약학박사학위논문

NR1D1과 IFI16의 DNA 손상 복구 및 항암제 감수성 조절 효과에 관한 연구

Identification of NR1D1 and IFI16 as key regulators in DNA damage response: Roles in chemosensitization against breast cancer

2019년 8월

서울대학교 대학원

약학과 병태생리학전공

가 나 리

ABSTRACT

Identification of NR1D1 and IFI16 as key regulators in DNA damage response: Roles in chemosensitization against breast cancer

Na-Lee Ka
Department of Pathology & Physiology
College of Pharmacy
The Graduate School
Seoul National University

Chemotherapy resistance still remains a major problem in the treatment of cancer. Many chemotherapeutic agents exert cytotoxic effects by inducing excessive DNA damage in cancer cells. Therefore, DNA repair capacity is a critical determinant of tumor sensitivity to chemotherapy. This study identified novel functions of nuclear receptor subfamily 1, group D, member 1 (NR1D1; Rev-erbα) and interferon γ-inducible protein 16 (IFI16) in DNA repair, which enhance chemosensitivity in breast cancer cells.

The first part of the study identified that NR1D1 inhibited both non-homologous recombination (NHEJ) and homologous recombination (HR)

DNA double strand breaks (DSB) repair, and delayed the clearance of doxorubicin-induced γH2AX and p53-binding protein 1 foci. Poly(ADP-ribose) polymerase 1 (PARP1) was identified as an NR1D1-interacting protein, which was confirmed by coimmunoprecipitation and proximity ligation assays. Notably, NR1D1 was PARylated and recruited to damaged DNA lesions. Interaction with PARP1 and subsequent PARylation were critical steps that allow NR1D1 to translocate to DNA damaged sites. NR1D1 inhibited the recruitment of DNA damage response (DDR) components such as SIRT6, pNBS1, and BRCA1 to the damaged DNA sites. In agreement, depletion of NR1D1 in MCF7 cells resulted in resistance to DNA damage-inducing chemotherapeutic agents both *in vitro* and *in vivo* experiments. Finally, the NR1D1 expression level was correlated positively with the clinical outcomes in breast cancer patients who received chemotherapy when analyzed using four public datasets. These findings suggest that NR1D1 and its ligands may offer therapeutic options to enhance chemosensitivity in breast cancer.

The second part of the study identified a novel function of IFI16 in DNA repair, which amplified type I interferon (IFN) signaling in triple negative breast cancer (TNBC) cells. The expression of IFI16 was induced by treatment of DNA damage-inducing chemotherapeutic agents and further increased by cotreatment with type I IFNs. Notably, type I IFNs inhibited the efficiency of

both NHEJ and HR, which was abolished when IFI16 was depleted in MDA-MB-231 cells. Interestingly, IFI16 was rapidly accumulated to histone-evicted regions near DSB sites. IFI16 inhibited the recruitment of DDR factors to DSB sites, thereby impairing DNA repair. Subsequently, IFI16 translocated into cytoplasm along with double stranded DNA, where it triggered stimulator of IFN genes activation and type I IFN production. Depletion of IFI16 suppressed doxorubicin- and type I IFN-induced activation of caspase-3 and production of T cell chemotactic factors. In agreement, synergistic cytotoxic effects of doxorubicin and type I IFNs were attenuated when IFI16 was depleted in MDA-MB-231 cells. Analysis of public patient datasets indicated that IFI16 expression correlates positively with clinical outcomes in breast cancer patients who received chemotherapy. These results suggest that IFI16 is essential for the DNA damage-induced amplification of type I IFN signaling in TNBC. These findings provide mechanistic insights and rationale for potential therapeutic use of type I IFNs in treating TNBC.

Taken together, NR1D1 and IFI16 may provide better therapeutic options that could enhance the outcomes of chemotherapy in breast cancer patients.

Keywords : DNA damage response, NR1D1, IFI16, PARP1, type I IFN, chemosensitivity, breast cancer

Student Number : 2013-21566

CONTENTS

LIST OF TABLES

LIST OF FIGURES

I . INTRODUCTION

1. Chemotherapy for breast cancer

1.1. Breast cancer biology and therapeutics

Breast cancer is the most commonly diagnosed cancer and the leading cause of cancer-related death in women worldwide (Torre et al., 2017). Genetic predisposition or family history, hormone exposure, lifecycle factors, and other environmental factors have been associated with increased risk for breast cancer development (Shah et al., 2014). Breast cancer is a heterogeneous disease characterized by specific morphological patterns and distinct biological features (Reis-Filho and Pusztai, 2011). Clinically, breast cancer is classified into four distinct subtypes based on their molecular expressions of estrogen receptor (ER), progesterone receptor, and erb-b2 receptor tyrosine kinase 2 (ERBB2, also known as human epidermal growth factor receptor 2 (HER2)): luminal A, luminal B, ERBB2/HER, and basal-like types (Yersal and Barutca, 2014).

In general, the primary treatment for early breast cancer is surgery and subsequent adjuvant therapy is treated to improve the survival of patients by eradicating residual cancer cells (Senkus et al., 2015). Systemic therapy of breast cancer includes chemotherapy, endocrine therapy, and anti-HER2 targeted therapy. These agents are employed based on the molecular subtypes, tumor grade, and lymph node involvement (Curigliano et al., 2017). For luminal types

of breast cancer, endocrine therapy is a primary treatment option. In patients with HER2-positive tumors, anti-HER2 therapy, such as trastuzumab, as well as chemotherapy are usually given. For triple-negative breast cancer (TNBC), chemotherapy is the only available therapy (Figure 1). In addition, tumors are characterized by proliferative fraction measured by Ki67, which also affect the treatment decisions (Curigliano et al., 2017). In contrast with early breast cancer, metastatic breast cancer is much more difficult to treat, thus is generally considered incurable. Systemic therapy is the first therapeutic options in metastatic breast cancer (Liedtkea and Kolberg, 2016). Biopsy of first metastatic site is recommended and systemic therapies are employed based on the tumor biology (Harbeck and Gnant, 2017).

1.2. Chemotherapy as a treatment option for most types of breast cancer

According to the 2017 St Gallen Consensus, chemotherapy should be provided to patients with HER2-positive breast cancer with stage pT1b pN0 and higher (Curigliano et al., 2017). Chemotherapy is also a treatment option for luminal-B-like and/or node-positive cancer with intermediate or high genomic risk scores (Curigliano et al., 2017). In particular, TNBC is characterized by lack of well-defined molecular targets, thus cytotoxic chemotherapy remains the

mainstay of treatment (Wahba and El-Hadaad, 2015). Anthracyclines (e.g., doxorubicin and epirubicin), alkylating agents (e.g., cyclophosphamide), and taxanes (e.g., paclitaxel and doxetaxel) constitute standard chemotherapy regimens for the treatment of breast cancer (Hernandez-Aya and Gonzalez-Angulo, 2013). In addition, platinum-based agents (e.g., cisplatin and carboplatin) have shown to be effective in TNBC, especially in breast cancer susceptibility gene (BRCA)-mutated tumors, thus being explored to addition to the standard chemotherapy (La Belle et al., 2017). However, despite their known efficacy, drug resistance develops frequently in breast cancer patients, which is still a major hurdle in the treatment of cancer. Therefore, there is an urgent need to develop more effective therapeutic strategies to enhance the effectiveness of chemotherapy while reducing resistance rate.

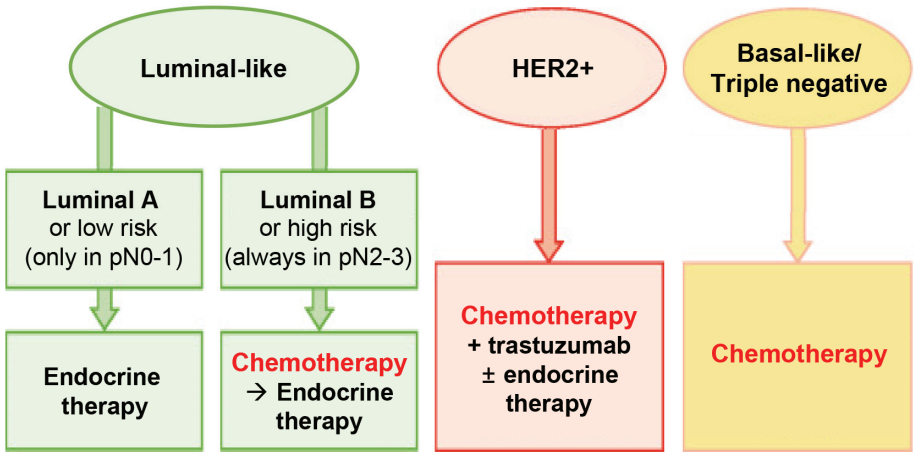

Figure 1. Systemic therapy in early breast cancer

Systemic therapy of early breast cancer includes chemotherapy, endocrine therapy, and targeted therapy. These treatment strategies are employed based on the molecular subtypes of breast cancer. Among them, chemotherapy is a treatment option for most types of breast cancer. (modified from Harbeck and Gnant, 2017).

2. DNA damage response in cancer chemotherapy

2.1. Chemotherapy induced DNA damage response

Most chemotherapeutic agents used to treat breast cancer exert their cytotoxic effect by inducing excessive DNA lesions, which is sufficient to effectively kill cancer cells (Goldstein and Kastan, 2015). For example, anthracyclines induce DNA single-strand breaks (SSBs) and double-strand breaks (DSBs) by poisoning topoisomerases (TOP) and by inducing reactive oxygen species (Kizek et al., 2012). Platinum agents and alkylating agents lead to intrastrand and interstrand crosslinks (ICLs) with purine bases (Dasari and Tchounwou, 2014). Upon recognizing DNA damage, cells normally initiate a series of DNA damage response (DDR) signaling to arrest the cell cycle and repair damaged DNA (Lord and Ashworth, 2012). SSBs are restored by base excision repair and tyrosyl-DNA-phosphodiesterase pathway (Caldecott, 2008). ICLs are repaired by nucleotide excision repair, translesion synthesis and homologous recombination (HR) (Schärer, 2005). DSBs are considered to be the most hazardous lesions and generated from SSBs in the S phase, or directly by ionizing radiation or TOPⅡ inhibitors. DSBs are repaired by two major pathways; non-homologous end joining (NHEJ) and HR (Hühn et al., 2013; Figure 2).

2.2. DNA damage response as a determinant of susceptibility to chemotherapy

DDR pathways play a critical role in cancer initiation, proliferation, and therapeutic response (Hühn et al., 2013; Furgason and Bahassi, 2013). Failure to DNA repair may lead to genomic instability and promote various cancers, including breast cancer (Luo et al., 2009). Indeed, germline or somatic mutations in DNA repair genes extensively increase the risk of breast cancer (Liu et al., 2014). However, these DDR defects in cancer cells can be exploited as targets for anticancer therapy. Cancer cells with specific abnormalities in DDR machinery make them more susceptible to chemotherapy (O'Connor, 2015). In particular, TNBC have been shown to harbor many of the DNA repair deficiencies including mutations in BRCA1/2 and p53, thus providing significant benefit of DNA-damaging agents (Cancer Genome Atlas Network, 2012).

However, some cancer cells develop the capacity to back-up DNA repair pathways such as genetic reversion of DDR defects or alterations of their choice of DNA repair pathway, which could induce resistance to chemotherapy in cancer cells (Figure 3). For example, HR-deficient ovarian tumors acquire platinum resistance by genetic reversion of BRCA1 or BRCA2, leading to restoration of protein function (Edwards et al., 2008; Sakai et al., 2008; Swisher et al., 2008; Norquist et al., 2011). Elevated expression of several DNA damage

repair genes was also observed in cisplatin-resistant mouse models of human non-small-cell lung cancer (Oliver et al., 2010). These studies suggest that regulating the components of DNA repair networks is a critical factor that determines the response as well as resistance to chemotherapeutic drugs. Therefore, development of novel strategies to enhance DNA damage in cancer cells by preventing DDR-associated therapy resistance would be critical to treatment of cancers.

2.3. Approaches to enhance chemosensitivity by modulating DNA damage response

Given the importance of DDR in tumor response to therapy, many attempts have been made to target DDR in cancer cells to enhance the effectiveness of therapy. Studies have identified several novel regulatory factors that confer sensitivity to chemo- or radiosensitivity by contoling DDR components in breast cancer cells. For example, tumor protein D52 increased sensitivity to ionizing radiation-induced DNA damage by compromising ataxia telangiectasia mutated (ATM)-mediated DDR in breast cancer cells (Chen et al., 2013). FOXP3, an X-linked tumor suppressor gene, decreased HR-mediated DNA repair and sensitizes cancer cells to γ-irradiation by repressing transcriptional expression of BRCA1 (Li et al., 2013). Recently, studies have reported that circadian clock

machineries as well as immune response genes are closely related to DDR, which could provide potential targets for enhancing the chemosensitivity of breast cancer.

2.3.1. Circadian clock genes modulate DNA damage response

Several components of DNA repair networks are modulated by circadian clock gene products such as Clock, Bmal, NPAS2, and Period2, which regulate a molecular time-keeping mechanism that orchestrates the daily oscillations of behavior and biochemical processes (Fu and Kettner, 2013; Sancar et al., 2010). Recently, cryptochrome (Cry) 1 was shown to modulate ataxia-telangiectasia and Rad3-related (ATR)-mediated DNA damage checkpoint responses (Kang et al., 2014). Furthermore, the activity of 8-oxoguanine DNA glycosylase, a rate-limiting factor in base excision repair, exhibits circadian rhythmicity (Manzella et al., 2015). Importantly, these circadian clock gene products are closely associated with sensitivity to DNA damage-inducing chemotherapeutic drugs; circadian mutant mice such as a transactivation-defective mutant of Per2, loss-of-function mutants of Cry1, and Cry2 genotypes exhibit differences in their sensitivity to g-irradiation or anticancer drugs such as cyclophosphamide (Fu et al., 2002, Gorbacheva et al., 2005, Antoch et al., 2005). These observations strongly suggest that there is a link between the circadian clock system and

DDR, which may affect the sensitivity of cancer cells to chemotherapy or radiotherapy.

2.3.2. Type I interferon signaling is closely linked to DNA damage response

Emerging evidences have suggested that DDR pathway is closely linked to type I interferon (IFN) signaling pathways. For instance, defects in Ataxia-telangiectasia mutated (ATM) results in release of DNA into cytoplasm, where it triggers type I IFN signaling (Härtlova et al., 2015). Similarly, downregulation of RAD51, a key component of DNA repair machinery, leads to the activation of stimulator of IFN genes protein (STING)-mediated innate immune response, which in turn primes the type I IFN signaling (Bhattacharya et al., 2017). Moreover, it has been shown that poly ADP-ribose polymerase (PARP) or checkpoint kinase 1 (CHK1) inhibition promotes activation of cytotoxic T lymphocytes, thereby potentiates the anti-tumor effect of programmed death-ligand 1 (PD-L1) blockade (Sen et al., 2019). Thus, targeting DNA repair pathways could provide a strategy that amplify both DNA damage-induced cancer cell death and tumor inherent type I IFN signaling that enhances therapeutic responses of cancer patients.

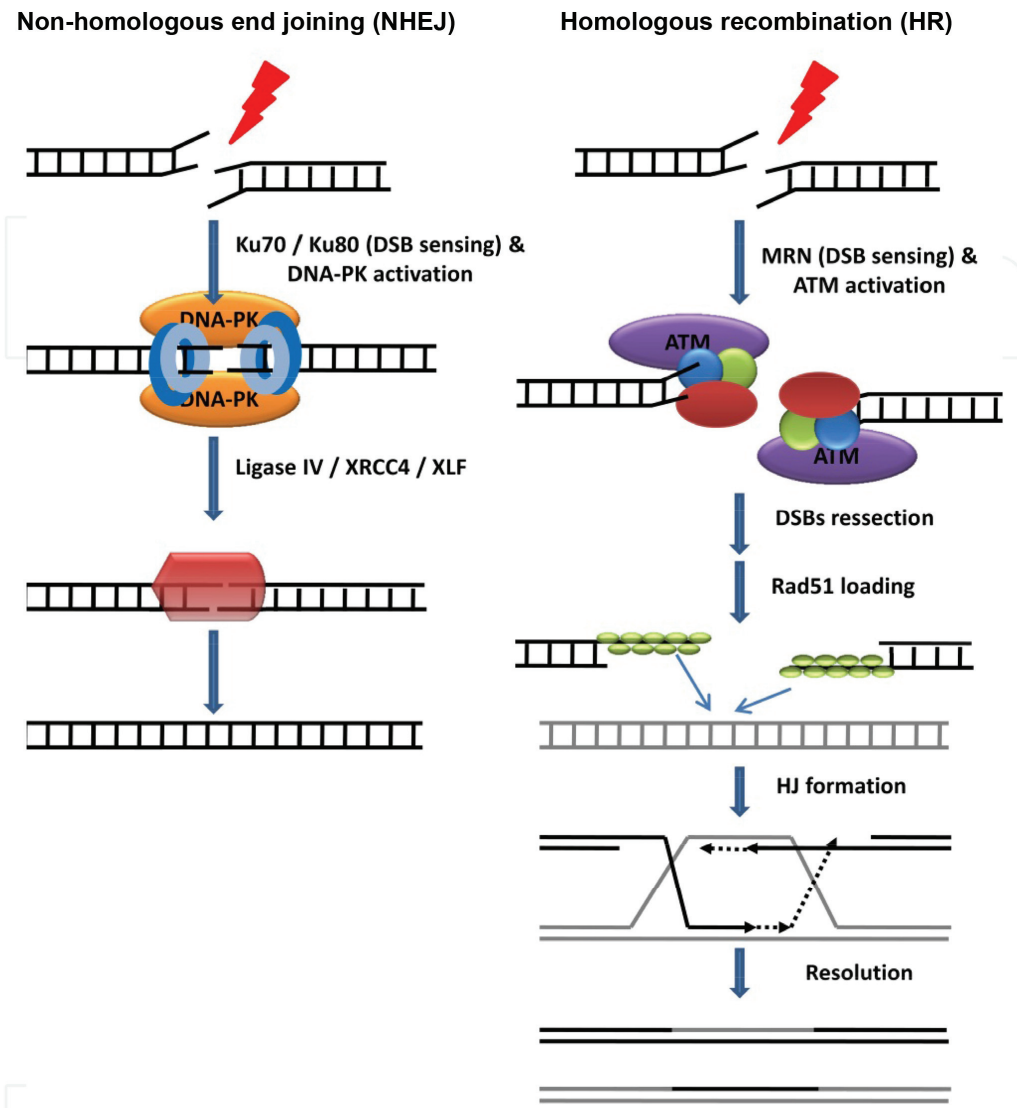

Figure 2. DNA double-strand break repair pathway

DNA double strand breaks (DSBs) are considered to be the most hazardous lesions. The two major DSB repair pathways are non-homologous recombination (NHEJ), an error-prone process, and homologous recombination (HR), an error-free process. NHEJ occurs throughout the cell cycle and mainly presents in G1 phase, whereas HR acts in the S and G2 phases, since homologous sister chromatid is used as a template for repair (Lopez-Contreras and Fernandez-Capetillo, 2012).

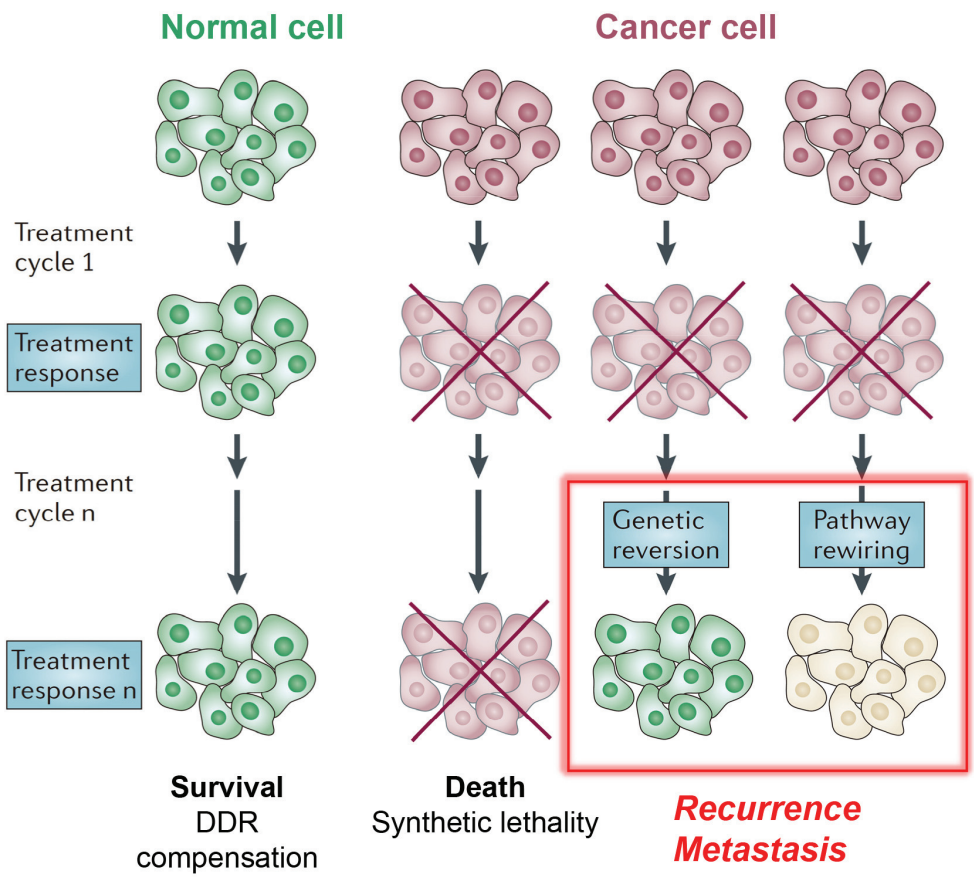

Figure 3. DNA damage response-related mechanisms of cancer drug resistance

DNA damage response (DDR) deficiency confers sensitivity of tumor cells to DSB-inducing agents. However, some cancer cells undergo genetic reversion of DDR defect or rewiring of DNA repair pathway that may induce therapy resistance (Bouwman and Jonkers, 2012).

3. Nuclear receptor subfamily 1, group D, member 1 (NR1D1)

3.1. Structure and functions of NR1D1

NR1D1 (also known as Rev-erbα) belongs to the nuclear receptor superfamily of ligand-regulated transcription factors (Everett and Lazar, 2014). NR1D1 consists of an N-terminal activation function (AF)-1 region, a conserved DNA binding domain, a hinge domain, and a ligand binding domain (LBD). Unlike most of the nuclear receptors, NR1D1 lacks a AF-2 domain which is necessary for the recruitment of coactivators (Figure 4A). NR1D1 binds to specific DNA response elements called ROR response element or Rev-erb direct repeat 2 as a monomer or a homodimer. Upon binding, NR1D1 recruits nuclear receptor corepressor (NcoR)-histone deacetylase 3 (HDAC3) complexes to repress target gene transcription (Yin et al., 2010).

NR1D1 has been implicated in the modulation of circadian rhythm. NR1D1 represses the transcription of core clock component Bmal1, which contributes to the formation of feedback loops to maintain circadian oscillations (Preitner et al., 2002; Figure 4B). Subsequent studies have revealed that NR1D1 represses transcription of additional circadian clock genes, including Clock, Cry1, and Npas2 (Crumbley et al., 2010; Crumbley and Burris, 2011; Ukai-Tadenuma et al., 2011). In addition to its circadian regulatory function, NR1D1 also

regulates the transcription of several genes involved in metabolism, autophagy, and inflammatory responses (Everett and Lazar, 2014). Thus, NR1D1 is a crucial components of the clock that link circadian rhythm to metabolic homeostasis.

3.2. Synthetic ligands of NR1D1

The identification of heme as an endogenous ligand for NR1D1 has facilitated the development of synthetic ligands that modulate the transcriptional activity of NR1D1 (Yin et al., 2007; Raghuram et al., 2007). The first identified synthetic agonist was GSK4112 (SR6452). GSK4112 increases the recruitment of NcoR and HDAC3 to the NR1D1 target gene promoters and increases the NR1D1-mediated transrepression (Grant et al., 2010; Kumar et al., 2010). However, GSK4112 possesses unfavorable pharmacokinetic properties when administered intraperitoneally, which limits its pharmacological uses (Grant et al., 2010). Modifications of GSK4112 led to the identification of two NR1D1 agonists, SR9009 and SR9011. Both compounds are more potent and efficacious than GSK4112 and have improved pharmacokinetic properties. Intraperitoneal administration of these compounds resulted in alteration of circadian behavior and the expression pattern of core clock genes (Solt et al., 2012). Later, four additional NR1D1 agonists were developed. These compounds have reasonable plasma exposure to be used *in vivo* and they are orally bioavailable (Trump et

al., 2013). These potent synthetic ligands could be used to target NR1D1 for therapeutic purposes (Table 1).

3.2. Role of NR1D1 in breast cancer

NR1D1 gene is encoded within ERBB2 amplicon (17q12 – q21), a maker of aggressive breast tumor, and its expression is correlated with poor prognosis (Chin et al., 2006; Davis et al., 2007). Consistent with these observations, NR1D1 together with peroxisome proliferator activated receptor binding protein, also a gene resides in the ERBB2 amplicon, enhanced survival of breast cancer cells by upregulating several genes in the *de novo* fatty acid synthase network associated with aerobic glycolysis (Kourtidis et al., 2010). However, results from recent studies raised controversies in that expression of NR1D1 was lower in both ER-positive and ER-negative breast cancer cohorts compared with normal breast (Muscat et al., 2013). Furthermore, synthetic NR1D1 and NR1D2 agonist, SR9011, suppressed the proliferation of breast cancer cells independent of their ER or ERBB2 status (Wang et al., 2015). In a more recent study, SR9011 and another NR1D1 agonist, SR9009, were lethal to various types of cancer cells including breast cancer, brain cancer, leukemia, colon cancer, and melanoma, through their inhibitory effects on *de novo* lipogenesis and autophagy (Sulli et al., 2018). Although these studies suggest a role of NR1D1 in breast cancer

proliferation and cellular energy metabolism, its role in DNA repair and chemosensitivity has not been revealed.

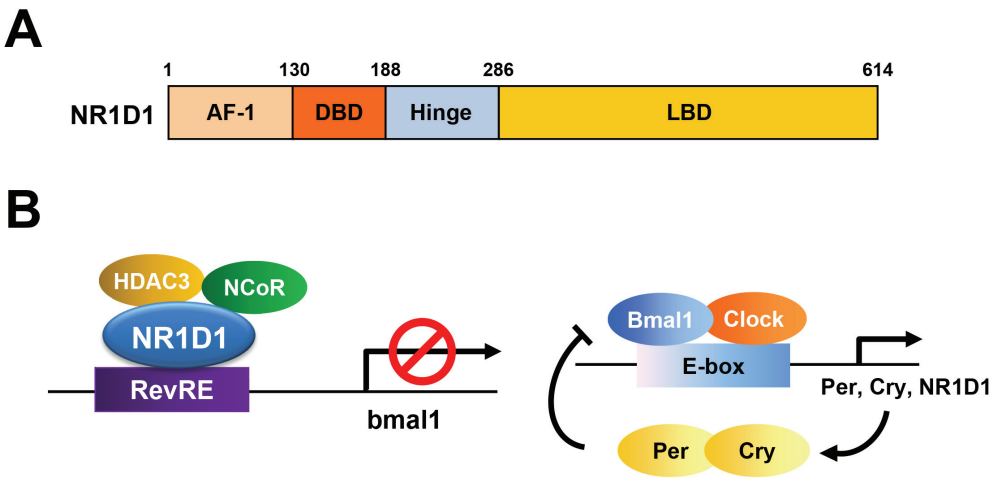

Figure 4. The nuclear receptor, NR1D1

(A) Structure of the NR1D1. NR1D1 contains a DNA binding domain (DBD) and a ligand binding domain (LBD), which are responsible for ligand-dependent transcriptional regulation.

(B) Role of NR1D1 in regulation of circadian rhythm. NR1D1 represses the transcription of clock components including Bmal1, which contributes to the formation of feedback loops to maintain circadian oscillations.

Compound	Structure	Ligand type	EC_{50} value and actions
GSK4112 (SR6452)	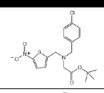	Agonist	▪ NR1D1 EC_{50} = 0.4 μM (measured by FRET assay) ▪ NR1D1 EC_{50} = 2.3 μM (measured by Bmal1 luciferase reporter assay) ▪ Has a limited *in vivo* exposure
SR9009	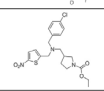	Agonist	▪ NR1D1 EC_{50} = 0.67 μM (measured by Gal4 reporter assay) ▪ NR1D1 EC_{50} = 0.71 μM (measured by full-length Bmal1 reporter assay) ▪ Suppresses expression of NR1D1 target genes *in vitro* and *in vivo*
SR9011	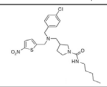	Agonist	▪ NR1D1 EC_{50} = 0.79 μM (measured by Gal4 reporter assay) ▪ NR1D1 EC_{50} = 0.62 μM (measured by full-length Bmal1 reporter assay) ▪ Suppresses expression of NR1D1 target genes *in vitro* and *in vivo*
GSK2945	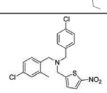	Agonist	▪ NR1D1 EC_{50} = 50 nM (measured by NCOR peptide recruitment) ▪ Pharmacokinetics suitable for 20-30 mg per kg dosing daily
GSK0999	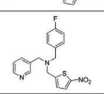	Agonist	▪ NR1D1 EC_{50} = 160 nM (measured by NCOR peptide recruitment) ▪ Pharmacokinetics suitable for acute dosing
GSK5072	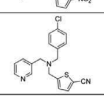	Agonist	▪ NR1D1 EC_{50} = 200 nM (measured by NCOR peptide recruitment) ▪ Pharmacokinetics suitable for acute dosing
GSK2667	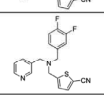	Agonist	▪ NR1D1 EC_{50} = 200 nM (measured by NCOR peptide recruitment) ▪ Pharmacokinetics suitable for acute dosing
SR8278	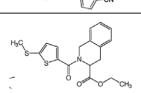	Antagonist	▪ NR1D1 IC_{50} = 2.3 μM (measured by full-length Bmal1 reporter assay) ▪ Limited *in vivo* exposure

Table 1. Synthetic ligands of NR1D1 (Reviewed by Kojetin and Burris, 2014)

4. Interferon γ-inducible protein 16 (IFI16)

4.1. Structure and functions of IFI16

IFI16 is a member of the IFN-inducible p200-protein family. The family includes structurally related human (e.g., IFI16, AIM2, MNDA, and IFIX) and mouse (e.g., p204, p202a, p202b, and p203) proteins (Cridland et al., 2012). IFI16 consists of a pyrin domain and two hematopoietic interferon-inducible nuclear (HIN) protein domains, HINa and HINb (Figure 5A). The pyrin domain is a putative protein-protein interaction domain, which mediates signal transduction in cellular functions, including innate immunity, inflammation, differentiation, apoptosis, and cancer (Stehlik, 2007). The HIN domain consists of two consecutive oligonucleotide/oligosaccharide-binding folds, which is responsible for the binding to either single or double-stranded DNA (dsDNA) (Albrecht et al., 2005).

IFI16 is expressed in a variety of human tissues and organs (Gariglio et al., 2002). The IFI16 protein contains a multipartite nuclear localization signal (NLS), and the acetylation of NLS has been reported to modulate its subcellular distribution (Li et al., 2012). Accordingly, IFI16 protein is localized in both nuclear and cytoplasmic, depending on the cell type (Veeranki and Choubey, 2012). The expression of IFI16 is induced by IFNs (α, β, or γ) in a variety of cells (Duan et al., 2011; Veeranki et al., 2011). Furthermore, expression of IFI16

is also regulated by transcriptional factors, such as activator protein 1, Wilms tumor gene, p53, and NF-κB, hormones, proinflammatory cytokines, and hypoxia (Choubey et al., 2008).

IFI16 acts as an innate immune sensor for cytosolic and nuclear dsDNA (Unterholzner et al., 2010, Kerur et al., 2011). Molecular mechanism underlying assembly of IFI16 on DNA has been demonstrated (Unterholzner et al., 2010, Morrone et al., 2014, Stratmann et al., 2015). IFI16 binds dsDNA in a length-dependent manner and assembles into distinct oligomeric clusters. Since IFI16 binds dsDNA with a footprint of ~15 base pairs, about 4 IFI16 molecules and minimal length of 60 base pairs of exposed dsDNA are required to initiate assembly, and about 10 IFI16 molecules and ~150 base pairs of dsDNA comprise an optimal binding cluster (Stratmann et al., 2015). Recently, IFI16 was shown to be required for the activation of STING by cooperating with cyclic GMP-AMP synthase (cGAS) in the detection of cytosolic DNA (Jønsson et al., 2017; Almine et al., 2017). Besides its function in dsDNA sensing, IFI16 also plays a critical role in transcriptional regulation, cell growth regulation, cell differentiation, and autoimmunity (Jakobsen and Paludan, 2014).

4.2. Tumor suppressive functions of IFI16

IFI16 has been shown to function as a tumor suppressor. Studies have indicated

that expression level of IFI16 is decreased or down-regulated in several types of cancers including breast cancer, prostate cancer, and hepatocellular carcinoma (Xin et al., 2003; Fujiuchi et al., 2004; Lin et al., 2017). Forced expression of IFI16 in breast cancer cell lines increased transcriptional activity of p53, as well as the expression of p53 target genes, including p21, Hdm2, and Bax (Fujiuchi et al., 2004). IFI16 downregulated the expression of androgen receptor (AR) and its target genes in prostate cancer cells (Alimirah et al., 2006). In addition, IFI16 expression is inversely correlated with proliferation and transforming activity in head and neck squamous cell carcinomas (HNSCCs) (De Andrea et al., 2007). Furthermore, recent studies have shown that the spleen of Lewis lung carcinoma-induced p204 knockout mice showed altered expressions in cytokines, chemoattractant molecules, and adhesion molecules compared with tumor-bearing wild type mice, suggesting that IFI16/p204 regulated anti-tumor immune network (Jian et al., 2018).

4.3. Role of IFI16 in DNA damage response

Studies have provided evidence that IFI16 is involved in cellular response to DNA damage. IFI16 expression is induced by oxidative stress, which is accompanied by the interaction and activation of p53 in endothelial cells (Gugliesi et al., 2005). Other studies have reported that IFI16 is constitutively

associated with BRCA1, which enhances p53-mediated apoptosis in response to DNA damage (Aglipay et al., 2003; Fujiuchi et al., 2004). Similarly, IFI16 restoration in HNSCC-derived cell line increased doxorubicin-induced cell death by accumulating the cells at the G2/M phase (De Andrea et al., 2007). More recently, it was reported that IFI16 is required for the non-canonical activation of STING in response to etoposide-induced DNA damage (Dunphy et al., 2018). These studies imply the involvement of IFI16 in DNA damage response. However, so far, no clear evidence has been provided for the role of IFI16 in the process of DNA repair and chemosensitivity of breast cancer cells.

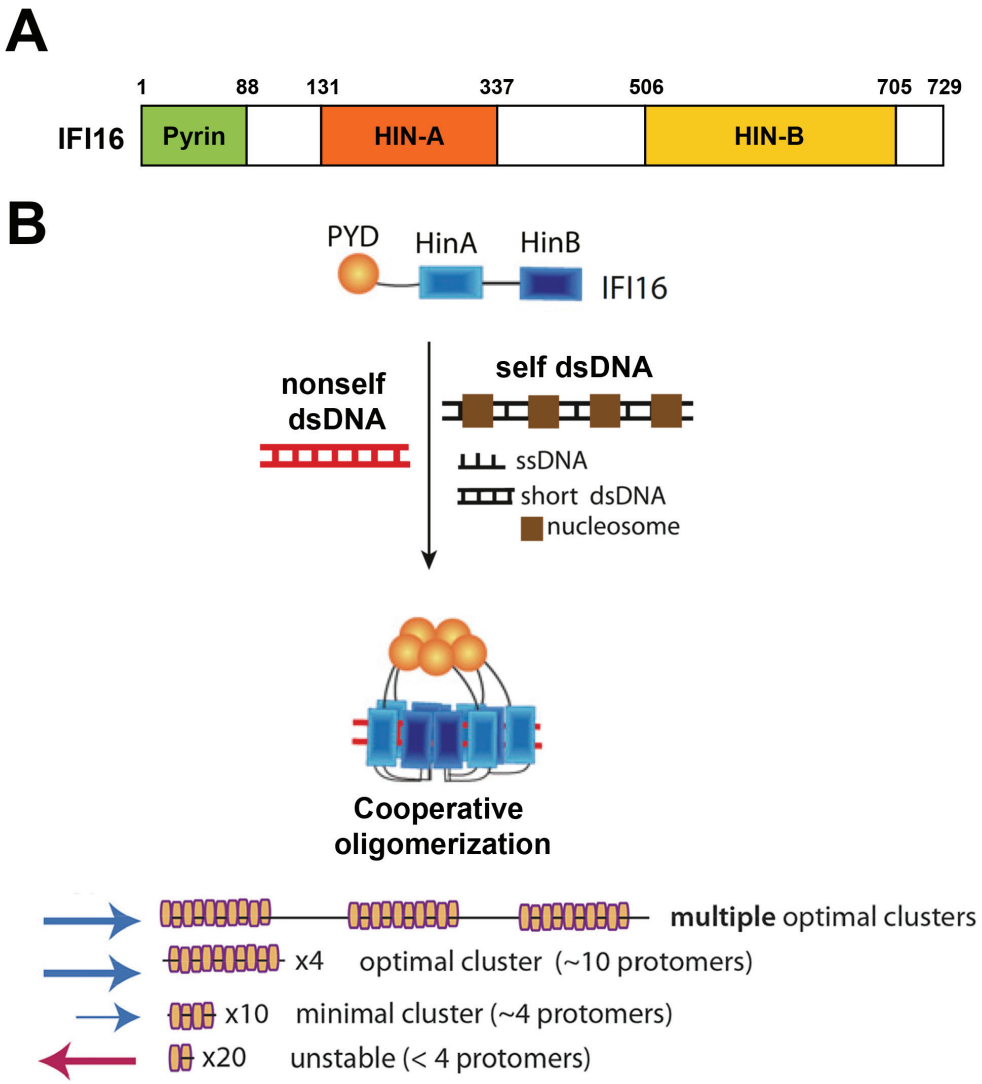

Figure 5. The innate immune sensor, IFI16

(A) Molecular structure of IFI16. IFI16 contains two C-terminal HIN domains that bind dsDNA and an N-terminal pyrin domain that is responsible for downstream signaling.

(B) IFI16 binds dsDNA in a length-dependent manner and assembles into oligomers, which represent a molecular mechanism that distinguish self from nonself dsDNA (Morrone et al., 2013; Stratmann et al., 2015).

II. PURPOSE OF THIS STUDY

Breast cancer is the most commonly diagnosed cancer in women and the fifth leading cause of cancer-related death worldwide (Torre et al., 2017). The primary treatment for patients with breast cancer is surgery and subsequent adjuvant chemotherapy is treated to improve the survival of patients by eradicating residual cancer cells. However, despite their known efficacy, drug resistance develops frequently in breast cancer patients, which is still a major obstacle in the treatment of cancer. Therefore, there is an urgent need to develop new therapeutic strategies to enhance the effectiveness of chemotherapy while reducing the rate of resistance.

Most chemotherapeutic agents exert their cytotoxic effect by inducing DNA damage. Upon recognizing DNA damage, cells normally initiate a series of DDR signaling to arrest the cell cycle and repair damaged DNA. However, many types of cancer cells possess specific abnormalities in DDR machinery, which make them more susceptible to chemotherapy (O'Connor, 2015). However, some cancer cells develop the capacity to back-up DNA repair pathways such as genetic reversion of DDR defects or alterations of their choice of DNA repair pathway, which could induce resistance to chemotherapy in cancer cells (Bauwman et al., 2012). Therefore, development of novel strategies to enhance

DNA damage in cancer cells by preventing DDR-associated therapy resistance would be critical for cancer treatment.

Studies have demonstrated that several DNA repair factors are modulated by circadian clock genes response. NR1D1 functions as a circadian clock that participates in regulation of the circadian rhythm and metabolic homeostasis (Everett and Lazar, 2014). Several studies have identified a role of NR1D1 in breast cancer proliferation. NR1D1 enhanced the survival of breast cancer cells by upregulating several genes in the *de novo* fatty acid synthase network associated with aerobic glycolysis (Kourtidis et al., 2010). In contrast, recent studies showed that expression of NR1D1 was lower in breast cancer cohorts compared with normal breast subjects (Muscat et al., 2013). Furthermore, a synthetic NR1D1 and NR1D2 agonist, SR9011, suppressed the proliferation of breast cancer cells (Wang et al., 2015). These studies suggest a role for NR1D1 in breast cancer proliferation and cellular energy metabolism, but its roles in DNA repair and chemosensitivity are not known.

Emerging evidences have suggested that DDR pathway is closely linked to type I IFN signaling. Previously, our group has reported that expression of IFI16 is significantly higher in ERα-negative breast cancer compared with ERα -positive cancer (Kang et al., 2014). Scattered data in literature suggest that IFI16 is involved in both cellular response to DNA damage and immune sensing

of intracellular dsDNA (Jakobsen and Paludan, 2014; Choubey and Panchanathan, 2016). Recently, it was reported that IFI16 is required for the activation of STING by cooperating with cGAS which detects cytosolic DNA (Jønsson et al., 2017; Almine et al., 2017). Furthermore, it has been shown that IFI16 is required for the non-canonical activation of STING in response to etoposide-induced DNA damage (Dunphy et al., 2018). Given the importance of linking DNA repair to innate immunity to enhance the effect of cytotoxic anticancer therapy, I asked whether IFI16 interconnects the process of DNA repair with tumor inherent type I IFN signaling in TNBC.

Therefore, this study aimed to investigate whether NR1D1 and IFI16 affected DNA repair after damage induced by chemotherapeutic agents and whether these factors could confer sensitivity to chemotherapy in breast cancer cells. Furthermore, the correlations between the expression levels of these regulatory factors with the overall survival rate after chemotherapy in breast cancer patients were analyzed. Ultimately, this study could provide potential therapeutic strategies for breast cancer treatment.

III. MATERIALS AND METHODS

1. Cell culture and reagents

1.1. Cells and cell culture

Human breast cancer cell lines, *i.e.,* MCF7, T47D, ZR75-1, BT474, SKBR3, MDA-MB-231, Hs578T, and BT549, and a human T lymphocyte cell line, Jurkat, were obtained from the American Type Culture Collection (ATCC). These cells were authenticated by ATCC, by short tandem repeat profiling and monitoring cell morphology. The DSB reporter cell line (U2OS) was provided by Dr. Janicki (The Wistar Institute, Philadelphia, PA). MCF7, ZR75-1, BT474, MDA-MB-231, Hs578T, and U2OS cells were maintained in Dulbecco's modified Eagle's medium supplemented with 10% fetal bovine serum. T47D, SKBR3, BT549, and Jurkat cells were maintained in RPMI-1640 medium supplemented with 10% fetal bovine serum. The cells were grown in an incubator with 5% CO_2/95% air at 37°C.

1.2. Establishment of stable cell lines

MCF7 stable cell lines with NR1D1 overexpression or knockdown were generated using a lentivirus-based system. The lentiviral vector encoding NR1D1 (pLJM1-NR1D1) or shNR1D1 (pLKO.1-shNR1D1) was constructed by inserting full-length NR1D1 or an annealed oligomer, respectively, into the *Age*I/*Eco*RI site of the corresponding viral vector (Table 2). The lentiviral targeting vector, packaging vector (psPAX2), and envelope vector (pMD2.G) were cotransfected into HEK293T packaging cells using Lipofercamine 2000 (Thermo Fisher Scientific). After 60 h incubation, the lentivirus in the supernatant was collected and used to infect MCF7 cells with 8 μg/ml

hexadimethrine bromide (Sigma Aldrich). Stable clones were selected with 2 μg/ml puromycin (Santa Cruz Biotechnology) for 3 weeks.

MDA-MB-231 stable cell lines with knockout of IFI16 were generated using CRISPR/Cas9 system. MDA-MB-231 cells were transfected with 1 μg of IFI16 CRISPR/Cas9 knockout plasmid (sc-416568, Santa Cruz Biotechnology) or control CRISPR/Cas9 plasmid (sc-418922, Santa Cruz Biotechnology) using Lipofectamine 2000 according to manufacturer's protocol. Three days after transfection, GFP-positive cells were sorted by FACS Aria (BD Biosciences) and seeded as single cells in 96-well plates. Clones were expanded and subsequently confirmed by western blotting.

All stable sublines were authenticated using short tandem repeat analysis by Cosmo Genetech.

1.3. Reagents

Doxorubicin, fluorouracil (5-FU), cisplatin, etoposide, GSK4112, 4',6-diamidino-2-phenylindole (DAPI), 6-(5H)-phenanthridinone (PHEN), and 3-(4,5-dimethylthiazol-2-yl)-2,5-diphenyltetrazolium bromide (MTT) were purchased from Sigma Aldrich. Recombinant human IFNα, IFNβ, and IFNɣ were purchased from R&D systems. Recombinant human IFNβ-1a (REBIF®) used in the animal experiments was purchased from Merck Serono.

2. Plasmids and transient transfection

2.1. Plasmids

Myc-, FLAG-, or GFP- tagged NR1D1 were constructed by inserting a

PCR-amplified full-length human NR1D1 into pCMV-Myc (Clontech), p3XFLAG-CMV-10 (Sigma-Aldrich) or pEGFP-C3 (Clontech), respectively. FLAG- or Myc-tagged deletion mutants of NR1D1, *i.e.*, N-terminus (NT; amino acids (aa), 1 – 130), DNA binding domain (DBD; aa 131 – 188), hinge (aa 189 – 286), ligand binding domain (LBD; aa 287 – 614), hinge with LBD (HinL; aa 189 – 614), △Hinge (hinge deleted), and △LBD (aa 1 – 286) were constructed by inserting the corresponding cDNA into p3XFLAG-CMV-10 or pCMV-Myc. FLAG-tagged deletion mutants of PARP1, *i.e.*, DBD (aa 1 – 372), BRCA1 C-terminal domain (BRCT; aa 373 – 524), and catalytic domain (CatD; aa 525 – 1014), were constructed by inserting the corresponding cDNA into p3XFLAG-CMV-10. NHEJ and HR reporter plasmids, as well as the I-SceI expression vector were kindly provided by Dr. Vera Gorbunova (University of Rochester, Rochester, NY) (Mao et al., 2011). DsRed expression vector was purchased from Clontech. The wild-type and the nuclease-deficient D450A mutant of FokI were kindly provided by Dr. Price (Dana-Farber Cancer Institute, Boston, MA) (Shanbhag et al., 2010). H2AX-GFP and GFP-RAP80 were provided by Dr. Hyeseong Cho (Ajou University, Suwon, South Korea) and Dr. Hongtae Kim (Sungkyunkwan University, Suwon, South Korea), respectively (Min et al., 2014, Soo Lee et al., 2016). Myc-, GFP-, or RFP-tagged IFI16 were constructed by inserting a PCR-amplified full-length human IFI16 into pCMV-Myc, pEGFP-C3, or pmRFP-C1 vector, respectively. RFP-tagged H2B or H1.5 were constructed by inserting a PCR-amplified full-length human H2B or H1.5, respectively, into pmRFP-C1 vector. GFP-SMARCA4 was kindly provided by Dr. Kyle Miller (Addgene plasmid #65391) (Gong et al., 2015).

2.2. Transient transfection

Transient transfection into MCF7 cells was carried out using X-tremeGENE HP DNA Transfection Reagent (Roche). Transient transfection into MDA-MB-231 cells was performed using TransIT-X2 Dynamic Delivery System (Mirus Bio). Transient transfections into BT474 and SKBR3 cells were performed using Lipofectamine 2000.

3. Protein and mRNA expression analysis

3.1. Western blotting

Cells were lysed in a lysis buffer containing 50 mM Tris (pH 7.4), 150 mM NaCl, 5 mM EDTA, 1% Nonidet P-40 (NP-40), and protease inhibitor cocktail (Roche). Chromatin fractionation was performed as described previously (Wang et al., 2013). Western blotting was performed using specific antibodies against NR1D1 (#14506-1-AP, Proteintech), PARP1 (sc-1561), IFI16 (sc-8023), Myc (sc-40), HMGB1 (sc-56698), HP1α (sc-130446), Actin (sc-1616) (all from Santa Cruz Biotechnology); Mre11 (ab33125), Rad50 (ab3623), IFNβ (ab140211) (all from Abcam); NBS1 (#3002), ATM (#2873), pNBS1 (#3001), KAP1 (#4123), pKAP1 (#4127), STING (#13647), pSTING (#85735), Caspase-3 (#9665) (all from Cell Signaling Technology); pATM (#200-301-400, Rockland Immunochemicals), PAR (#551813; BD Biosciences), FLAG (#F3165, Sigma-Aldrich), or α-tubulin (#05-829, Calbiochem), as described previously (Yeo et al., 2005).

3.2. Quantitative real-time polymerase chain reaction (qRT-PCR)

Total RNA was isolated using easy-BLUE reagents (iNtRON Biotechnology)

according to the manufacturer's instructions. cDNA was synthesized as previously described (Han et al., 2014). qRT-PCR was performed using the StepOnePlusTM Real-time PCR system (Applied Biosystem) using specific primers (Table 3). Relative mRNA level of target gene was analyzed by the equation $2^{-\triangle Ct}$ ($\triangle$Ct = Ct of target gene - Ct of β-actin).

4. Analysis of DNA damage and repair

4.1. DSB repair assay and FACS analysis

Cells were cotransfected with the *Hind*III-linearized NHEJ or I-*Sce*I-linearized HR reporter plasmid, Myc-NR1D1 or Myc-IFI16, and DsRed expression vector. Or the cells were cotransfected with the *Hind*III-linearized NHEJ or I-*Sce*I-linearized HR reporter plasmid, and DsRed expression vector, and then treated with 100 IU/ml recombinant IFNα, IFNβ, or IFNɣ. After 48 h, the numbers of GFP-positive cells and DsRed-positive cells were quantified by flow cytometry. The ratio of GFP-positive cells to DsRed-positive cells was used to determine the DSB repair efficiency.

4.2. Immunofluorescence : Analysis of ɣH2AX and 53BP1 foci

Cells were fixed and stained with the antibodies against ɣH2AX (ab22551, Abcam) or 53BP1 (ab36823, Abcam). The foci were counted and the data were presented as the mean number of foci per nucleus from at least 50 cells. Nuclei were stained by DAPI.

4.3. Laser microirradiation assay

Cells were transfected with GFP- and/or RFP-tagged vectors and pre-sensitized with 10 μM 5-bromo-2'-deoxyuridine (Sigma Aldrich) for 24 h. Laser microirradiation was carried out using a Zeiss LSM 710 confocal microscope (Carl Zeiss) equipped with 405 nm laser diode focused through a C-Apochromat 40x/1.2 water immersion objective. The laser setting was set to 100% output with 20 iterations. Data were normalized to the initial fluorescence intensity and the average intensity from at least 20 cells was plotted.

4.4. Fok I assay

U2OS-DSB reporter cells, containing 256 Lac operator repeats integrated into the genome, were transfected with mCherry-LacI-Fok I wild-type (Fok I WT) or nuclease-deficient mCherry-LacI-Fok I (Fok I D450A), with GFP-NR1D1 or GFP-IFI16. After 24 or 48 h, live cell imaging was performed with confocal microscopy. For chromatin immunoprecipitation (ChIP) assay, U2OS-DSB reporter cells were transfected with Fok I WT or Fok I D450A with Myc-IFI16. After 24 h, ChIP assay was performed using antibodies against H2B (ab1790), H3 (ab1791), INO80 (ab118787) (all from Abcam), or Myc (sc-40, Santa Cruz Biotechnology), with specific primers, as described previously (Shanbhag et al., 2010) (Table 4).

4.5. I-SceI-based assay

Cells were cotransfected with NHEJ or HR reporter plasmid, I-*Sce*I expressing vector, and Myc-NR1D1 or Myc-IFI16. At the indicated time points, cells were

fixed and subjected to ChIP analysis using specific antibodies against Myc (sc-40, Santa Cruz Biotechnology); ATM (ab78), γH2AX (ab22551), NBS1 (ab175800), MDC1 (ab50003) (all from Abcam). Recruitment of NR1D1, IFI16, or DDR factors to I-*Sce*I-induced DSBs was analyzed by qRT-PCR using a primer set that amplifies the region 7 to 315 nt downstream of the I-*Sce*I recognition site (Table 4).

5. Analysis of protein-protein interactions and post-translational modifications

5.1. Immunoprecipitation (IP)

Cells were lysed in a lysis buffer containing 20 mM Tris (pH 7.5), 150 mM NaCl, 0.1 mM EDTA, 0.2% NP-40, and protease inhibitor cocktail (Roche). Immunoprecipitation were performed using specific antibodies against PARP1 (sc-1561) and Myc (sc-40) (both from Santa Cruz Biotechnology); FLAG (#F3165, Sigma-Aldrich); Mre11 (ab33125), Rad50 (ab3623), NBS1 (ab175800) (all from Abcam), as described previously (Yeo et al., 2005).

5.2. In situ proximity ligation assay (PLA)

Cells were fixed with 4% formaldehyde, permeabilized with 0.1% Triton X-100, followed by incubation with antibodies against NR1D1 (#14506-1-AP, Proteintech) and PARP1 (sc-1561, Santa Cruz Biotechnology). The PLA assay was performed using Duolink In Situ PLA Probes (Sigma Aldrich) and Detection Reagents Red (Sigma Aldrich) according to the manufacturer's instructions.

5.3. In vitro PARylation assay

The recombinant GST-PARP1 protein (#SRP0192, Sigma Aldrich) was incubated with a reaction buffer containing 20 mM Tris-HCl (pH 8.0), 100 mM NaCl, 10 mM $MgCl_2$, 10% glycerol, 1 mM DTT, 0.1 mg/ml sonicated salmon sperm DNA, and 300 μM NAD^+, in the presence or absence of the recombinant GST-NR1D1-His for 30 min at 30°C. The reaction mixture was analyzed by western blotting using anti-PAR antibody (#551813, BD Biosciences). The purified recombinant GST-NR1D1-His protein was obtained using a conventional protocol. Briefly, the pET21a$^+$-NR1D1-His construct was transformed into BL21 (DE5) cells, and the protein expression was induced with 0.5 mM isopropyl β-D-1-thiogalactopyranoside for 18 h at 16 °C. The cells were lysed and broken by sonication. After centrifugation, the supernatant was loaded to Ni^+-NTA resin (Qiagen), and the resin-bound GST-NR1D1-His proteins were eluted by increasing the concentration of imidazole.

6. Analysis of cytosolic DNA and STING signaling

6.1. PicoGreen Staining

PicoGreen staining was performed using Quant-iT PicoGreen dsDNA reagent (Thermo Fisher Scientific). Cells were treated with doxorubicin and/or IFNβ for 16 h and then stained with 1 μl/ml PicoGreen for 1 h. Cells were mounted with Fluoro-Gel (Electron Microscopy Sciences) and analyzed using a confocal microscope (Carl Zeiss).

6.2. In vitro migration assay

Migration assay was performed using Transwell chambers with 8-μm pore size polycarbonate membrane (Corning Costar). The Transwell membrane was coated with 10 μg/ml fibronectin (Sigma Aldrich) for 1 h at 37 ℃. Jurkat cells (5×10^5 cells) were seeded into the upper chamber and allowed to migrate to the lower chamber containing conditioned medium from MDA-MB-231 stable cells pretreated with doxorubicin and/or IFNβ. The number of cells that migrated to the lower chamber within 4 h was counted using a hemocytometer.

6.3. IFNβ ELISA

Cells were treated with doxorubicin and/or IFNβ for 16 h. The amount of IFNβ protein in the culture supernatants was measured using commercial ELISA kit (#MBS2513798, MyBioSource) according to the manufacturer's instructions.

7. Analysis of cellular sensitivity to chemotherapeutic agents

7.1. MTT assay

Cells were seeded onto 96-well plates and treated with doxorubicin and/or GSK4112 for 3 days. At the end of the treatment, MTT reagent was added to each well and the plates were incubated for 4 h. The formazan crystals were dissolved with dimethyl sulfoxide (Sigma Aldrich). To assess the viability of cells in 3D cultures, 48-well plates were coated with Matrigel (BD Biosciences) and the cell suspension mixed with Matrigel was then seeded on top. Cells were incubated in medium containing doxorubicin and/or GSK4112. At the end of the treatment, MTT reagent was added, and then the formazan crystals were

dissolved with 10% sodium dodecylsulfate and 0.01 N HCl. The absorbance was measured at 570 nm using a SpectraMax M5 microplate reader (Molecular Devices).

7.2. Clonogenic survival assay

MCF7 or MDA-MB-231 cells were seeded at 1,000 cells/plate in 35-mm plates. After incubation for 48 h, MCF7 cells were treated with doxorubicin and/or GSK4112 for 14 days. MDA-MB-231 cells were treated with 2 nM doxorubicin and/or 100 IU/ml IFNβ for 12 days. At the end of the treatment, colonies were fixed with methanol, stained with 0.5% crystal violet (Sigma-Aldrich). Colonies that composed of more than 50 cells were counted.

8. Analysis of *in vivo* susceptibility to doxorubicin

8.1. Xenograft experiments

For MCF7 xenografts, female 6-week-old athymic (nu/nu) BALB/c mice (Central Lab. Animal Inc.) were housed in an air-conditioned room at a temperature of 22°C to 24°C and humidity of 37% to 64%, with a 12 h light/dark cycle. Mice were implanted subcutaneously with 17β-estradiol pellets (60-day release, Innovative Research of America) and then injected in both flanks with 5×10^6 MCF7 cells mixed 1:1 with Matrigel (BD Biosciences). When the tumor volume reached approximately 100 mm^3, mice were separated randomly into two groups and given intraperitoneal injections with saline or doxorubicin (4 mg/kg body weight) at 4-day intervals, with a total of three injections. The tumor diameter was measured every 3 days with a caliper and

the tumor volume was calculated using the following formula: tumor volume (mm^3) = $width^2$ × length × 0.5.

For MDA-MB-231 xenografts, female 5-week-old athymic (nu/nu) BALB/c mice (Orient Bio Inc.) were injected subcutaneously in the flanks with 2.5×10^6 MDA-MB-231 cells mixed 1:1 with Matrigel. When the tumor volume reached approximately 100 mm^3, mice were separated randomly into four groups. Mice were given subcutaneous injection with IFNβ-1a (2×10^5 IU/mouse), and after 6 h, given intraperitoneal injection of doxorubicin (2 mg/kg body weight). IFNβ-1a injections were repeated for 3 consecutive days for a total of four administrations. Tumor diameter was measured every 4 days with a caliper.

All animal experiments were approved by Seoul National University Institutional Animal Care and Use Committee.

8.2. Histological analysis

For immunohistochemical staining or PLA of xenograft tumor sections, 3-μm paraffin sections were deparaffinized and processed for antigen retrieval. Slides were subjected to immunostaining using specific antibodies against NR1D1 (#14506-1-AP, Proteintech); PARP1 (sc-1561) and IFI16 (sc-8023) (both from Santa Cruz Biotechnology); γH2AX (ab22551), 53BP1 (ab36823), IFNβ (ab140211), and CXCL11 (ab9955) (all from Abcam).

For PicoGreen staining, slides were deparaffinized and stained with PicoGreen and wheat germ agglutinin (WGA) for 1 h. The slides and cells were mounted with Fluoro-Gel (Electron Microscopy Sciences) and analyzed using a confocal microscope (Carl Zeiss).

9. Clinical significance in human breast cancer

9.1. Human tissue array

For immunohistochemistry or PLA assays of breast cancer tissues, tissue microarray slides (#T088c, US Biomax) were deparaffinized and processed for antigen retrieval. Slides were subjected to immunostaining using antibodies against γH2AX (#ab22551, Abcam) and NR1D1 (#14506-1-AP, Proteintech). Tissue microarray slides (#BR1201a, US Biomax) that contain most of TNBC tissue sections were subjected to immunostaining using antibodies against IFI16 (sc-8023, Santa Cruz Biotechnology) and 53BP1 (ab36823, Abcam). For PicoGreen staining, slides (#BC081116b, US Biomax) were subjected to staining with PicoGreen and WGA for 1 h. The stained slides were analyzed using a confocal microscope (Carl Zeiss).

9.2. Breast cancer patient cohort analysis based on public datasets

The public datasets, GSE4056, GSE34138, and GSE1456, were downloaded from NCBI Gene Expression Omnibus (GEO; http://www.ncbi.nlm.nih.gov/geo/) and the NKI dataset was obtained from a Web site provided by Dr. Bernards and his colleagues (http://ccb.nki.nl/data/). The GSE4056 dataset (DKFZ/Operon Human Oligo Set v2.1) contained the gene expression profiles of a 100-patient cohort, among which 44 patients in the validation set had received gemcitabine, epirubicin, and docetaxel as primary standard chemotherapy (Thuerigen et al., 2006). The GSE34138 dataset (HumanWG-6 v3.0 Expression BeadChip; Illumina, San Diego, CA, USA) contained the gene expression profiles of a 178-patient cohort treated with a single dose-dense doxorubicin and cyclophosphamide

chemotherapy regimen (de Ronde et al., 2013). The GSE1456 dataset (Affymetrix Human Genome U133A Array) contained the gene expression profiles of a 159-patient cohort who had mostly been treated with intravenous cyclophosphamide, methotrexate, and 5-fluorouracil as adjuvant chemotherapy (Pawitan et al., 2005). The NKI dataset (Agilent chip containing NKI annotated probes) included the gene expression profiles of a 295-patient cohort, among which 110 patients who received chemotherapy were selected for analysis (van de Vijver et al., 2002). Data that lacked expression signals in the microarrays or without clinical information records were excluded from all analyses. The processed data including normalization procedures were obtained from the corresponding websites and no additional transformations were performed.

10. Statistical analyses

Statistical analyses were performed using GraphPad Prism software. Experimental values were expressed as the mean ± standard deviation based on three independent experiments, unless indicated otherwise. Statistically significant differences between two groups were determined using the nonparametric Mann - Whitney *U* test. Statistical analyses of multiple groups were performed using two-way ANOVA followed by the Bonferroni posttest. $P < 0.05$ was considered significantly different. Flow cytometry results, laser microirradiation data, immunofluorescence data, immunoblots, *in situ* PLAs, FokI assays, clonogenic survival assays, and PicoGreen staining were taken from a representative experiment, which was qualitatively similar to at least three experiments.

Table 2. Oligonucleotide for gene deletion targeting by lentivirus

shRNA	Nucleotide sequence
shGFP	5′-GCAAGCTGACCCTGAAGTTCAT-3′
shNR1D1	5′-GGCATGGTGTTACTGTGTAAA-3′

Table 3. Primer sequences for qPCR

Gene	Accession number		Nucleotide sequence
NR1D1	NM_021724.5	Sense	5′-CAAGGCTGTCCCACCTACTT-3′
		Antisense	5′-ACGACGAGGAAGATGAGGAA-3′
CCL5	NM_001278736.2	Sense	5′-ATCCTCATTGCTACTGCCCTC-3′
		Antisense	5′-GCCACTGGTGTAGAAATACTCC-3′
CXCL11	NM_001302123.2 NM_005409.5	Sense	5′-TGCTACAGTTGTTCAAGGCTTCC-3′
		Antisense	5′-GGTACATTATGGAGGCTTTCTCAAT ATC-3′
b-actin	NM_001101.5	Sense	5′-CGTGGGCCGCCCTAGGCACCA-3′
		Antisense	5′-TTGGCTTAGGGTTCAGGGGGG-3′

Table 4. Primer sequences for ChIP assay

Target region		Nucleotide sequence
Fok I site	Sense	5′-TGTACGGTGGGAGGCCTATATAA-3′
	Antisense	5′-GCGTCTCCAGGCGATCTG-3′
I-*Sce*I site	Sense	5′-CCTGAAGATTTGGGGGATTGTGCTTC-3′
	Antisense	5′-CTTGGAAACACCCATGTTGAAATATC-3′

IV. RESULTS

1. Role of NR1D1 in DNA repair and chemosensitivity of breast cancer

1.1. NR1D1 inhibits DSB repair in various breast cancer cells

To examine the expression of NR1D1 in different breast cancer subtypes, I first analyzed two public patient datasets, TCGA and METABRIC breast cancer datasets (Ciriello et al., 2015, Pereira et al., 2016). The expression level of NR1D1 was higher in luminal B and HER2-positive subtypes compared with luminal A and TNBC subtypes. In addition, copy number alterations of NR1D1 displayed positive correlations with those of HER2 in these datasets (Figure 6), consistent with the previous reports (Chin et al., 2006, Davis et al., 2007).

To investigate the role of NR1D1 in DNA repair, I examined whether NR1D1 affected DNA repair after DSB using the plasmid-based NHEJ and HR reporter assays. Notably, NHEJ and HR efficiency were reduced when NR1D1 was transiently overexpressed in MCF7 cells (Figure 7A). Similar results were obtained in several different types of breast cancer cell lines, suggesting that NR1D1 disrupt the proper DNA repair process in breast cancer cells (Figure 7B). In addition, the mRNA level of NR1D1 and the NHEJ efficiency in these cell lines were negatively correlated (Figure 7C). Thus, I asked whether NR1D1

could alter the rate of recruitment of DDR factors to DSB sites. The cells that expressed NR1D1 were subjected to laser-microirradiation analysis using a live cell imaging system. The rate of recruitment and the intensity of RAP80 and H2AX were significantly lower at the damaged sites in the NR1D1-expressing cells compared with those in the control cells (Figure 8A). Next, I employed doxorubicin, a DNA intercalating agent that causes DSB, to analyze the clearance of γH2AX and 53BP1 foci. The number of γH2AX and 53BP1 foci, hallmarks of unrepaired DSBs, increased greatly after doxorubicin treatment but it disappeared with time after the removal of doxorubicin. However, both γH2AX and 53BP1 foci remained longer when NR1D1 was overexpressed, indicating a delayed DNA repair by NR1D1 (Figure 8B). These results indicate that NR1D1 impairs the correct DNA repair process.

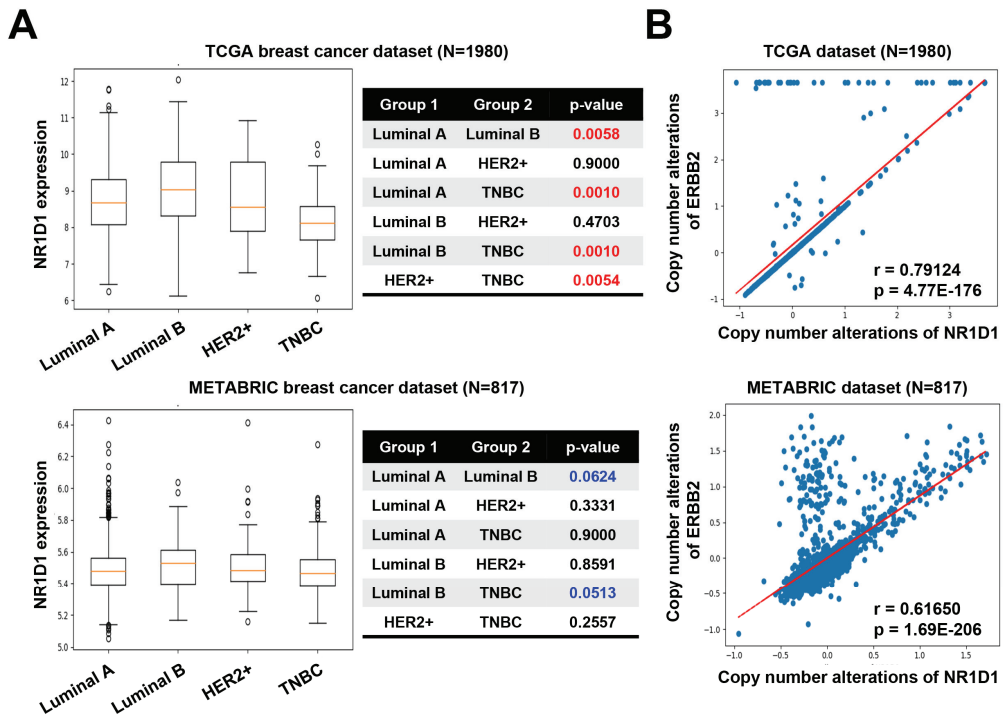

Figure 6. Expression of NR1D1 is higher in HER2-positive and luminal B subtypes compared with luminal A and TNBC subtypes

(A) Database-based gene expression analysis was conducted using TCGA and METABRIC breast cancer datasets (Ciriello et al., 2015, Pereira et al., 2016). The NR1D1 expression level was analyzed in different molecular subtypes of breast cancer.

(B) Copy number alterations of NR1D1 and ERBB2 were analyzed in TCGA and METABRIC breast cancer datasets.

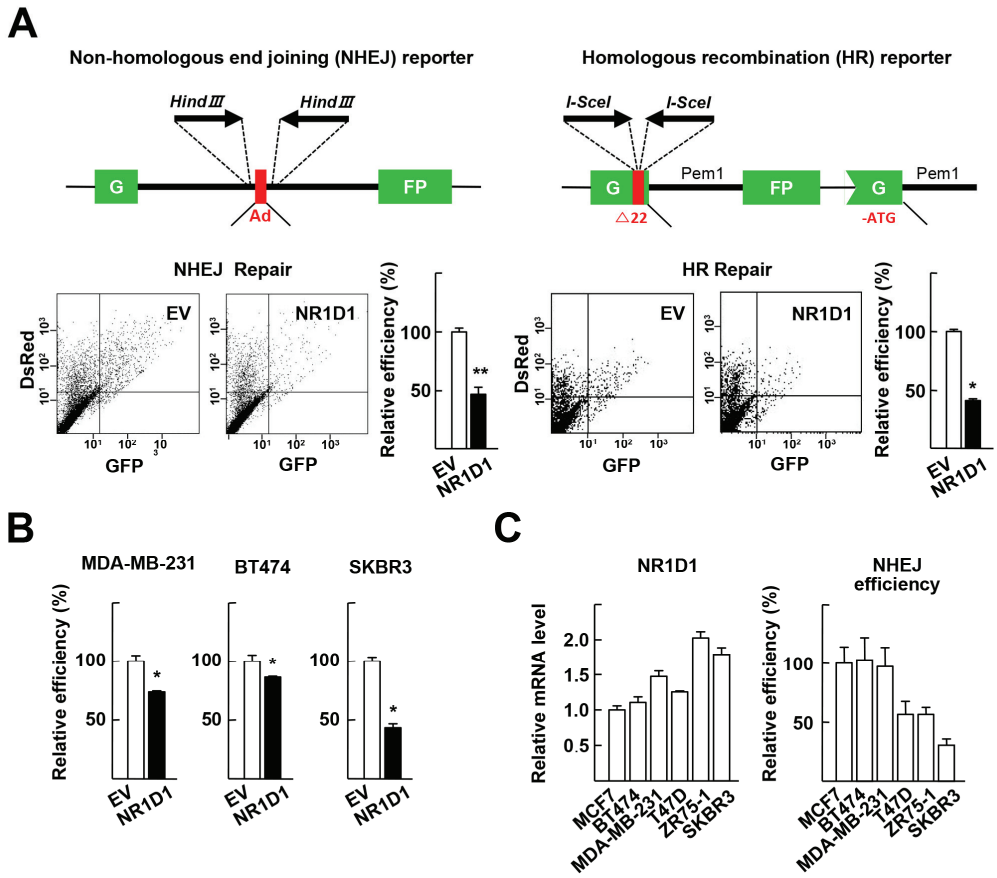

Figure 7. NR1D1 inhibits DSB repair efficiencies in various breast cancer cell lines

(A) Constructs of NHEJ and HR reporters (top). NHEJ or HR efficiency was measured in MCF7 cells that were cotransfected with the HindⅢ-linearized NHEJ or I-*Sce*I-linearized HR reporter plasmid, Ds-Red, and either empty vector (EV) or Myc-NR1D1. The ratio of number of GFP-positive cells *vs* that of DsRed-positive cells were determined by flow cytometry. The NHEJ or HR efficiency was normalized to that of EV-transfected samples (bottom). $*P < 0.05$ and $**P < 0.01$ *vs* EV (n=4).

(B) NHEJ efficiency was measured as described in panel (A) from the indicated cells. $*P < 0.05$ *vs* EV (n=3).

(C) Expression level of NR1D1 in the indicated cells was analyzed by qRT-PCR (left). NHEJ efficiency was measured as described in panel (A) (right) (n=3).

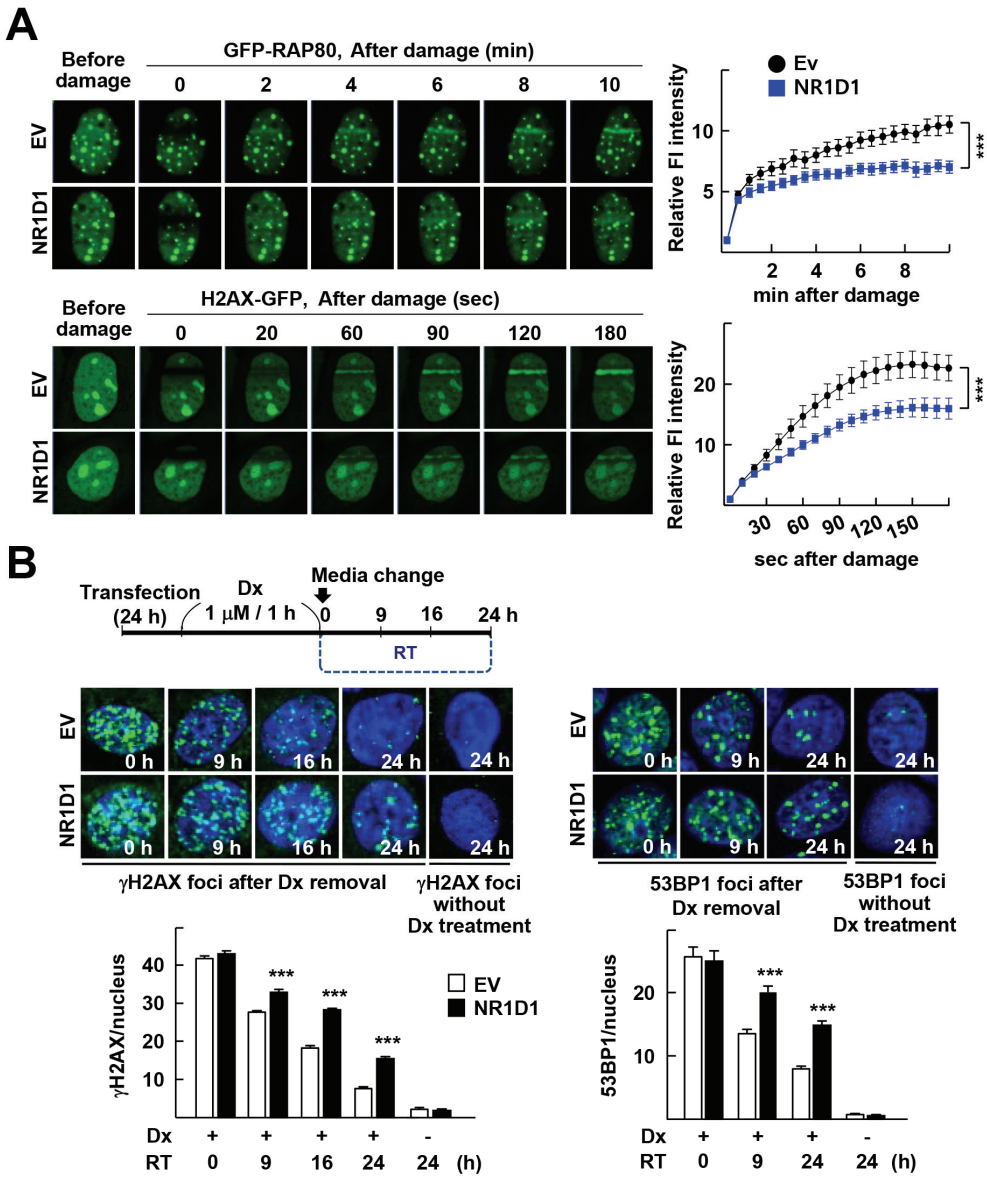
A
Before damage
GFP-RAP80, After damage (min)
0
2
4
6
8
10
EV
NR1D1
Ev
NR1D1
Relative FI intensity
10
5
2
4
6
8
min after damage
***
Before damage
H2AX-GFP, After damage (sec)
0
20
60
90
120
180
EV
NR1D1
Relative FI intensity
20
10
30
60
90
120
150
sec after damage
***
B
Transfection (24 h)
Dx 1 μM / 1 h
Media change
0
9
16
24 h
RT
EV
NR1D1
0 h
9 h
16 h
24 h
γH2AX foci after Dx removal
γH2AX foci without Dx treatment
γH2AX/nucleus
40
30
20
10
***
EV
NR1D1
Dx + + + + -
RT 0 9 16 24 24 (h)
53BP1 foci after Dx removal
53BP1 foci without Dx treatment
53BP1/nucleus
20
10
Dx + + + -
RT 0 9 24 24 (h)

Figure 8. NR1D1 delays DNA repair

(A) Laser microirradiation experiments were performed with MCF7 cells that stably expressing EV or Myc-NR1D1 after transfection of GFP-RAP80 or H2AX-GFP (left). The mean fluorescence (Fl) intensity at the microirradiated site was analyzed from 20 cells (right). $***P < 0.001$.

(B) Clearance of γH2AX and 53BP1 was monitored in MCF7 cells that transfected with EV or FLAG-NR1D1 and treated with 1 μM doxorubicin (Dx) for 1 h. Cells were fixed at the indicated recovery time (RT) points after Dx removal and immunostained with anti-γH2AX or anti-53BP1 antibody (green). Nuclei were visualized by DAPI staining (blue) (top). The numbers of γH2AX and 53BP1 foci were quantified from 50 cells (bottom). $***P < 0.001$ *vs* EV at each time point (n=3).

1.2. PARP1 interacts with NR1D1 and induces PARylation in response to DNA damage

Next, I asked the mechanism that allows the NR1D1-mediated inhibition of DSB repair. Because both NHEJ and HR repair were impaired by NR1D1, I hypothesized that NR1D1 may mediate the inhibition of DSB repair at the early stage of DDR. Since PARP1 functions in the initial steps of DDR by recognizing DNA breaks, I examined the potential interaction of NR1D1 with PARP1 (Sousa et al., 2012). Coimmunoprecipitation experiments demonstrated that both endogenous and FLAG-tagged NR1D1 interacted physically with PARP1 and this interaction was enhanced in response to DNA damage induced by doxorubicin (Figure 9A). Interestingly, the interaction between NR1D1 and PARP1 was also increased by treatment with GSK4112, a ligand of NR1D1, which was further enhanced by cotreatment of both doxorubicin and GSK4112 (Figure 9B). *In situ* PLA also confirmed the physical interaction of NR1D1 and PARP1 (Figure 9C). Domain mapping studies demonstrated that the ligand-binding domain (LBD) of NR1D1 and the DNA-binding domain of PARP1 were responsible for this interaction (Figure 10A and 10B). In agreement, deletion of NR1D1 LBD resulted in a loss of PLA signals, indicating that LBD of NR1D1 served as the binding site for PARP1 (Figure 10C).

PARP1 regulates the recruitment of various DDR proteins to DNA

breakage sites by catalyzing the attachment of PAR chains to target proteins, so we investigated whether NR1D1 was PARylated (Sousa et al., 2012). Interestingly, NR1D1 was PARylated and the PARylation was stronger under DNA damage induced by doxorubicin (Figure 11A). *In vitro* PARylation assay using recombinant NR1D1 and PARP1 proteins also confirmed the PARylation of NR1D1 (Figure 11B). Domain mapping studies demonstrated that the hinge domain of NR1D1 was PARylated (Figure 11C). Furthermore, the hinge domain deletion mutant (△Hinge), as well as the LBD deletion mutant (△LBD) that was unable to bind PARP1, were not PARylated (Figure 11D). The △Hinge and △LBD were less effective in inhibiting NHEJ and HR repair compared with the full-length NR1D1 (Figure 12). Thus, these observations strongly suggest that PARylation of NR1D1 is essential for the NR1D1-induced inhibition of DNA repair.

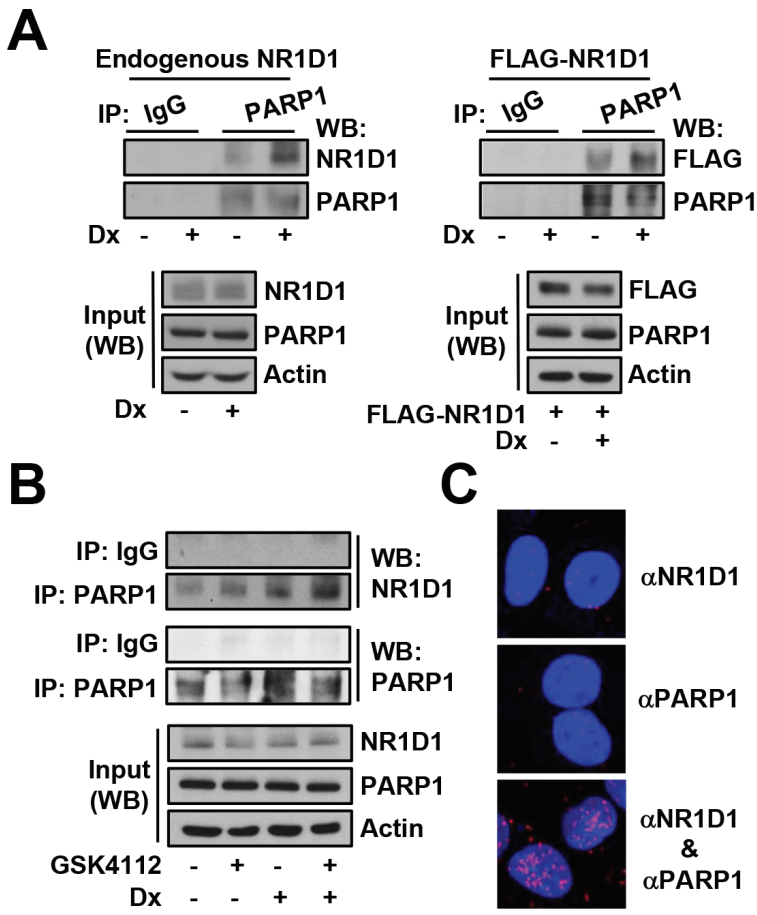

Figure 9. NR1D1 interacts with PARP1, which is enhanced in response to DNA damage

(A) Co-immunoprecipitation of NR1D1 and PARP1 was examined in MCF7 cells (left) or MCF7 cells that were transfected with FLAG-NR1D1 (right) after 0.5 μM doxorubicin (Dx) treatment for 4 h. Whole cell lysates were immunoprecipitated (IP) and probed by western blotting (WB).

(B) MCF7 cells were treated with 10 μM GSK4112 for 24 h and then treated with 0.5 μM doxorubicin for 4 h. Whole cell lysates were immunoprecipitated and probed by western blotting.

(C) MCF7 cells were subjected to *in situ* PLA. As a negative control, a single staining with the anti-NR1D1 or anti-PARP1 antibody was performed. Nuclei were stained by DAPI (blue).

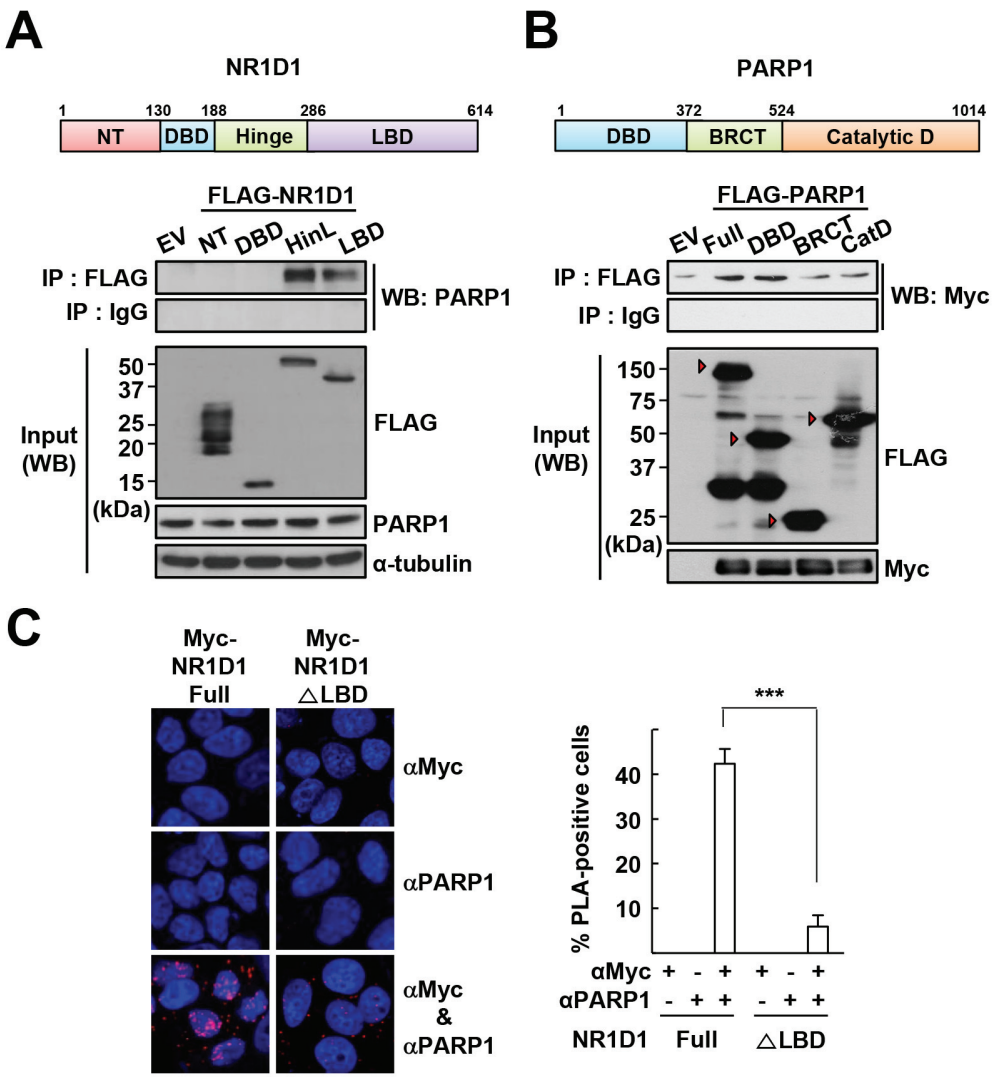
A
NR1D1
1
130
188
286
614
NT
DBD
Hinge
LBD
FLAG-NR1D1
EV
NT
DBD
HinL
LBD
IP : FLAG
IP : IgG
WB: PARP1
Input (WB)
50
37
25
20
15
(kDa)
FLAG
PARP1
α-tubulin
B
PARP1
1
372
524
1014
DBD
BRCT
Catalytic D
FLAG-PARP1
EV
Full
DBD
BRCT
CatD
IP : FLAG
IP : IgG
WB: Myc
Input (WB)
150
75
50
37
25
(kDa)
FLAG
Myc
C
Myc-NR1D1 Full
Myc-NR1D1 △LBD
αMyc
αPARP1
αMyc & αPARP1
***
% PLA-positive cells
40
30
20
10
αMyc + - + + - +
αPARP1 - + + - + +
NR1D1 Full △LBD

Figure 10. LBD of NR1D1 binds to PARP1

(A) MCF7 cells were transfected with FLAG-tagged N-terminus (NT), DNA-binding domain (DBD), hinge with LBD (HinL), or ligand-binding domain (LBD) of NR1D1, or empty vector (EV). Whole cell lysates were immunoprecipitated (IP) and probed by western blotting (WB).

(B) MCF7 cells were transfected with Myc-NR1D1 and FLAG-tagged full-length (Full), DBD, BRCA1 C-terminal domain (BRCT), or catalytic domain (CatD) of PARP1, or EV. Whole cell lysates were immunoprecipitated and probed by western blotting.

(C) MCF7 cells that were transfected with Myc-tagged full-length or LBD deletion mutant (△LBD) of NR1D1 were subjected to *in situ* PLA (left). The percentage of PLA-positive cells (>five nuclear spots) was quantified from 200 cells (right). $***P < 0.001$ (n=3).

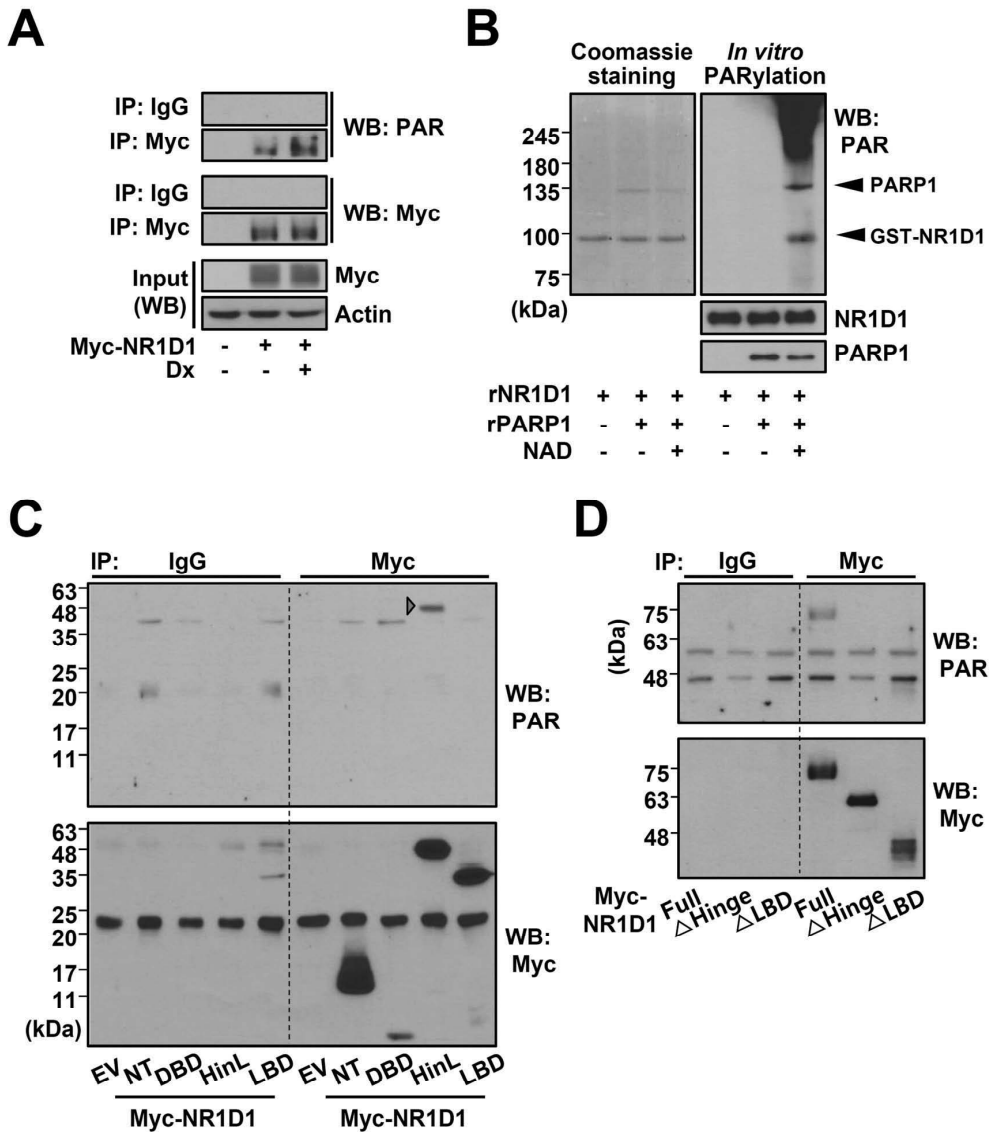
A
IP: IgG
IP: Myc
WB: PAR
IP: IgG
IP: Myc
WB: Myc
Input (WB)
Myc
Actin
Myc-NR1D1 - + +
Dx - - +
B
Coomassie staining
In vitro PARylation
245
180
135
100
75
(kDa)
WB: PAR
PARP1
GST-NR1D1
NR1D1
PARP1
rNR1D1 + + + + + +
rPARP1 - + + - + +
NAD - - + - - +
C
IP: IgG Myc
63
48
35
25
20
17
11
WB: PAR
63
48
35
25
20
17
11
(kDa)
WB: Myc
EV NT DBD HinL LBD EV NT DBD HinL LBD
Myc-NR1D1
Myc-NR1D1
D
IP: IgG Myc
(kDa)
75
63
48
WB: PAR
75
63
48
WB: Myc
Myc-NR1D1 Full △Hinge △LBD Full △Hinge △LBD

Figure 11. NR1D1 is PARylated by PARP1

(A) PARylation of NR1D1 was determined in the MCF7 cells that transfected with Myc-NR1D1 after 0.5 μM doxorubicin (Dx) treatment for 4 h. Whole cell lysates were immunoprecipitated (IP) and probed by western blotting (WB).

(B) *In vitro* PARylation assay was performed using the recombinant GST-PARP1 (rPARP1) and GST-NR1D1-His (rNR1D1) proteins. The reaction mixtures were stained with Coomassie (left) and immunoblotted using anti-PAR antibody (right).

(C) PARylation at the hinge domain of NR1D1. PARylation was determined as described in panel (A).

(D) Lack of PARylation in the hinge deletion mutant (△Hinge) or the LBD deletion mutant (△LBD) of NR1D1. PARylation was determined as described in panel (A).

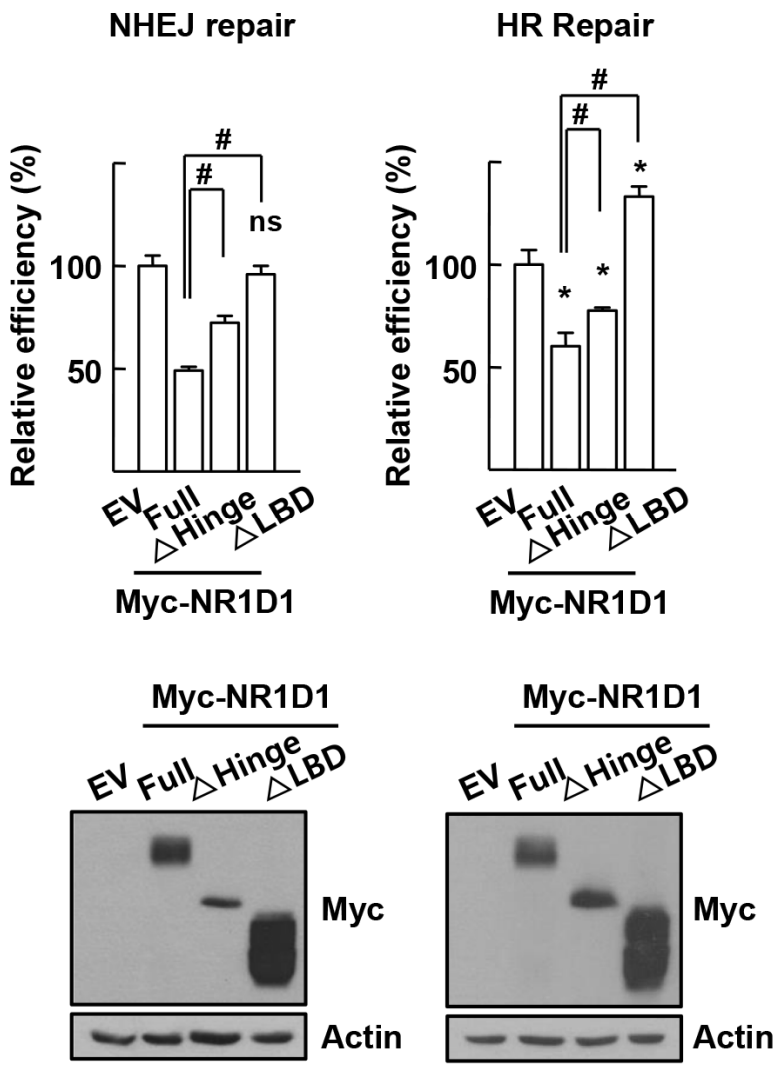

Figure 12. PARylation of NR1D1 is required for the inhibition of DNA repair

NHEJ and HR efficiency was determined in MCF7 cells that were cotransfected with the indicated constructs. $*P < 0.05$ and not significant (ns) *vs* EV; $^{\#}P < 0.05$ *vs* NR1D1 Full (n=4) (top). Expression level of NR1D1 was shown (bottom).

1.3. NR1D1 is recruited to DSB sites and then suppresses further recruitment of DDR factors

Since many DDR factors are PARylated to access DNA damage sites, I examined the possibility that PARylated NR1D1 is recruited to DNA breakage sites. I employed a DSB reporter system where single DSB is created by mCherry-Lac I -Fok I nuclease fusion protein in U2OS cells. Surprisingly, NR1D1 was co-localized with Fok I wild-type nuclease but not with the Fok I D450A mutant, which was unable to generate the DSB (Figure 13A). To confirm the recruitment of NR1D1 to DSB sites, I analyzed the recruitment of NR1D1 to the DSB sites generated by exogenously introduced I-*Sce* I on the NHEJ or HR reporter plasmid. ChIP analysis showed that NR1D1 was recruited to the DSB sites on both reporters at 24 h after I-*Sce* I transfection (Figure 13B). NR1D1 was also rapidly accumulated to the sites of DNA damage when examined by laser microirradiation analysis. However, in the presence of PARP1 inhibitor, PHEN, the NR1D1 recruitment was dramatically decreased. In addition, the △LBD was defective to access the damaged DNA (Figure 14A). Interestingly, NR1D1 formed nuclear foci following doxorubicin treatment, which were overlaid with γH2AX foci. In the presence of PHEN, however, the number of overlaid γH2AX/NR1D1 foci decreased mainly due to the disapperance of NR1D1 foci (Figure 14B). These results suggest that bnding to PARP1 and

subsequent PARylation is essential for the recruitment of NR1D1 to DNA breakage sites.

Recruitment of DDR factors such as γH2AX, PARP1, SIRT6, pNBS1, and BRCA1 peaked at 24 h after I-*Sce* I transfection in control cells, whereas most of the peaks were delayed until 36 h in the NR1D1-expressing cells. The overall amounts of DDR factors recruited to DSB sites were lower in the presence of NR1D1 (Figure 15). Taken together, these results show that NR1D1 is recruited to DNA damage sites in a PARP1-dependent manner and inhibits further recruitment of DDR complex.

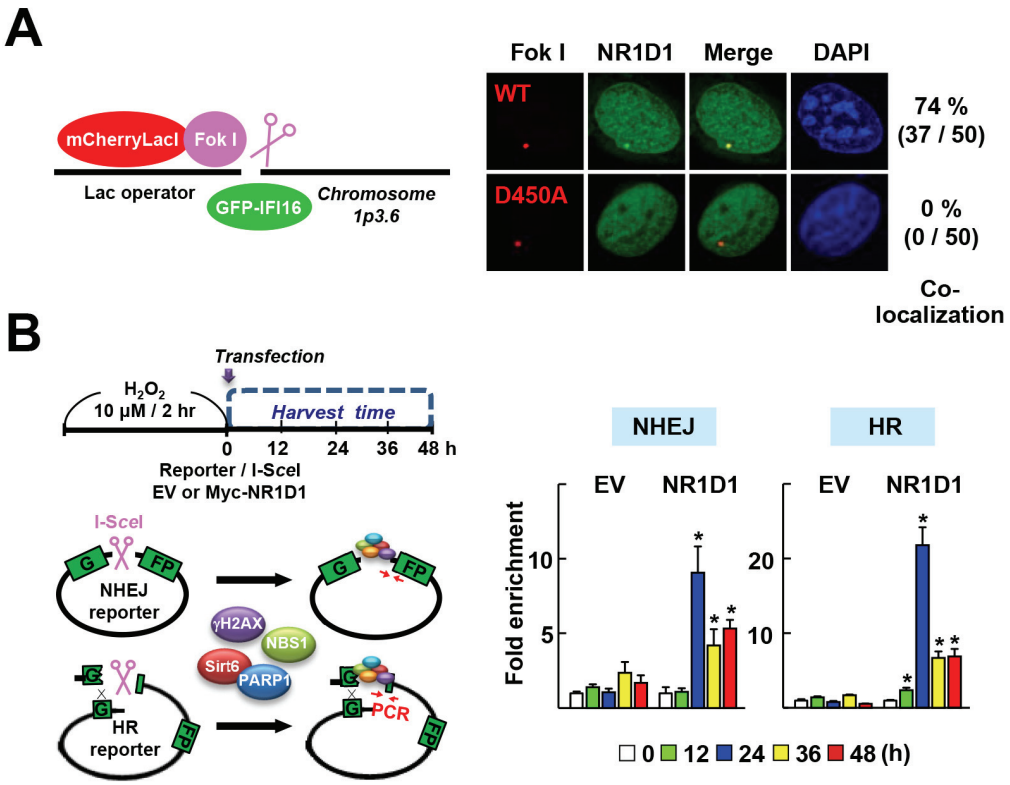

Figure 13. NR1D1 is recruited to DSB sites

(A) Schematic representation of Fok I assays (left). U2OS-DSB reporter cells were cotransfected with mCherry-LacI-FokI wild-type (WT) or nuclease-deficient mCherry-LacI-FokI (D450A) and GFP-NR1D1. After 48 h, cells were fixed and analyzed using confocal microscopy. The number of cells in which NR1D1 (green) was colocalized with FokI (red) was counted and presented as percentage of 50 FokI-positive cells.

(B) Schematic representation of ChIP assays (left). MCF7 cells were treated with 10 μM H_2O_2 for 2 h and then transfected with NHEJ or HR reporter plasmid, I-*Sce*I expressing vector, and empty vector (EV) or Myc-NR1D1. Cells were fixed at the indicated time and subjected to ChIP assays using anti-Myc. $*P < 0.05$ *vs* 0 h (n=3) (right).

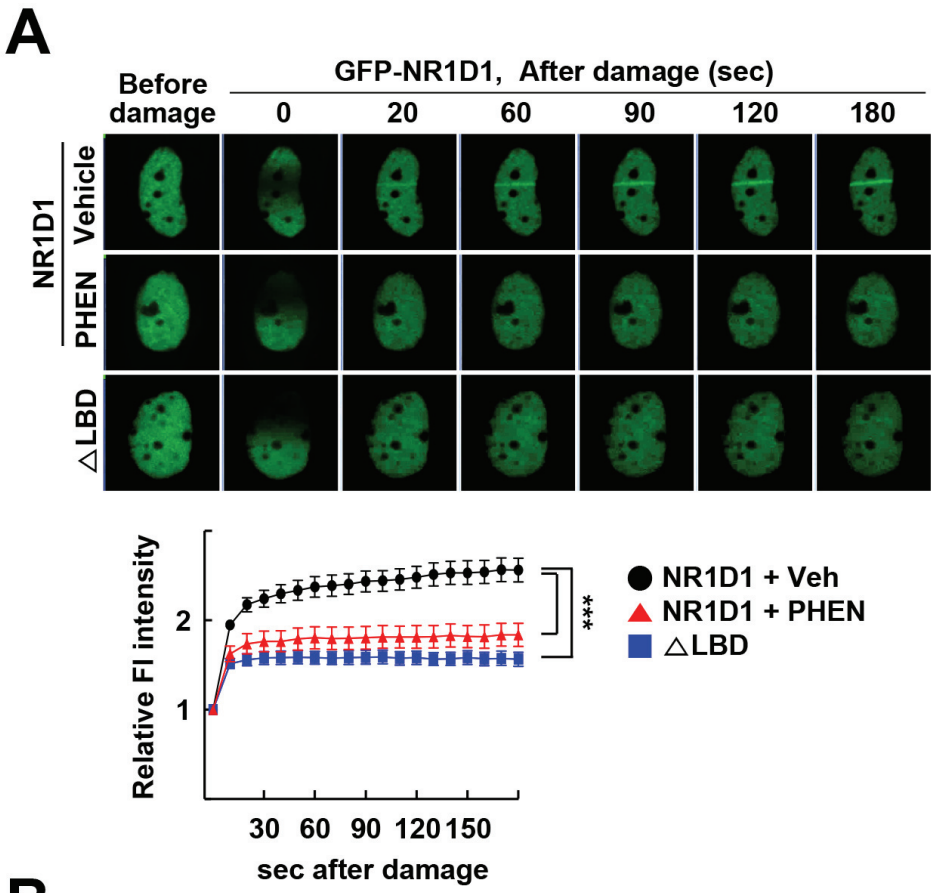
A
Before damage
GFP-NR1D1, After damage (sec)
0
20
60
90
120
180
NR1D1
Vehicle
PHEN
△LBD
Relative FI intensity
2
1
30 60 90 120 150
sec after damage
***
NR1D1 + Veh
NR1D1 + PHEN
△LBD

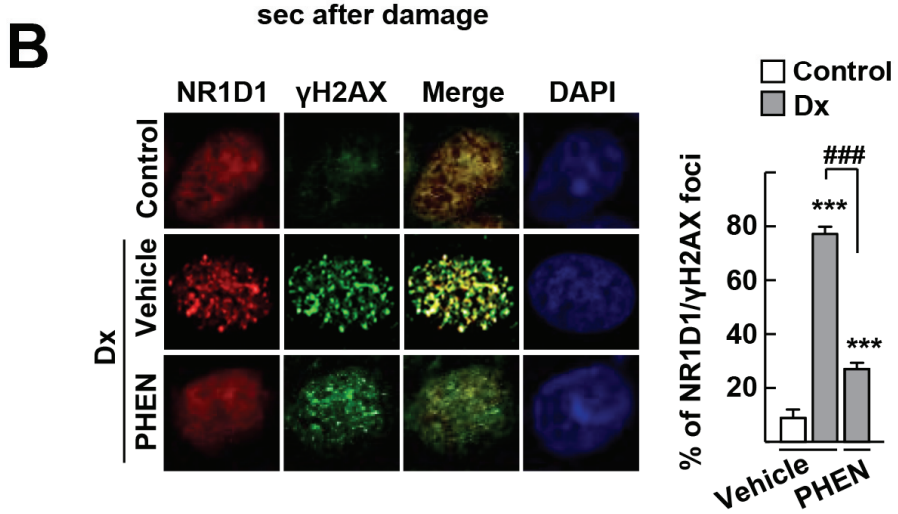
B
NR1D1
γH2AX
Merge
DAPI
Dx
Control
Vehicle
PHEN
Control
Dx
% of NR1D1/γH2AX foci
80
60
40
20
###
***
***
Vehicle
PHEN

Figure 14. Recruitment of NR1D1 to DSBs is dependent on PARP1

(A) Laser microirradiation experiments were performed with MCF7 cells transfected with GFP-fused NR1D1 or LBD deletion mutant (△LBD) in the presence or absence of 100 μM PHEN (top). The mean fluorescence (Fl) intensity at the microirradiated site was analyzed from 20 cells (bottom). $^{***}P < 0.001$ (n=3).

(B) MCF7 cells were treated with 1 μM doxorubicin (Dx) for 1 h in the presence of absence of 100 μM PHEN. Cells were fixed and immunostained with anti-NR1D1 (red) and anti-γH2AX antibody (green) (left). The number of γH2AX-positive foci that were also NR1D1-positive was quantified and presented as percentage of the number of total γH2AX-positive foci from 50 cells (right). $^{***}P < 0.001$ *vs* no treatment (control) and $^{\#\#\#}P < 0.001$ *vs* doxorubicin with vehicle (n=3).

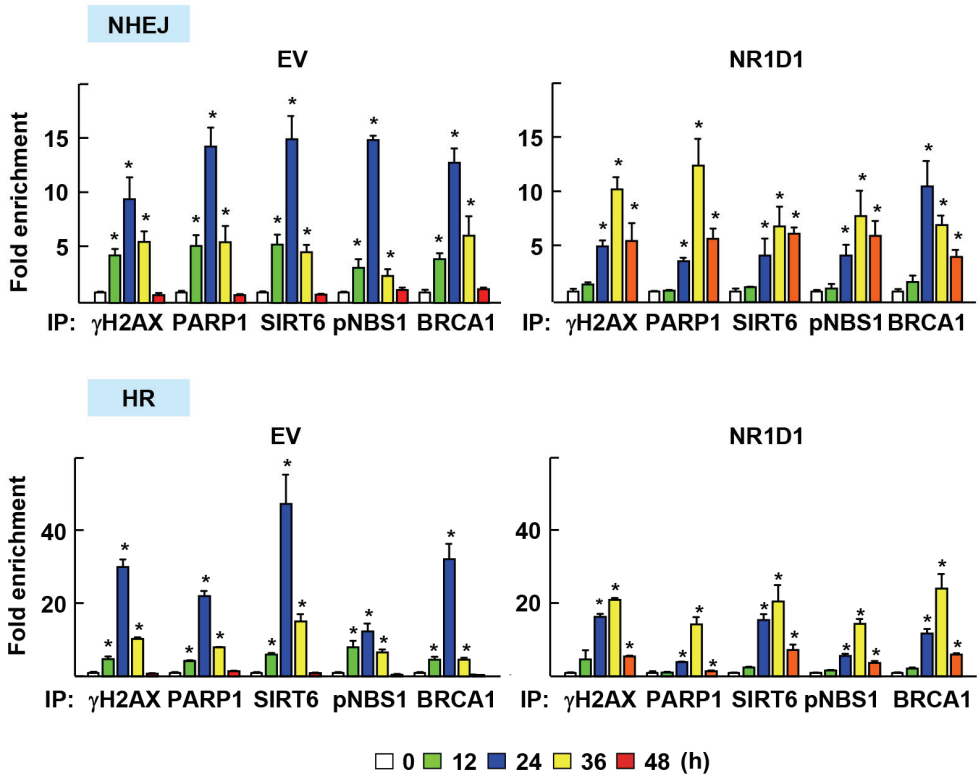

Figure 15. NR1D1 inhibits further recruitment of DDR factors to DSB sites

MCF7 cells were treated with 10 μM H_2O_2 for 2 h and then transfected with NHEJ or HR reporter plasmid, I-*Sce*I expressing vector, and empty vector (EV) or Myc-NR1D1. Cells were fixed at the indicated time and subjected to ChIP assays using specific antibodies as indicated. $*P < 0.05$ *vs* 0 h (n=3).

1.4. NR1D1 increases the sensitivity of breast cancer cells to DSB-inducing chemotherapeutic agents

Since DNA repair deficiency in cancer cells sensitizes them to DNA damaging agents, I determined whether NR1D1 makes cells sensitive to DNA damage-inducing chemotherapeutic agents. First, two stable MCF7 sublines in which NR1D1 expression was suppressed were established using the lentiviral delivery shRNA system (Figure 16A). To confirm the effect of NR1D1 on DNA repair, formation of γH2AX foci was examined in the shGFP control and shNR1D1-MCF7 cells. The number of γH2AX foci was increased by doxorubicin treatment in both cell lines, however, it decreased more rapidly in the shNR1D1-MCF7 than shGFP control cells, supporting that NR1D1 delays the DNA repair (Figure 16B). In agreement, shNR1D1-MCF7 cells were less sensitive to DSB-inducing agents, doxorubicin and etoposide, which are commonly used chemotherapeutics to treat breast cancer patients (Figure 17A). Doxorubicin-induced inhibition of clonal growth were significantly lower in shNR1D1 cells (Figure 17B). To investigate the effect of NR1D1 in the tumor microenvironment, three-dimensional (3D) culture was used. Cells were cultured in matrigel and the cellular sensitivity to doxorubicin was assessed by using MTT assay. Result shows that shNR1D1 cells were less sensitive to doxorubicin than shGFP control cells (Figure 17C). Importantly, GSK4112, an

NR1D1 agonist, increased the sensitivity to doxorubicin-induced suppression of cell survival in diverse culture systems (Figure 18A and 18B). This chemosensitizing effect of GSK4112 was also supported by clonal growth inhibition in shGFP control cells, but not in the shNR1D1 cells (Figure 18C).

To investigate the effect of NR1D1 on the *in vivo* susceptibility to doxorubicin, I injected the shRNA-MCF7 stable cell lines into athymic nude mice and monitored tumor growth. Tumor growth in shGFP control cells was significantly inhibited by doxorubicin treatment, whereas that in shNR1D1-MCF7 cells was not affected (Figure 19A). Immunohistochemical analysis of tumor tissues showed that the level of γH2AX, a marker of DSBs, increased greatly in the doxorubicin-treated shGFP control group, but not in the shNR1D1-MCF7 group (Figure 19B). Furthermore, PLA assay clearly showed the binding of NR1D1 with PARP1 in the specimens from the xenografted shGFP-MCF7 cells that were treated with doxorubicin (Figure 19C). Taken together, these results indicate that NR1D1 increases the sensitivity of breast cancer cells to chemotherapeutic agents by suppressing DNA repair.

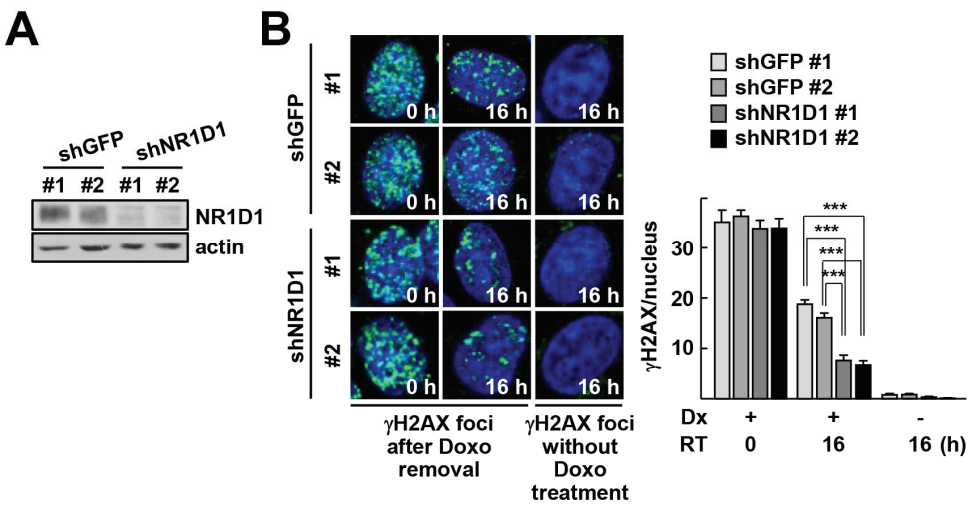

Figure 16. Establishment of the MCF7 stable cell lines expressing shGFP or shNR1D1

(A) Expression level of NR1D1 from the indicated cell lines was analyzed by western blotting.

(B) Clearance of γH2AX was monitored in the MCF7 stable cell lines that expressing shGFP or shNR1D1 after 1 μM doxorubicin (Dx) treatment for 1 h. Cells were fixed at 16 h after removal of doxorubicin and immunostained with anti-γH2AX antibody (green) (left). The numbers of γH2AX foci were quantified from 50 cells (right). $***P < 0.001$ (n=3).

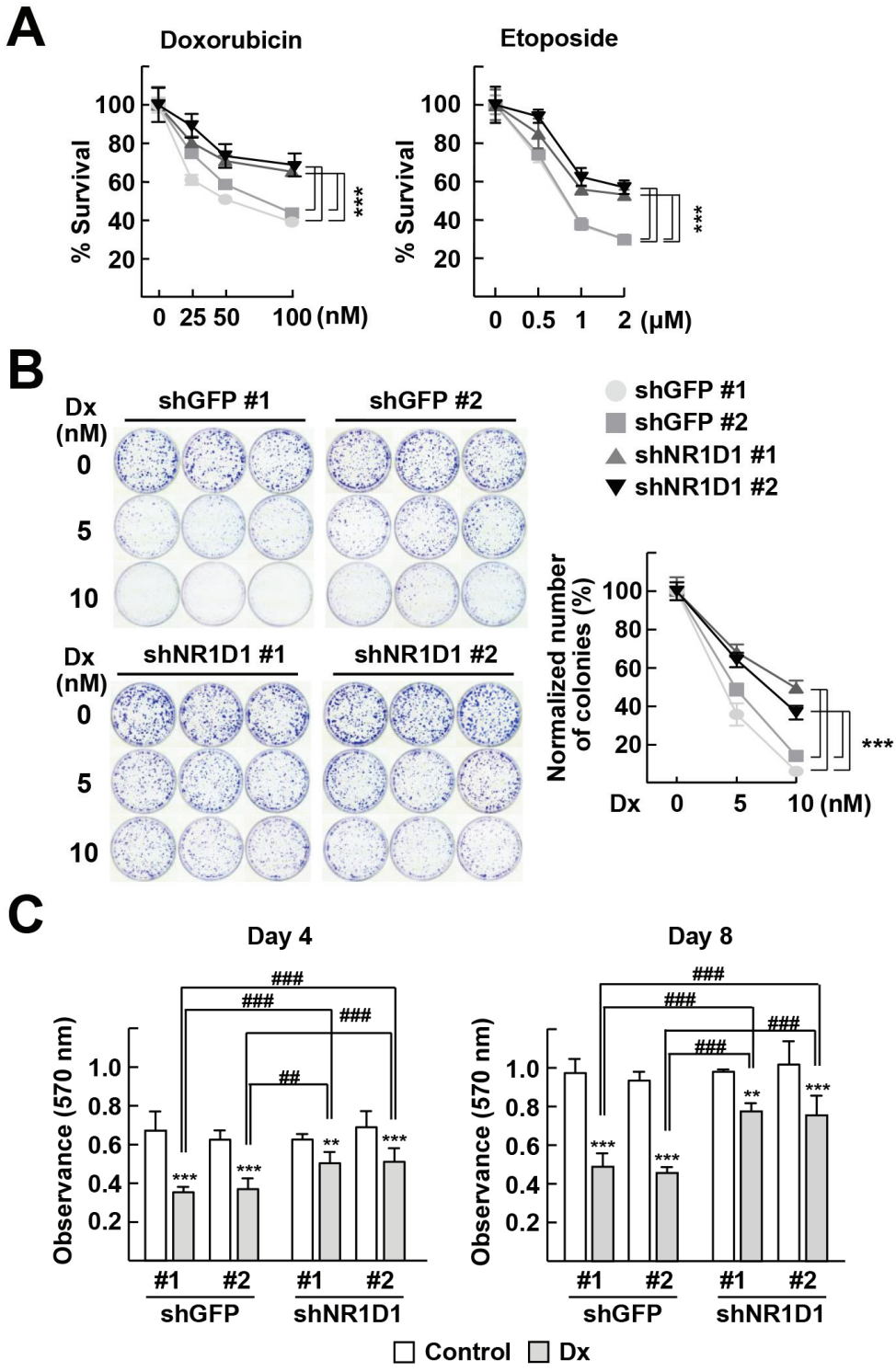
A
Doxorubicin
Etoposide
% Survival
100
80
60
40
20
0 25 50 100 (nM)
0 0.5 1 2 (μM)
***
B
Dx (nM)
shGFP #1
shGFP #2
shNR1D1 #1
shNR1D1 #2
0
5
10
Normalized number of colonies (%)
Dx 0 5 10 (nM)
C
Day 4
Day 8
Observance (570 nm)
1.0
0.8
0.6
0.4
0.2
###
##
**
#1 #2 #1 #2
shGFP shNR1D1
Control Dx

Figure 17. Lack of NR1D1 decreases sensitivity to DSB-inducing chemotherapeutic agents

(A) The MCF7-shGFP and -shNR1D1 cells were exposed to doxorubicin or etoposide for 72 h. Relative cell viability was analyzed using MTT assay. $^{***}P < 0.001$ (n=3).

(B) The MCF7 stable cells were exposed to doxorubicin (Dx) for 14 days, and clonogenic survival assays were performed. Images are representative of those obtained from three independent experiments (left). The number of colonies that composed of more than 50 cells was counted (right). $^{***}P < 0.001$ (n=3).

(C) The MCF7 stable cells were mixed with matrigel were seeded on top of matrigel-coated plates. A medium containing 1 μM doxorubicin was overlaid on the top of the gel. After the indicated days of incubation, relative cell viability was analyzed using MTT assay. $^{**}P < 0.01$ and $^{***}P < 0.001$ *vs* no treatment (control); $^{\#\#}P < 0.01$ and $^{\#\#\#}P < 0.001$ *vs* doxorubicin (n=3).

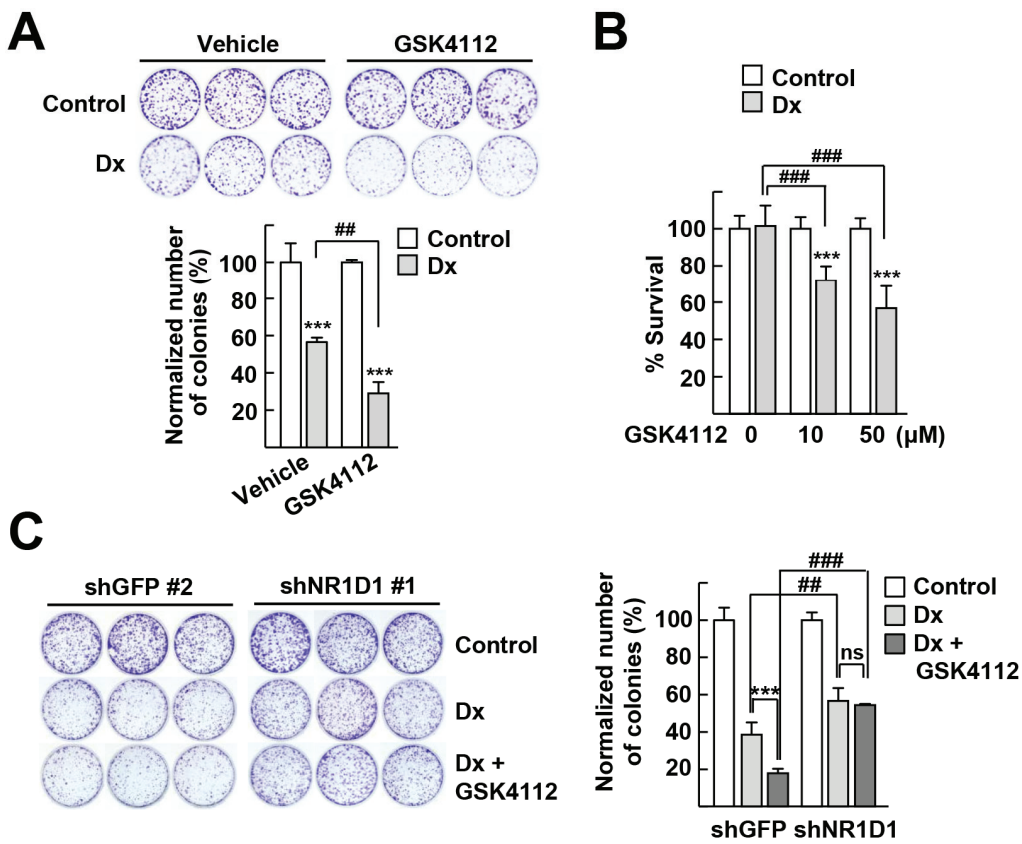

Figure 18. NR1D1 agonist, GSK4112, increases the sensitivity to doxorubicin

(A) MCF7 cells were exposed to 5 nM doxorubicin (Dx) and/or 5 μM GSK4112 for 14 days (top). Colonies that composed of more than 50 cells were counted (bottom). $^{***}P < 0.001$; $^{\#\#}P < 0.01$ and $^{\#\#\#}P < 0.001$ (n=3).

(B) MCF7 cells cultured in 3D matrigel were exposed to doxorubicin and/or GSK4112 for 8 days. Cell viability was analyzed using MTT assay. $^{***}P < 0.001$ *vs* doxorubicin; $^{\#\#\#}P < 0.001$ as indicated (n=3).

(C) The MCF7 stable cells were exposed to 5 nM doxorubicin and/or 5 μM GSK4112 for 14 days (left). Colonies that composed of more than 50 cells were counted (right). $^{***}P < 0.001$ and not significant (ns) *vs* doxorubicin; $^{\#\#}P < 0.01$ and $^{\#\#\#}P < 0.001$ (n=3).

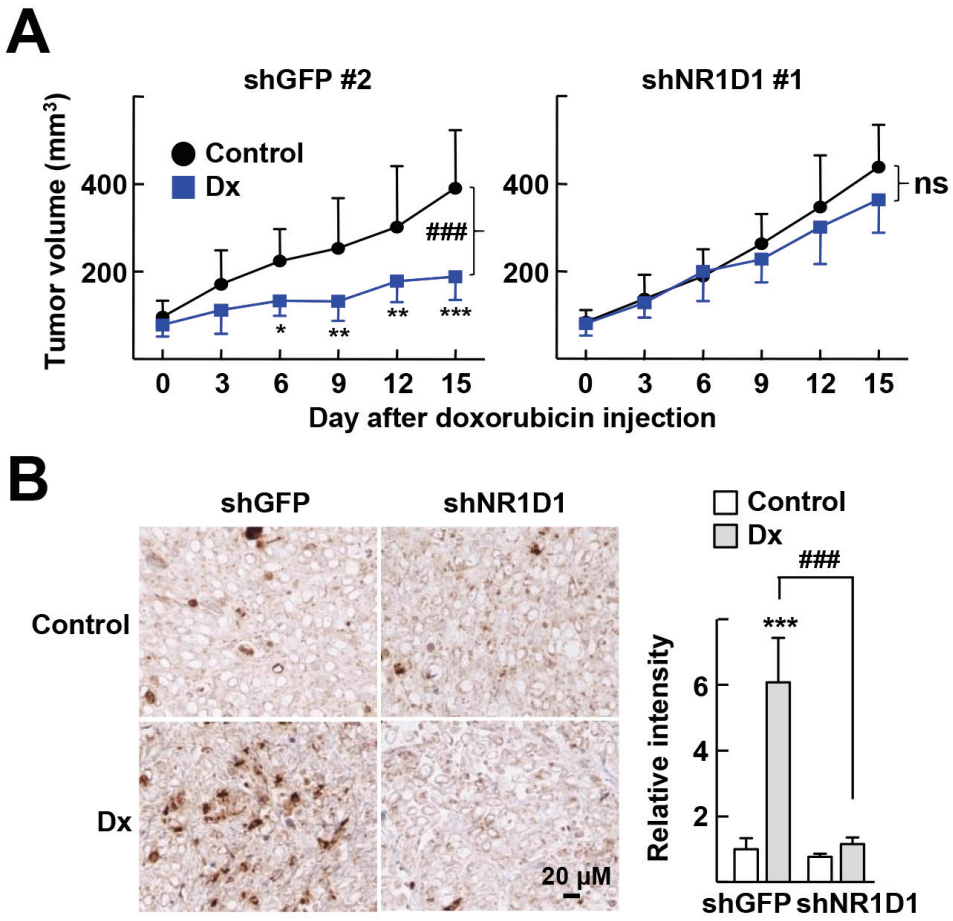
A
shGFP #2
shNR1D1 #1
Tumor volume (mm³)
Control
Dx
400
200
###
ns
*
**
**
***
0 3 6 9 12 15
Day after doxorubicin injection
B
shGFP
shNR1D1
Control
Dx
20 μM
Control
Dx
###
***
Relative intensity
6
4
2
shGFP shNR1D1
C
PLA
DAPI
Merge
αNR1D1
10 μM
αPARP1
αNR1D1
&
αPARP1

Figure 19. Lack of NR1D1 decreases sensitivity to doxorubicin *in vivo*

(A) Female athymic nude mice were injected subcutaneously with the MCF7 stable cells. When tumors were approximately 100 mm^3, mice were given intraperitoneal injections with doxorubicin at a dose of 4 mg/kg at 4-days interval, with a total of 3 injections. Tumor volume was measured with a caliper. The number of specimen of each group was as follow: shGFP-control (n=14), shGFP-doxorubicin (n=12), shNR1D1-control (n=8) and shNR1D1-doxorubicin (n=8). $*P < 0.05$, $**P < 0.01$ and $***P < 0.001$ vs control at the indicated time; $^{###}P < 0.001$ vs control.

(B) Immunohistochemistry staining for γH2AX in tumor sections (left). Immunohistochemistry staining was quantified in three random fields per section by densitometric analysis using ImageJ software (right). $***P < 0.001$ *vs* control, $^{###}P < 0.001$ *vs* doxorubicin in shGFP tumors.

(C) PLA was performed in tumor sections with anti-NR1D1 and anti-PARP1 antibodies. As a negative control, a single staining with the anti-NR1D1 or anti-PARP1 was shown. Nuclei were stained by DAPI.

1.5. High NR1D1 expression is correlated with an improved clinical outcome in breast cancer patients

Since NR1D1 modulated the chemosensitivity of breast cancer cells in both *in vitro* and *in vivo* experiments, I determined whether intratumoral NR1D1 expression is associated with the response to chemotherapy in breast cancer patients. I analyzed the gene expression profiles obtained from public datasets, which included clinical outcome information such as pathological complete response (pCR), disease-free survival (DFS), and relapse-free survival (RFS). In two independent datasets, GSE4056 and GSE34138, the groups of patients with high NR1D1 expression levels had higher pCR rates (Thuerigen et al., 2006, de Ronde et al., 2013). The odds ratio was 3.75 for GSE4056 and 2.11 for GSE34138, thereby indicating a positive correlation between the intratumoral NR1D1 expression level and a better clinical outcome in breast cancer patients (Table 5). In agreement, the NR1D1 expression levels were higher in the achieved pCR group than in the nonachieved pCR group, with statistical or marginal significance in these datasets (Figure 20A). In addition, I analyzed the survival rates in breast cancer patients using the Kaplan-Meier method with the log-rank test in two independent datasets, GSE1456 and NKI (Pawitan et al., 2005, van de Vijver et al., 2002). DFS or RFS was improved in the high NR1D1 expression group compared with that in low NR1D1 expression group, which

indicates a beneficial effect on recurrence in patients with hgh NR1D1 expression levels (Figure 20B). Overall, these findings suggest that breast cancer patients with high intratumoral NR1D1 expression are moe sensitive to chemotherapy. Lastly, I observed the co-localization of NR1D1 with γH2AX and the specific interaction of NR1D1 with PARP1 in human breast cancer specimens, which is probably associated with chemosensitivity of breast cancer cells (Figure 21A and 21B).

Table 5. Increased therapeutic response in breast cancer patients with high NR1D1 expression[a]

Data set	NR1D1 expression[b]	Non-pCR	pCR	p-value	Odd ratio of pCR[c] (95% CI)
GSE4056 (test set)	low	20 (90.9%)	2 (9.1%)	0.2404	3.75 (0.6647~21.1546)
	high	16 (72.7%)	6 (27.3%)		
GSE34138	low	67 (75.3%)	22 (24.7%)	0.0254	2.1084 (1.1092~4.0077)
	high	52 (59.1%)	36 (40.9%)		

[a] The GSE4056 and GSE34138 datasets that have therapeutic response information were obtained from NCBI GEO site.

[b] Patients were categorized into a low (below median) NR1D1 expression group and a high (above median) NR1D1 expression group. The expression levels of NR1D1 in individual patient in each NR1D1 low and high group and their median values were shown in Figure 20A.

[c] The Fisher's exact probability test was performed for determination of significance by a web-based program (http://vassarstats.net/). CI, confidence interval.

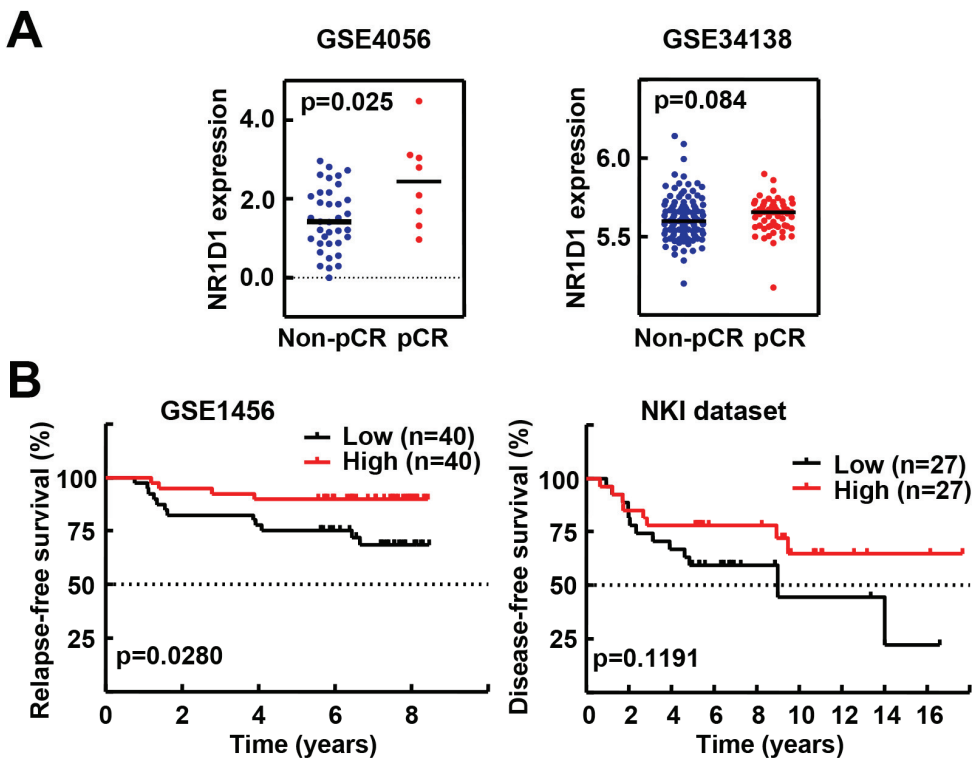

Figure 20. High NR1D1 expression is correlated with an improved clinical outcome in breast cancer patients received chemotherapy

(A) Expression level of NR1D1 was higher in pCR group of breast cancer. The GSE4056 and GSE34138 datasets were obtained from NCBI GEO site (Thuerigen et al. 2006, de Ronde et al. 2013). Scattered dot plots show NR1D1 expression level in Non-pCR group and in pCR group. Bars indicate the median NR1D1 expression level in each group. Statistical significance was analyzed by Mann-Whitney *U* test.

(B) The GSE1456 and the NKI data sets were obtained from NCBI GEO site and a web site provided by Dr. Bernards and his colleagues, respectively. Patients were categorized into a low (lower quartile) NR1D1 expression group and a high (upper quartile) NR1D1 expression group. DFS or RFS rate (%) was plotted for each group. To analyze statistical differences, Log-rank (Mantel-Cox) tests were performed.

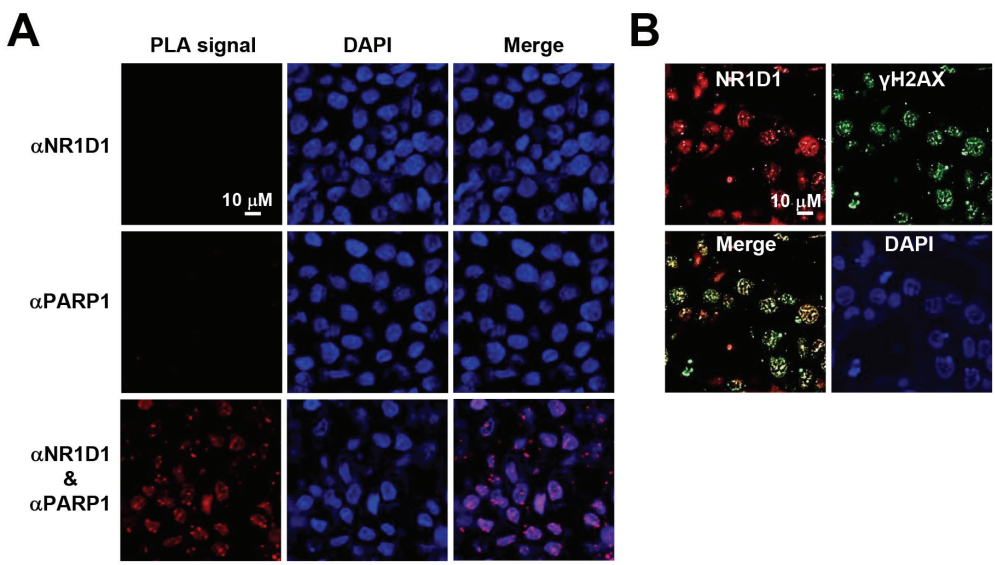

Figure 21. Clinical significance of NR1D1 in breast cancer

(A) PLA was performed in breast cancer specimens with anti-NR1D1 and anti-PARP1 antibodies. As a negative control, a single staining with the anti-NR1D1 or anti-PARP1 was performed. Nuclei were stained by DAPI (blue). (B) Co-localization of NR1D1 and γH2AX. Breast cancer specimens were immunostained with anti-NR1D1 (red) and anti-γH2AX (green).

2. Role of IFI16 in DNA repair and amplification of type I IFN signaling in TNBC

2.1. Type I IFNs and chemotherapeutic agents increase the expression of IFI16 in TNBC cells

According to the previous finding that IFI16 expression was higher in ERα-negative than ERα-positive breast carcinomas (Kang et al., 2014). I first examined the IFN inducibility of IFI16 in different subtypes of breast cancer cell lines. Interestingly, IFNα and IFNβ dramatically induced the expression of IFI16 only in TNBC cells, but not in other types of cells (Figure 22A). To examine the role of IFI16 in DNA damage response, I employed several DNA damaging agents, *i.e.*, doxorubicin, 5-FU, and cisplatin, which are commonly used chemotherapies to treat patients with TNBC (Wahba and El-Hadaad, 2015). The expression of IFI16 increased in response to these drugs in a dose-dependent manner in various TNBC cells (Figure 22B). The doxorubicin-induced expression of IFI16 was increased further by cotreatment with IFNα or IFNβ, suggesting that IFI16 may play a role in DNA damage response and type I IFN signaling (Figure 22C).

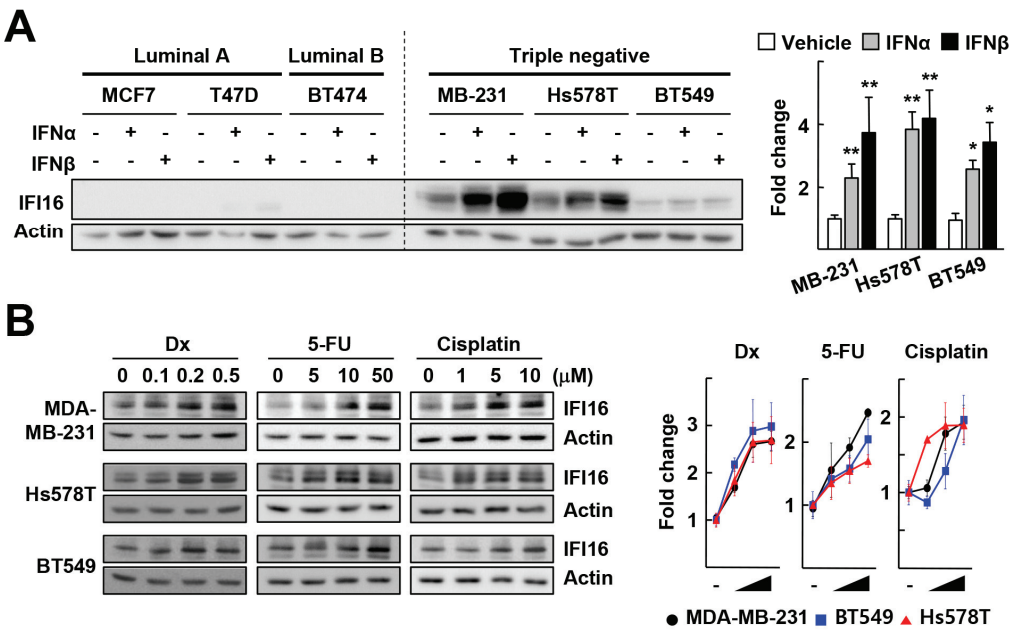
A
Luminal A
Luminal B
Triple negative
MCF7
T47D
BT474
MB-231
Hs578T
BT549
IFNα
IFNβ
IFI16
Actin
Vehicle
IFNα
IFNβ
Fold change
MB-231
Hs578T
BT549
B
Dx
5-FU
Cisplatin
0 0.1 0.2 0.5
0 5 10 50
0 1 5 10 (μM)
MDA-MB-231
Hs578T
BT549
IFI16
Actin
Fold change
MDA-MB-231
BT549
Hs578T
C
IFN
10
100 (IU/ml)
Dx
IFNα
IFNβ
IFNγ
IFI16
Actin
Fold change
Vehicle
IFN 10 U/ml
IFN 100 U/ml

Figure 22. Type 1 IFNs and chemotherapeutic agents induce the expression of IFI16

(A) MCF7, T47D, BT474, MDA-MB-231 (MB-231), Hs578T, and BT549 cells were treated with 100 IU/ml IFN for 16 h. Expression level of IFI16 was analyzed by western blotting (left). Band intensity was quantified using ImageJ and normalized to that of Actin band (right). $*P < 0.05$ and $**P < 0.01$ *vs* vehicle (n=4).

(B) Breast cancer cells were treated with doxorubicin (Dx), 5-FU, or cisplatin for 16 h. Expression level of IFI16 was analyzed by western blotting (left). Band intensity was quantified using ImageJ and normalized to that of Actin band (right) (n=3).

(C) MDA-MB-231 cells were treated with 0.5 μM doxorubicin and/or IFNs for 16 h. Expression level of IFI16 was analyzed by western blotting (left). Band intensity was quantified using ImageJ and normalized to that of Actin band (right) (n=3).

2.2. IFI16 inhibits DNA repair by impairing the ATM-mediated DDR signaling

Given that IFI16 was induced in response to DNA damage, I examined whether IFI16 is involved in DNA repair process. Notably, I found that IFNα and IFNβ, but not IFNγ, inhibited both NHEJ and HR efficiency (Figure 23). To investigate the involvement of IFI16 on the type I IFN-induced inhibition of DNA repair, we established IFI16 knockout (KO) cell lines using the CRISPR/Cas9 system (Figure 24A). The DSB repair inhibitory effects were blunted when IFI16 was depleted (Figure 24B). In agreement, both NHEJ and HR efficiency were reduced when IFI16 was transiently overexpressed in MDA-MB-231 cells (Figure 24C).

Since IFI16 inhibited both NHEJ and HR efficiency, I hypothesized that IFI16 may act during the early stages of DSB repair. The MRN complex, consisting of the Mre11, Rad50, and Nbs1 protein, is one of the first factors recognizing DSB and plays an essential role in processing of DSBs (Williams et al., 2007). I found that IFI16 interacted with MRN components and these interactions were enhanced in response to the doxorubicin treatment (Figure 25A). ChIP analysis showed that IFI16 inhibited the recruitment of ATM as well as its downstream targets, including γH2AX and MDC1, to DSB sites (Figure 25B). In agreement, DSB-induced phosphorylation of ATM and its downstream

substrates was attenuated when IFI16 was transiently overexpressed (Figure 25C). In contrast, depletion of IFI16 further enhanced the ATM activation in response to DSBs (Figure 25D). Taken together, these results show that IFI16 physically interacts with MRN complex, and it inhibits further recruitment of DDR proteins and impairs proper DNA repair process.

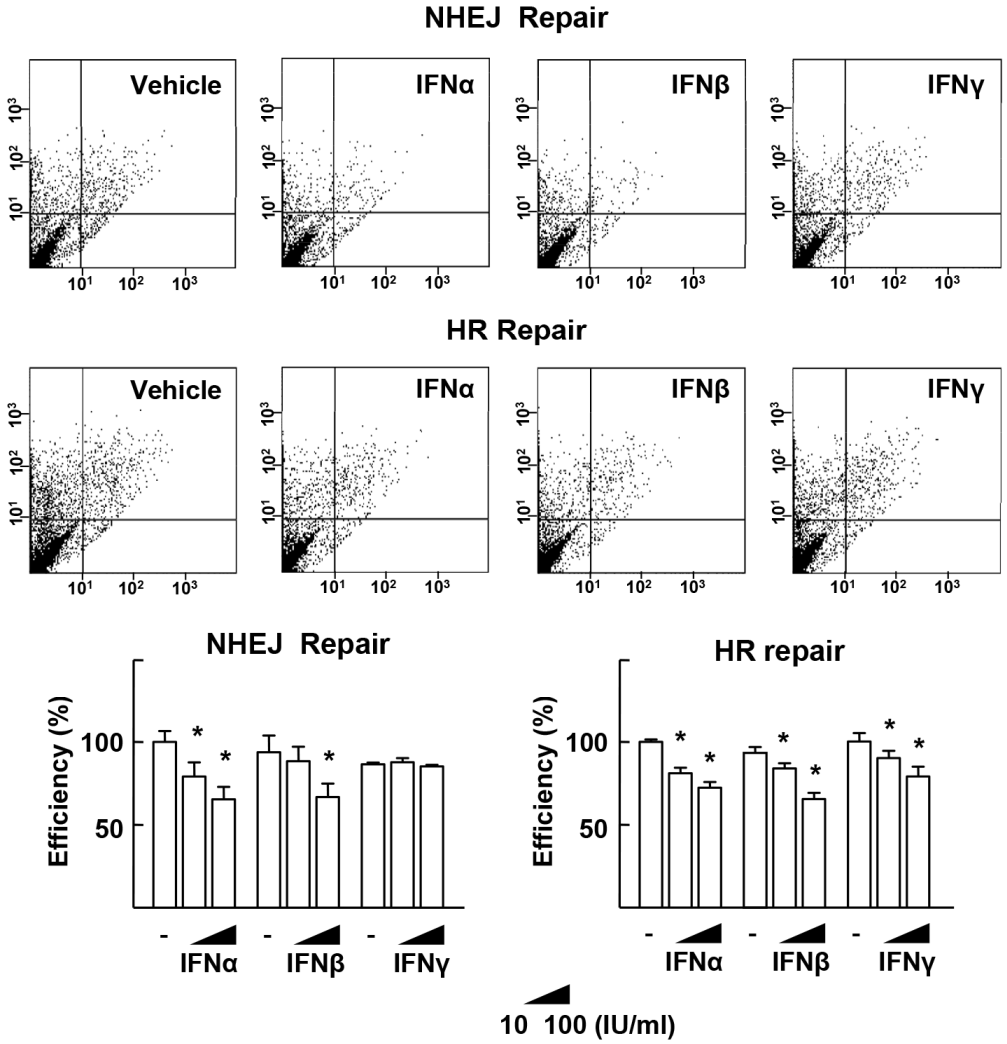

Figure 23. Type 1 IFNs inhibit DSB repair

MDA-MB-231 cells were cotransfected with the *Hind*Ⅲ-linearized NHEJ or I-*Sce*I-linearized HR reporter plasmid with Ds-Red, and then treated with IFNs. After 48 h, the ratio of number of GFP-positive cells *vs* that of DsRed-positive cells were determined by flow cytometry. Representative dot plots of 100 IU/ml IFN-treated samples are shown (top). The NHEJ or HR efficiency was normalized to that of vehicle-treated samples (bottom). $*P < 0.05$ *vs* vehicle (n=3).

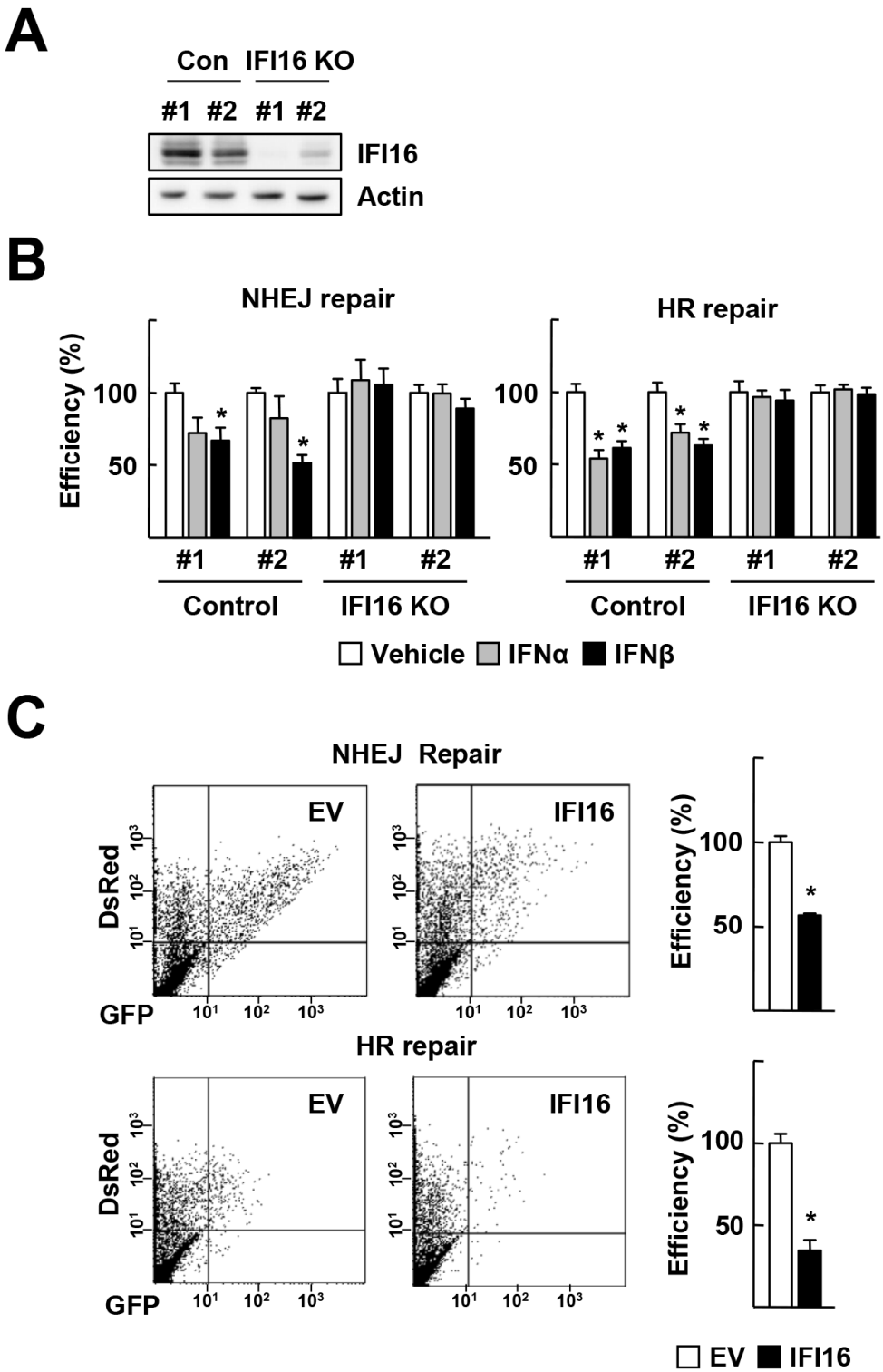
A
Con
IFI16 KO
#1 #2 #1 #2
IFI16
Actin
B
NHEJ repair
HR repair
Efficiency (%)
100
50
#1 #2 #1 #2
Control
IFI16 KO
Vehicle
IFNα
IFNβ
C
NHEJ Repair
HR repair
EV
IFI16
DsRed
GFP
Efficiency (%)
EV
IFI16

Figure 24. IFI16 is essential for the type I IFN-induced inhibition of DNA repair

(A) Establishment of the MDA-MB-231-IFI16 knockout (KO) cell lines. Expression level of the corresponding proteins was analyzed by western blotting. (B) MDA-MB-231 control or IFI16 KO cells were cotransfected with the *Hind*Ⅲ-linearized NHEJ or I-*Sce*I-linearized HR reporter plasmid with Ds-Red, and then treated with IFNs. After 48 h, the ratio of number of GFP-positive cells *vs* that of DsRed-positive cells were determined by flow cytometry. NHEJ or HR efficiency was normalized to that of vehicle-treated samples. $*P < 0.05$ *vs* vehicle (n=3).

(C) NHEJ or HR efficiency was measured in MDA-MB-231 cells that were cotransfected with the *Hind*Ⅲ-linearized NHEJ or I-*Sce*I-linearized HR reporter plasmid, Ds-Red, and either empty vector (EV) or Myc-IFI16, as described in panal (B). $*P < 0.05$ *vs* EV (n=3).

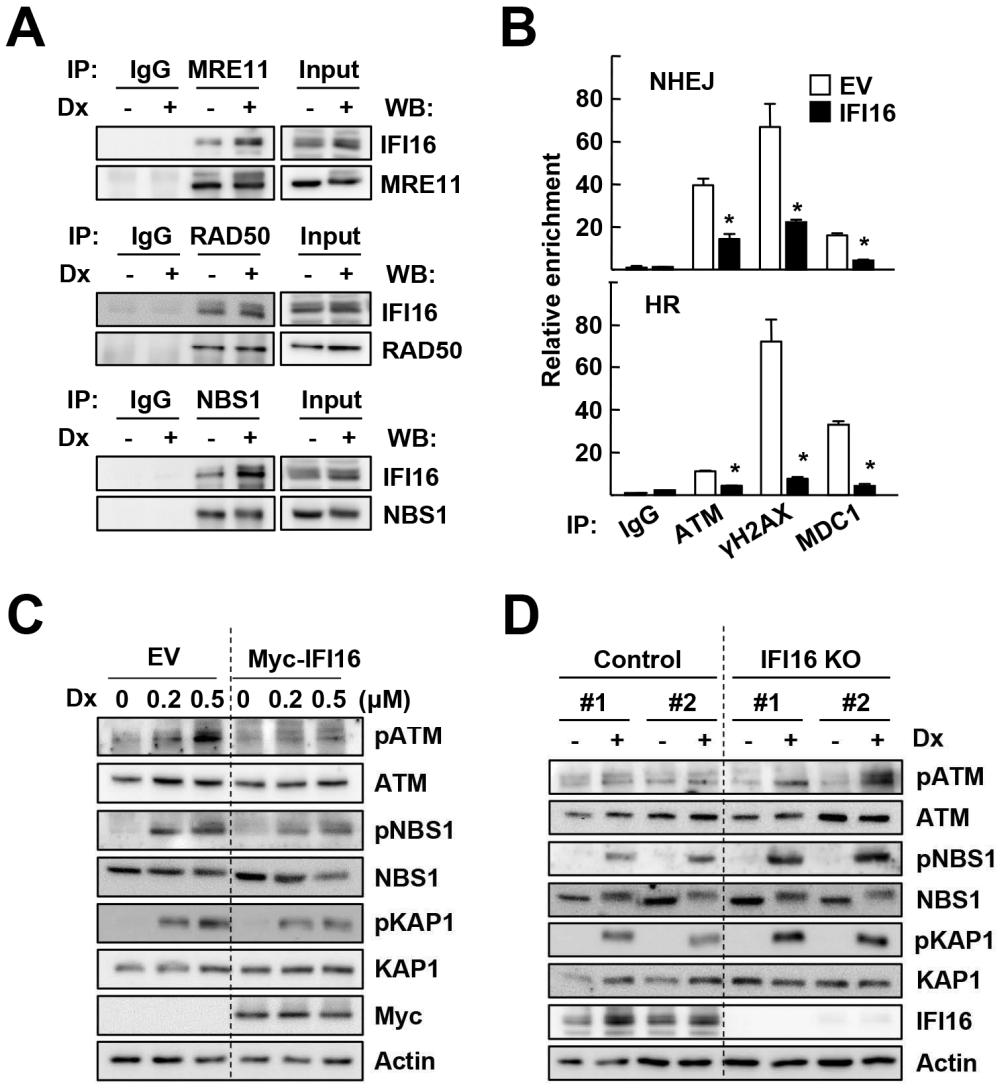
A
IP: IgG MRE11 Input
Dx - + - + - + WB:
IFI16
MRE11
IP: IgG RAD50 Input
Dx - + - + - + WB:
IFI16
RAD50
IP: IgG NBS1 Input
Dx - + - + - + WB:
IFI16
NBS1
B
NHEJ
EV
IFI16
Relative enrichment
80
60
40
20
HR
IP: IgG ATM γH2AX MDC1
C
EV
Myc-IFI16
Dx 0 0.2 0.5 0 0.2 0.5 (μM)
pATM
ATM
pNBS1
NBS1
pKAP1
KAP1
Myc
Actin
D
Control
IFI16 KO
#1 #2 #1 #2
- + - + - + - + Dx
pATM
ATM
pNBS1
NBS1
pKAP1
KAP1
IFI16
Actin

Figure 25. IIFI16 inhibits the recruitment of ATM to DNA damage sites, resulting in the impairment of downstream DDR signaling

(A) MDA-MB-231 cells were treated with 0.5 μM doxorubicin (Dx) for 16 h. Whole cell lysates were immunoprecipitated (IP) and probed by western blotting (WB).

(B) MDA-MB-231 cells were transfected with NHEJ or HR reporter plasmid, and I-*Sce*I expressing vector with empty vector (EV) or Myc-IFI16. After 24 h, cells were fixed and subjected to ChIP assays followed by qPCR analysis. $*P < 0.05$ *vs* EV (n=3).

(C) MDA-MB-231 cells were transfected with EV or Myc-IFI16 and then treated with doxorubicin for 16 h. Expression levels of protein was analyzed by western blotting.

(D) The MDA-MB-231 control or IFI16 KO cells were treated with 0.2 μM doxorubicin for 16 h. Expression levels of protein was analyzed by western blotting.

2.3. IFI16 is recruited to the sites of DNA damage

To understand the molecular mechanism by which IFI16 impairs DNA repair, I examined the possibility that IFI16 is recruited to DNA breakage sites. Surprisingly, IFI16 was rapidly accumulated to the sites of DNA damage when examined by laser microirradiation analysis. The accumulation of IFI16 was much faster than that of RAP80, a downstream mediator of DNA damage response (Figure 26A) (Yan et al., 2007). The wild type FokI, but not the D450A mutant, generated single DSB site in chromosome which was overlaid with IFI16, further demonstrating the association of IFI16 in DNA breakage sites (Figure 26B). Furthermore, ChIP analysis showed that IFI16 was recruited to the DSB sites generated by exogenously introduced I-SceI on the NHEJ or HR reporter plasmid (Figure 26C). These results demonstrate that IFI16 is mobilized and recruited to the sites of DNA damage.

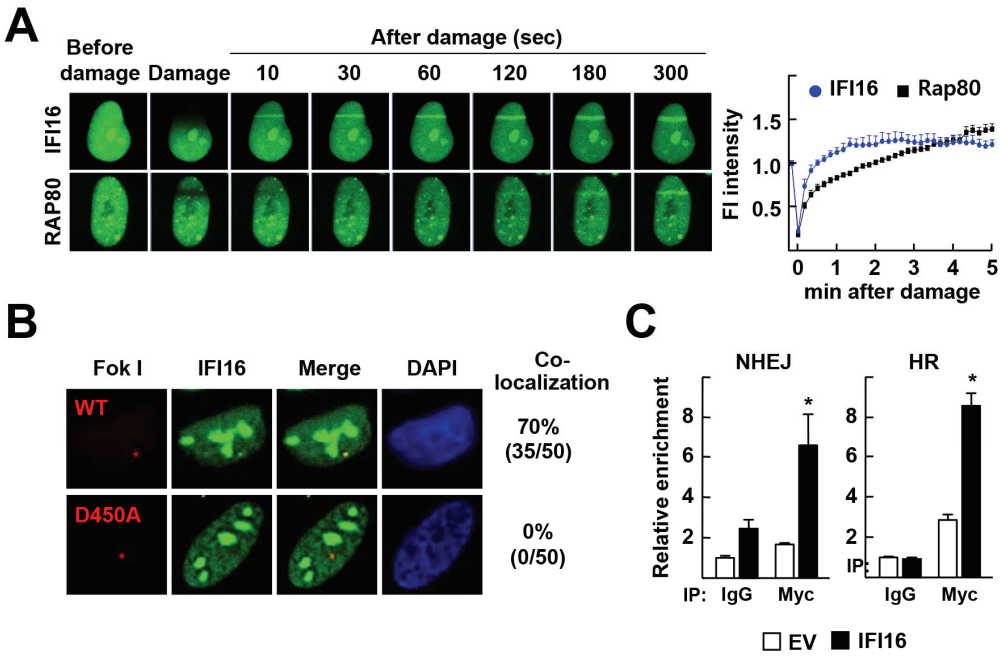

Figure 26. IFI16 is recruited to DSB sites

(A) Laser microirradiation experiments were performed with MDA-MB-231 cells that were transfected with GFP-IFI16 or GFP-RAP80 (left). The mean fluorescence (Fl) intensity at the microirradiated site was analyzed from 20 cells (right) (n=3).

(B) U2OS-DSB reporter cells were cotransfected with mCherry-LacI-Fok I wild-type (WT) or nuclease-deficient mCherry-LacI-Fok I (D450A) and GFP-IFI16. After 24 h, cells were fixed and analyzed using confocal microscope. The number of cells in which IFI16 (green) was colocalized with FokI (red) was counted and presented as percentage of 50 Fok I -positive cells.

(C) MDA-MB-231 cells were transfected with NHEJ or HR reporter plasmid, I-*Sce*I expressing vector with empty vector (EV) or Myc-IFI16. After 24 h, cells were fixed and subjected to ChIP assays using anti-Myc followed by qPCR analysis. $*P < 0.05$ *vs* EV (n=3).

2.4. IFI16 binds to histone-evicted regions near DSB sites

In response to DNA damage, chromatin undergoes a decondensation process within a few seconds-to-minutes to facilitate access of the DNA repair factors to the sites of DNA lesions. Several chromatin remodeling complexes are recruited to damage sites and modulate the chromatin architecture by sliding and/or evicting histones (Xu and Price, 2011; Price and D'Andrea, 2013). Recently, it was reported that IFI16 binds dsDNA in a length-dependent manner and assembles into distinct oligomeric clusters (Stratmann et al., 2015). Therefore, I hypothesized that IFI16 could recognize and bind the histone-evicted sites induced by DNA damage. I analyzed the dynamics of proteins in the same cell following microirradiation-induced DNA damage. Both core histone H2B and linker histone H1.5 were rapidly displaced from microirradiated sites, where IFI16 was accumulated within the first few seconds (Figure 27A). The recruitment kinetics of IFI16 to DSB sites was similar with that of SMARCA4, catalytic subunit of the SWI/SNF chromatin-remodelling complex responsible for histone eviction (Figure 27B) (Lans et al., 2012). ChIP analysis also showed that histones were depleted from the mCherry-LacI-FokI-induced DSB sites by the chromatin remodelers including INO80, where IFI16 was significantly enriched (Figure 28A). When cell extracts were separated into fractions enriched for open chromatin or compacted chromatin segments, IFI16 was abundant in the fraction

consisting nucleoplasm in the absence of stress. Doxorubicin treatment caused a portion of IFI16 to specifically enriched to the nuclease-sensitive open chromatin fraction (Figure 28B). Morever, doxorubicin cuase IFI16 to associate with chromatin and become resistant to detergent extraction (Figure 28C). Taken together, these results show that IFI16 could sense the exposed dsDNA regions generated by histone eviction upon DSBs.

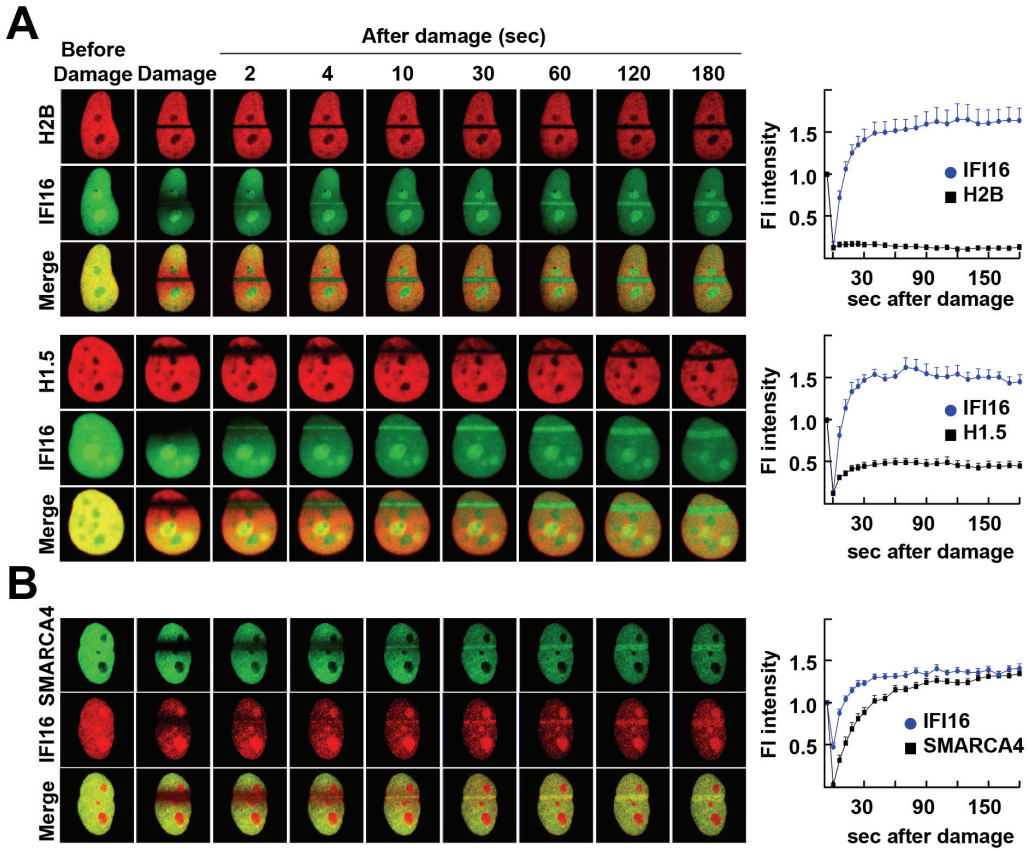

Figure 27. IFI16 is recruited to DNA damage-induced histone evicted regions

(A) Laser microirradiation experiments were performed with MDA-MB-231 cells that were transfected with GFP-IFI16 and RFP-H2B or RFP-H1.5 (left). The mean fluorescence (Fl) intensity at the microirradiated site was analyzed from 20 cells (right) (n=3).

(B) Laser microirradiation experiments were performed with MDA-MB-231 cells that were transfected with RFP-IFI16 and GFP-SMARCA4, as described in panal (A).

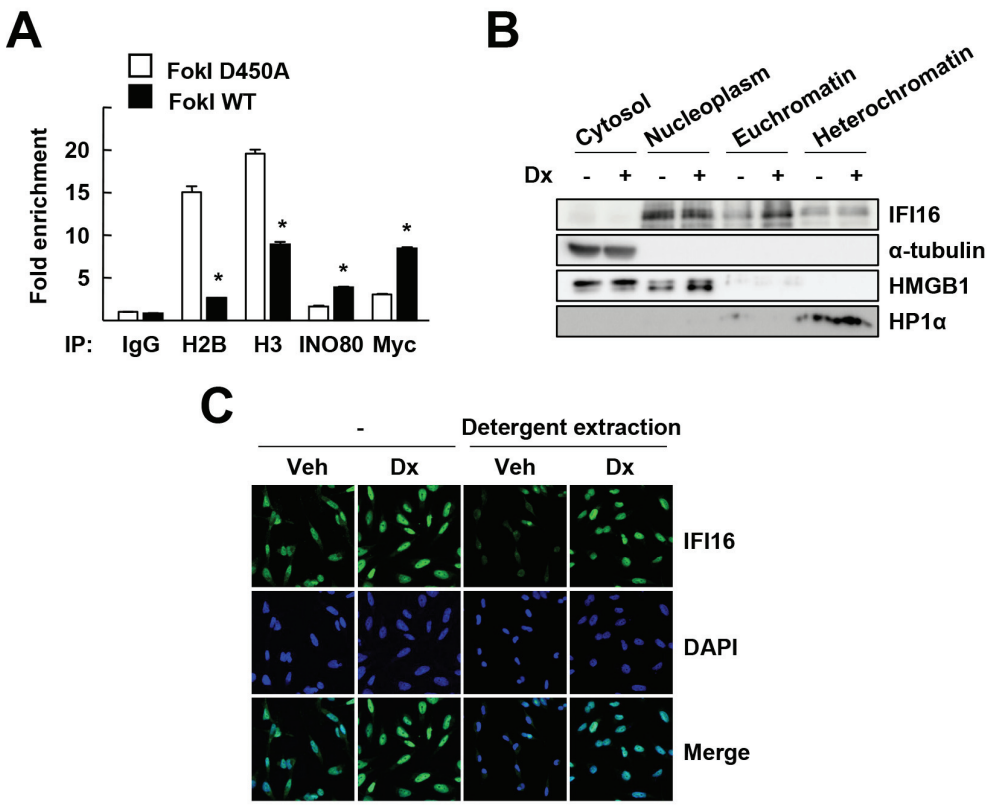

Figure 28. Association of IFI16 to open chromatin is enhanced in response to DNA damage

(A) U2OS-DSB reporter cells were cotransfected with nuclease-deficient mCherry-LacI-Fok I (Fok I D450A) or mCherry-LacI-Fok I wild-type (Fok I WT) and Myc-IFI16. After 24 h, cells were fixed and subjected to ChIP assays followed by qPCR analysis. $*P < 0.05$ *vs* Fok I D450A (n=3).

(B) MDA-MB-231 cells treated with 0.5 μM doxorubicin (Dx) for 16 h were processed for chromatin segregation. Two point five percent of each fraction was subjected to western blot analysis.

(C) MDA-MB-231 cells were treated with 0.5 μM doxorubicin for 16 h. Cells were fixed immediately to detect total proteins or pre-extracted with Triton X-100 before fixation to detect chromatin-bound proteins. Cells were immunostained with anti-IFI16 antibody (green). Nuclei were stained with DAPI (blue).

2.5. IFI16 translocates to cytoplasm along with double stranded DNA

DNA damage in the nucleus results in the release of DNA into cytoplasm, especially when cells have defects in DNA repair machinaries (Bhattacharya et al., 2017; Vanpouille-Box et al., 2017; Härtlova et al., 2015). Therefore I asked whether IFI16-induced DNA repair impairment results in the activation of cytosolic DNA-STING signaling pathways. Doxorubicin treatment increased the levels of cytosolic DNA in the control cells, but not in the IFI16 KO cells (Figure 29A). Consistently, doxorubicin-induced activation of STING signal was attenuated in the IFI16 KO cells, as judged by phosphorylation of STING at Ser366 (Figure 29B). Notably, IFI16 was co-localized with the dsDNA in the cytoplasm in response to DNA damage (Figure 30A). Time-lapse imaging revealed that IFI16 translocated from the nucleus to the cytosol along with dsDNA (Figure 30B). Thus, besides its role in inhibition of DNA repair in nucleus, IFI16 may also play a role in the cytosolic DNA sensing and subsequent STING signaling in tumor cells, as previously reported in macorphages and keratinocytes (Jønsson et al., 2017; Almine et al., 2017).

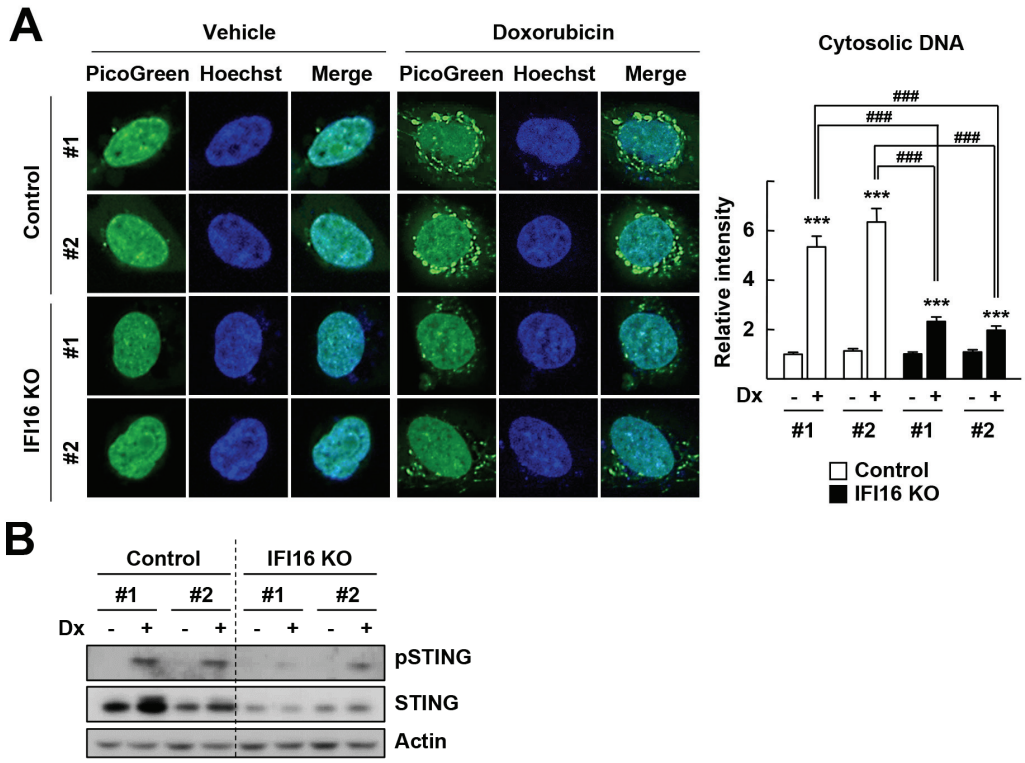

Figure 29. Deletion of IFI16 decreases cytosolic DNA and subsequent STING signaling

(A) MDA-MB-231 control or IFI16 KO cells were treated with 0.5 μM doxorubicin (Dx) for 16 h and then stained with dsDNA-specific dye PicoGreen (green) and Hoechst (blue) (left). Cytosolic intensity was quantified from at least 100 cells (right) (n=3). $^{***}P < 0.001$ *vs* vehicle of each cell, $^{\#\#\#}P < 0.001$ *vs* control cells.

(B) The MDA-MB-231 stable cells were treated with 0.5 μM doxorubicin for 40 h. Expression levels of protein were analyzed by western blotting.

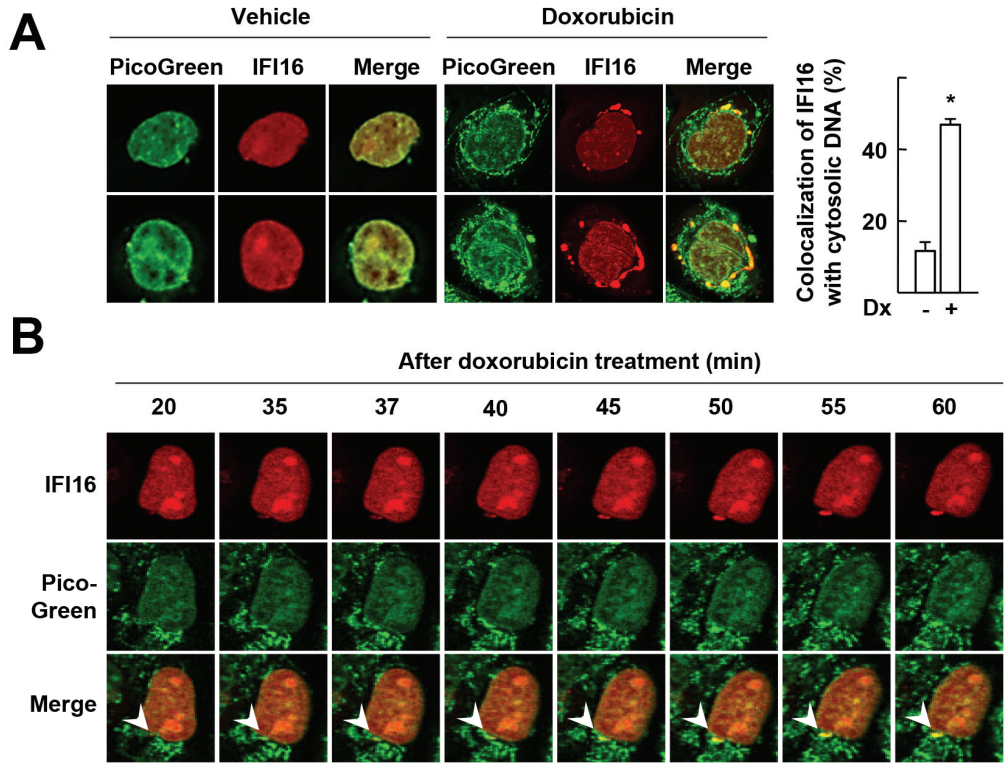

Figure 30. IFI16 translocates to cytoplasm along with dsDNA

(A) MDA-MB-231 cells transfected with RFP-IFI16 and treated with 0.5 μM doxorubicin (Dx) for 16 h were stained with PicoGreen (green). The number of cells in which IFI16 was colocalized with cytosolic DNA was counted from 100 cells and presented as percentage of total counted cells. $*P < 0.05$ *vs* vehicle (n=3).

(B) MDA-MB-231 cells were transfected with RFP-IFI16 and then treated with 0.5 μM doxorubicin and 1 μl/ml PicoGreen. Immediately, cells were subjected to real-time confocal imaging analysis. The arrows indicate IFI16 which is colocalized with dsDNA.

2.6. IFI16 is essential for the amplification of DNA damage-induced type I IFN signaling

The level of cytosolic DNA in the control cells was increased by each of IFNβ and doxorubicin treatment and further induced by combination of both IFNβ and doxorubicin. However, depletion of IFI16 notably suppressed this increment (Figure 31A). Consistently, the STING signal was activated by treatment of IFNs with or without doxorubicin, but not in the IFI16 KO cells. Interestingly enough, doxorubicin treatment increased the expression of IFNβ, which was further enhanced by cotreatment with IFNα and IFNβ in the control cells, but not in the IFI16 KO cells (Figure 31B).

Next, I examined whether IFI16 is involved in the antitumor effect of type I IFNs which is exerted via both cell intrinsic and extrinsic mechanisms (Parker et al., 2016). Cotreatment of IFNα or IFNβ further increased the doxorubicin-induced caspase-3 activation in the control cells, but not in the IFI16 KO cells (Figure 32A). Doxorubicin- and IFNβ-induced suppression of clonal growth induced was significantly lower in IFI16 KO cells (Figure 32B). The activation of STING pathway leads to the production of chemokine (CC motif) ligand 5 (CCL5) and chemokine (CXC motif) ligand 11 (CXCL11), which promote infiltration of NK cells and T cells into tumor (Sokolowska and Nowis, 2018). Doxorubicin treatment induced CCL5 and CXCL11 expression, which was

further enhanced by IFNα or IFNβ. However, it was attenuated in the IFI16 KO cells (Figure 33A and 33B). In agreement, conditioned media (CM) from the doxorubicin- and IFNβ-treated MDA-MB-231 control cells increased T cell migration, whereas CM from drug-treated IFI16 KO cells had a minimal impact on T cell migration (Figure 33C). These results suggest the importance of IFI16 in DNA damage-induced activation of the STING pathway, followed by the amplification of type I IFN signaling.

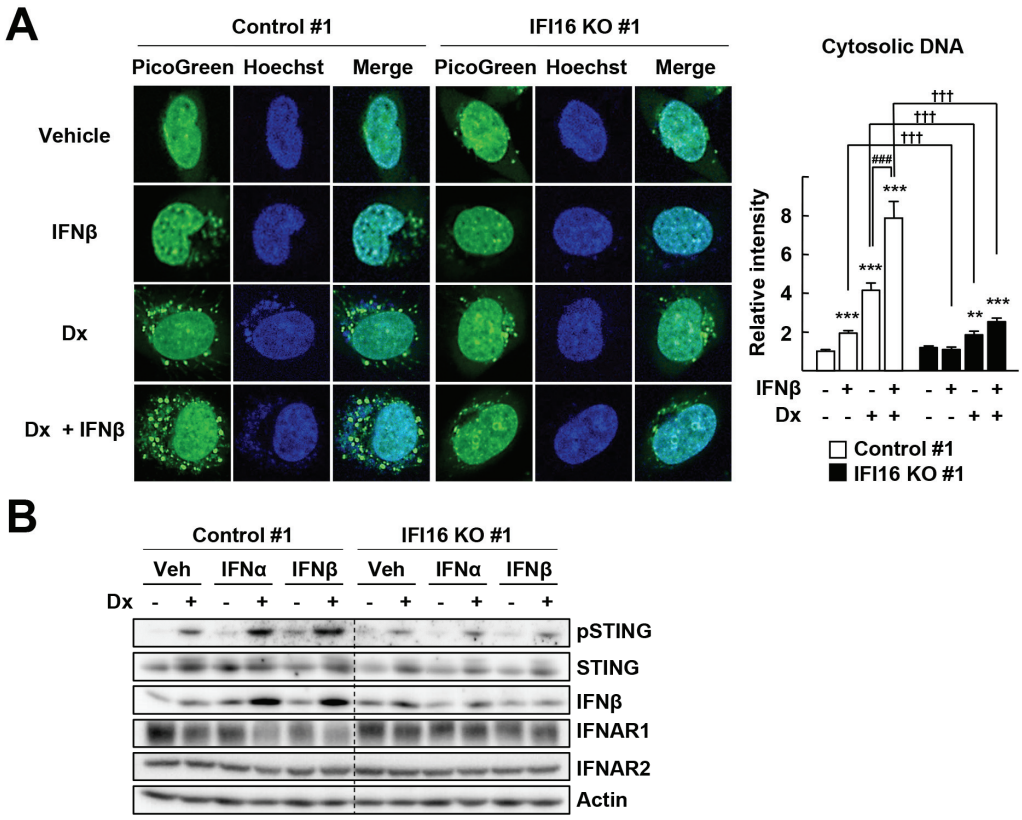

Figure 31. IFI16 is required for the DNA damage-induced type I IFN signaling

(A) MDA-MB-231 control or IFI16 KO cells were treated with 0.2 μM doxorubicin (Dx) and/or 100 IU/ml IFNβ for 16 h and then stained with 1 μl/ml PicoGreen (green) and Hoechst (blue) (left). Cytosolic intensity was quantified from at least 100 cells (right). $^{**}P < 0.01$ and $^{***}P < 0.001$ *vs* vehicle of each cell; $^{\#\#\#}P < 0.001$ *vs* Dx only; $^{\dagger\dagger\dagger}P < 0.001$ *vs* control cells (n=3).

(B) The MDA-MB-231 stable cells were treated with 0.2 μM doxorubicin and/or 100 IU/ml IFNβ for 40 h. Expression levels of protein were analyzed by western blotting.

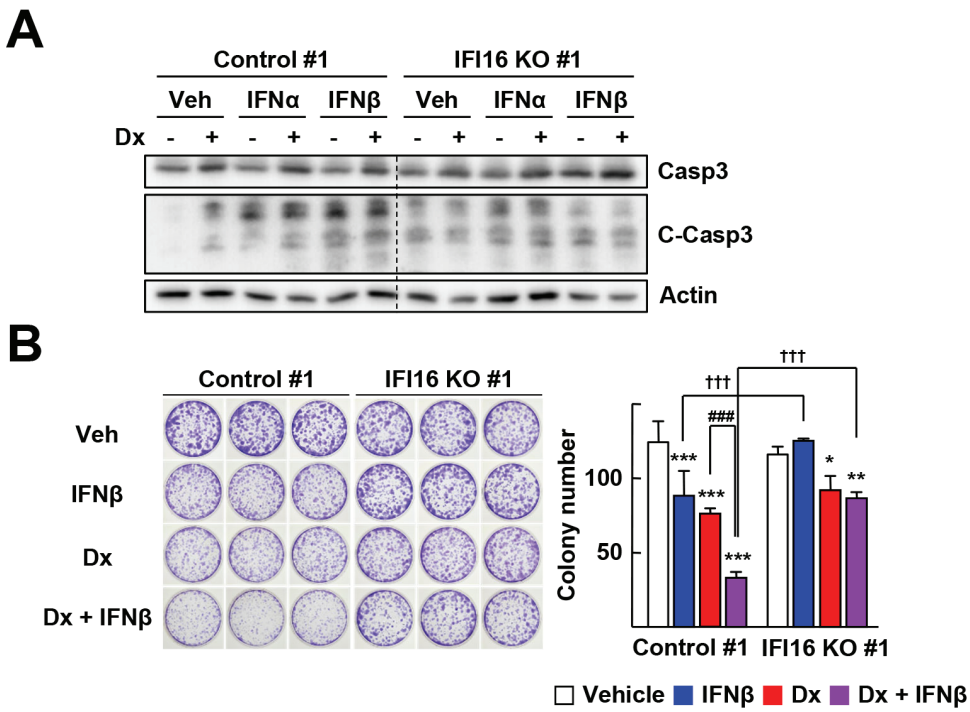

Figure 32. IFI16 is essential for the type I IFN-induced apoptotic cell death

(A) MDA-MB-231 control or IFI16 KO cells were treated with 0.2 μM doxorubicin (Dx) and/or 100 IU/ml IFNβ for 40 h. Expression levels of protein were analyzed by western blotting.

(B) The MDA-MB-231 stable cells were exposed to 2 nM doxorubicin and/or 10 IU/ml IFNβ for 12 days, and clonogenic survival assays were performed (left). Colonies that were composed of more than 50 cells were counted (right). $*P < 0.05$, $**P < 0.01$, and $***P < 0.001$ *vs* vehicle of each cell; $^{\#\#\#}P < 0.001$ *vs* Dx only; $^{\dagger\dagger\dagger}P < 0.001$ *vs* control cells (n=3).

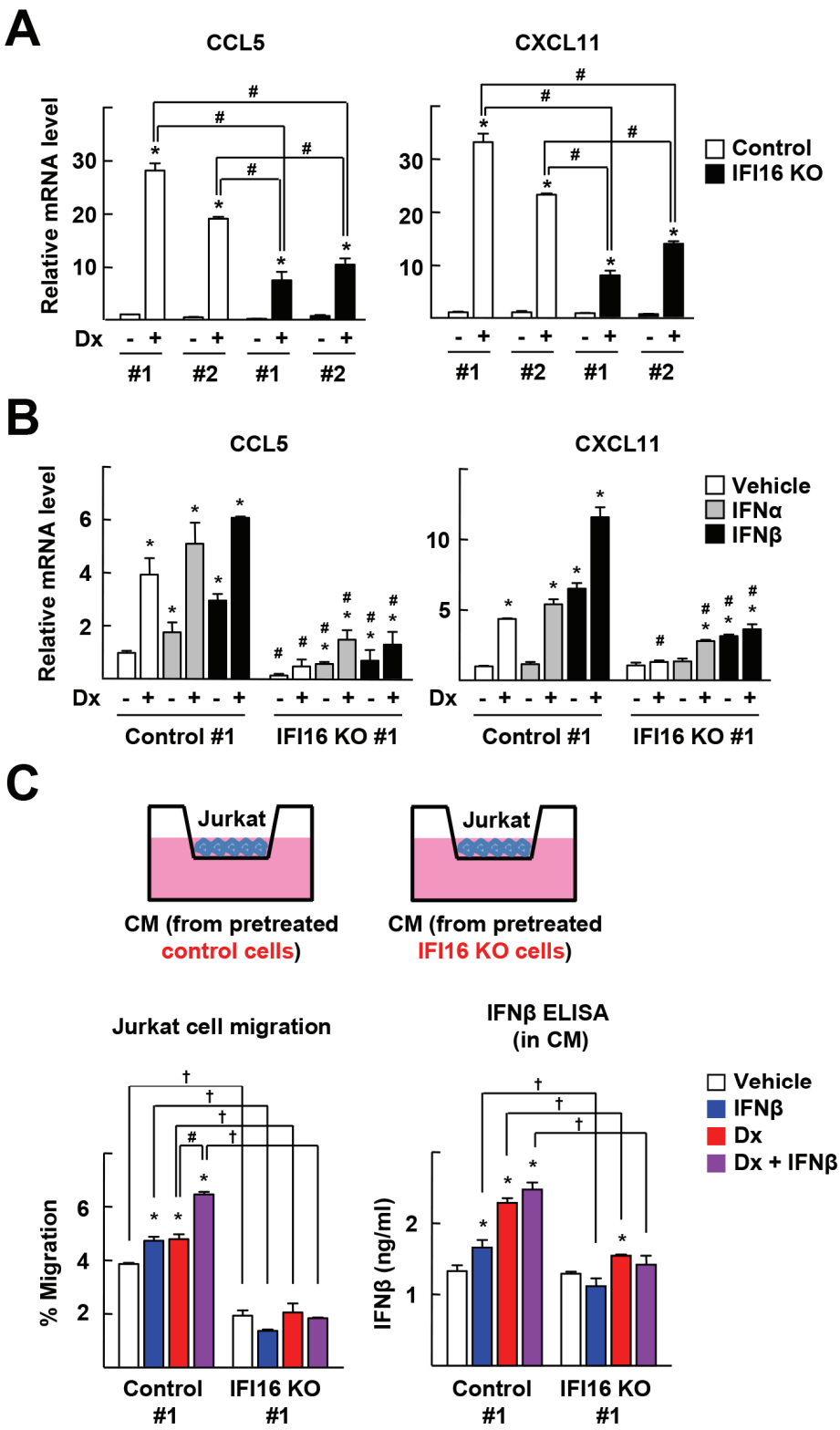
A
CCL5
CXCL11
Relative mRNA level
Control
IFI16 KO
Dx
#1
#2
B
CCL5
CXCL11
Relative mRNA level
Vehicle
IFNα
IFNβ
Control #1
IFI16 KO #1
C
Jurkat
CM (from pretreated control cells)
CM (from pretreated IFI16 KO cells)
Jurkat cell migration
IFNβ ELISA (in CM)
% Migration
IFNβ (ng/ml)
Vehicle
IFNβ
Dx
Dx + IFNβ

Figure 33. IFI16 is essential for the induction of T cell chemotactic factors

(A) MDA-MB-231 control or IFI16 KO cells were treated with 0.5 μM doxorubicin (Dx) for 16 h. The mRNA levels of CCL5 and CXCL11 were measured by qRT-PCR. $*P < 0.05$ *vs* vehicle of each cell; $^{\#}P < 0.05$ *vs* control cells with doxorubicin treatment (n=3).

(B) MDA-MB-231 control or IFI16 KO cells were treated with 0.2 μM doxorubicin (Dx) and/or 100 IU/ml IFNβ for 16 h. The mRNA levels of CCL5 and CXCL11 were measured by qRT-PCR. $*P < 0.05$ *vs* vehicle of each cell; $^{\#}P < 0.05$ *vs* control cells with doxorubicin treatment (n=3).

(C) Jurkat cells were allowed to migrate in Transwell inserts toward the conditioned media (CM) obtained from the MDA-MB-231 stable cells pretreated with 0.2 μM doxorubicin and/or 100 IU/ml IFNβ for 16 h. The number of the cells that migrated to the bottom chamber was counted using a hemocytometer and presented as percentage of migrated cells (left). The concentration of IFNβ in conditioned media was measured by ELISA (right). $*P < 0.05$ *vs* vehicle of each cell; $^{\#}P < 0.05$ *vs* Dx only; $^{\dagger}P < 0.05$ *vs* control cells (n=3).

2.7. IFN-IFI16 sensitizes doxorubicin-induced tumor growth inhibition in vivo

To further investigate the effect of IFI16 on the *in vivo* susceptibility of cancer cells to doxorubicin and type I IFN, the MDA-MB-231-control or -IFI16 KO cells were inoculated into athymic nude mice and treated with vehicle, IFNβ, doxorubicin, or doxorubicin/IFNβ (Figure 34A). Tumor growth in the control cells was slightly inhibited by doxorubicin treatment alone, but that was significantly inhibited by co-administration of doxorubicin and IFNβ. In contrast, tumor growth in the IFI16 KO cells was not affected by these drugs (Figure 34B and 34C). Body weights were unchanged and no apparent treatment-related toxicities were noted throughout the experiments (Figure 34D).

Immunohistochemical analyses of the tumor tissues showed that the expression of IFI16 increased in doxorubicin- or IFNβ-treated control group, which was further increased in cotreated control group (Figure 35A). The levels of 53BP1 and γH2AX, markers of DSBs, further increased in cotreated control group, but not in the IFI16 KO group, indicating an enhanced rate of DNA repair (Figure 35B). Moreover, the level of cytosolic DNA in the tumor tissues was increased in doxorubicin-treated group, and it was further increased in doxorubicin/IFNβ-cotreated control group, but not in the IFI16 KO group (Figure 36A). In agreement, the levels of IFNβ and CXCL11 were significantly

higher in doxorubicin/IFNβ-cotreated group of control mice compared with that of IFI16 KO mice (Figure 36B). These results show that type I IFNs increase the sensitivity of TNBC cells to doxorubicin, and IFI16 is essential for these chemosensitizing effects.

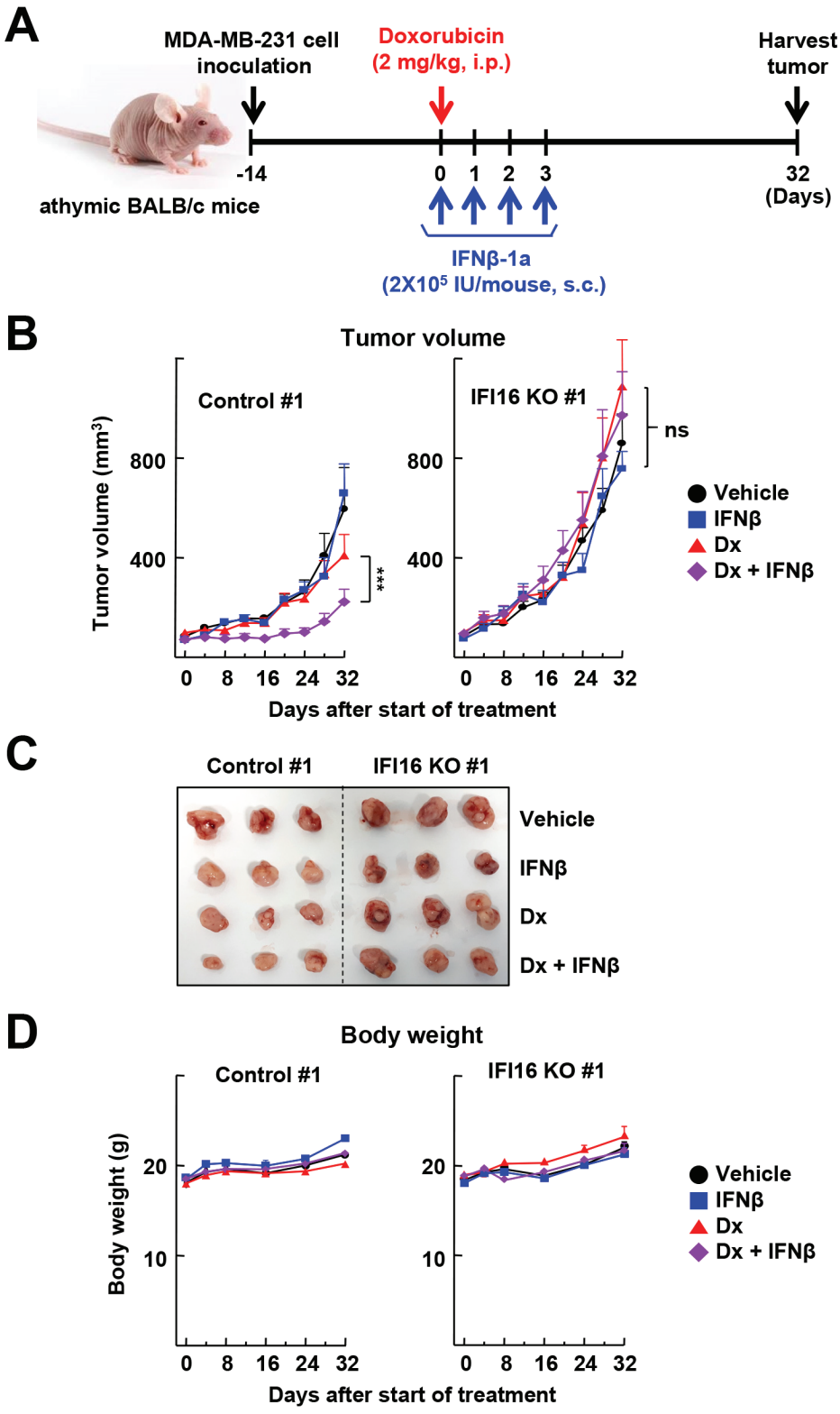
A
MDA-MB-231 cell inoculation
Doxorubicin (2 mg/kg, i.p.)
Harvest tumor
athymic BALB/c mice
-14
0 1 2 3
32 (Days)
IFNβ-1a (2X10⁵ IU/mouse, s.c.)
B
Tumor volume
Control #1
IFI16 KO #1
ns
***
Tumor volume (mm³)
800
400
0 8 16 24 32
Days after start of treatment
Vehicle
IFNβ
Dx
Dx + IFNβ
C
Control #1
IFI16 KO #1
Vehicle
IFNβ
Dx
Dx + IFNβ
D
Body weight
Control #1
IFI16 KO #1
Body weight (g)
20
10
0 8 16 24 32
Days after start of treatment
Vehicle
IFNβ
Dx
Dx + IFNβ

Figure 33. Lack of IFI16 decreases sensitivity to doxorubicin *in vivo*

(A) Treatment schedule for the MDA-MB-231 xenograft experiments.

(B) Tumor volume was measured with a caliper. The number of specimen of each group was as follow: Control-vehicle (n=8), control-IFNβ (n=7), control-Dx (n=6), control-IFNβ+Dx (n=8), IFI16 KO-vehicle (n=7), IFI16 KO-IFNβ (n=5), IFI16 KO-Dx (n=4), and IFI16 KO-IFNβ+Dx (n=8). ***$P < 0.001$; ns=not significant difference between the groups.

(C) Representative tumor images are shown.

(D) Measurement of the body weight of MDA-MB-231 xenograft mice throughout the experiments.

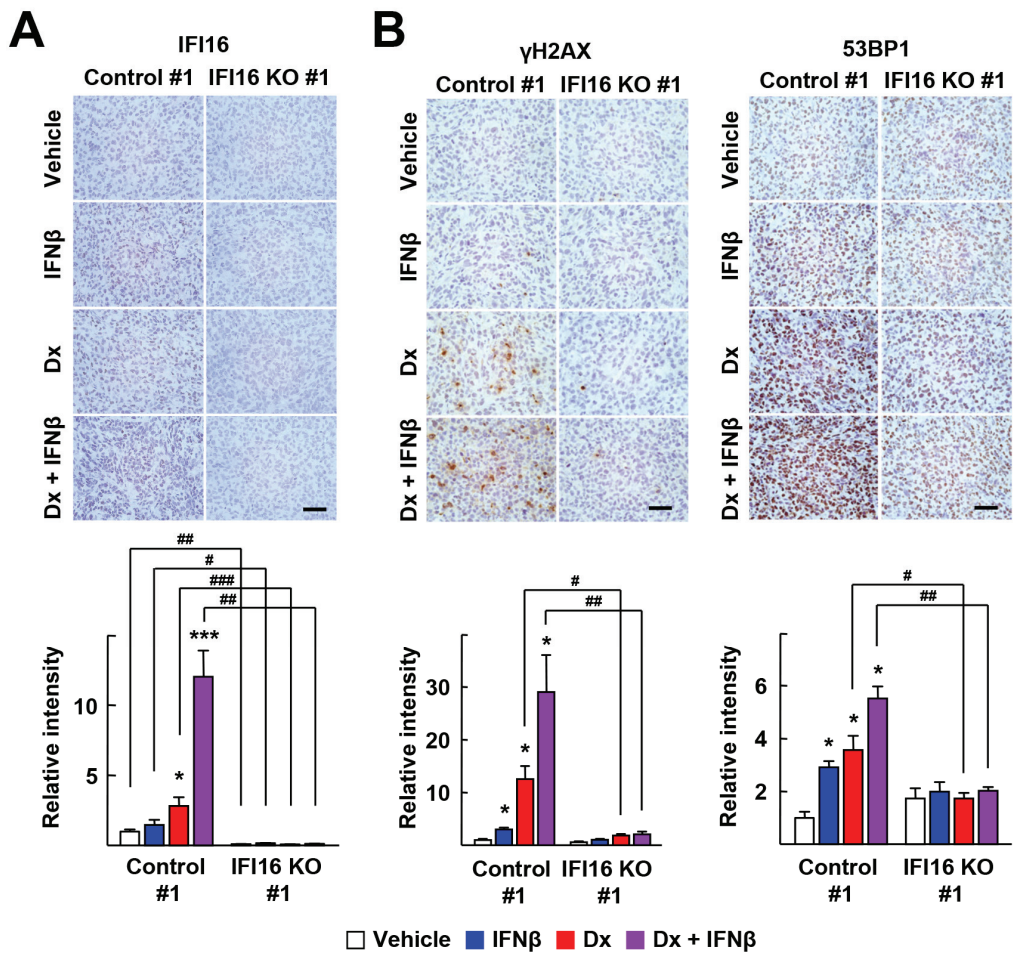

Figure 35. Lack of IFI16 enhances the rate of DNA repair *in vivo*

(A) Immunohistochemistry staining of IFI16 in tumor sections (top). Staining intensity was quantified in three tumor samples from each group and five random field per sample by densitometric analysis using ImageJ software (bottom). $*P < 0.05$ and $***P < 0.001$ *vs* vehicle of each cell; $^{\#}P < 0.05$, $^{\#\#}P < 0.01$, and $^{\#\#\#}P < 0.001$ *vs* control cells.

(B) Immunohistochemistry staining of IFNβ and CXCL11 in tumor sections. Staining intensity was quantified as described in panal (A). $*P < 0.05$ *vs* vehicle of each cell; $^{\#}P < 0.05$ and $^{\#\#}P < 0.01$ *vs* control cells.

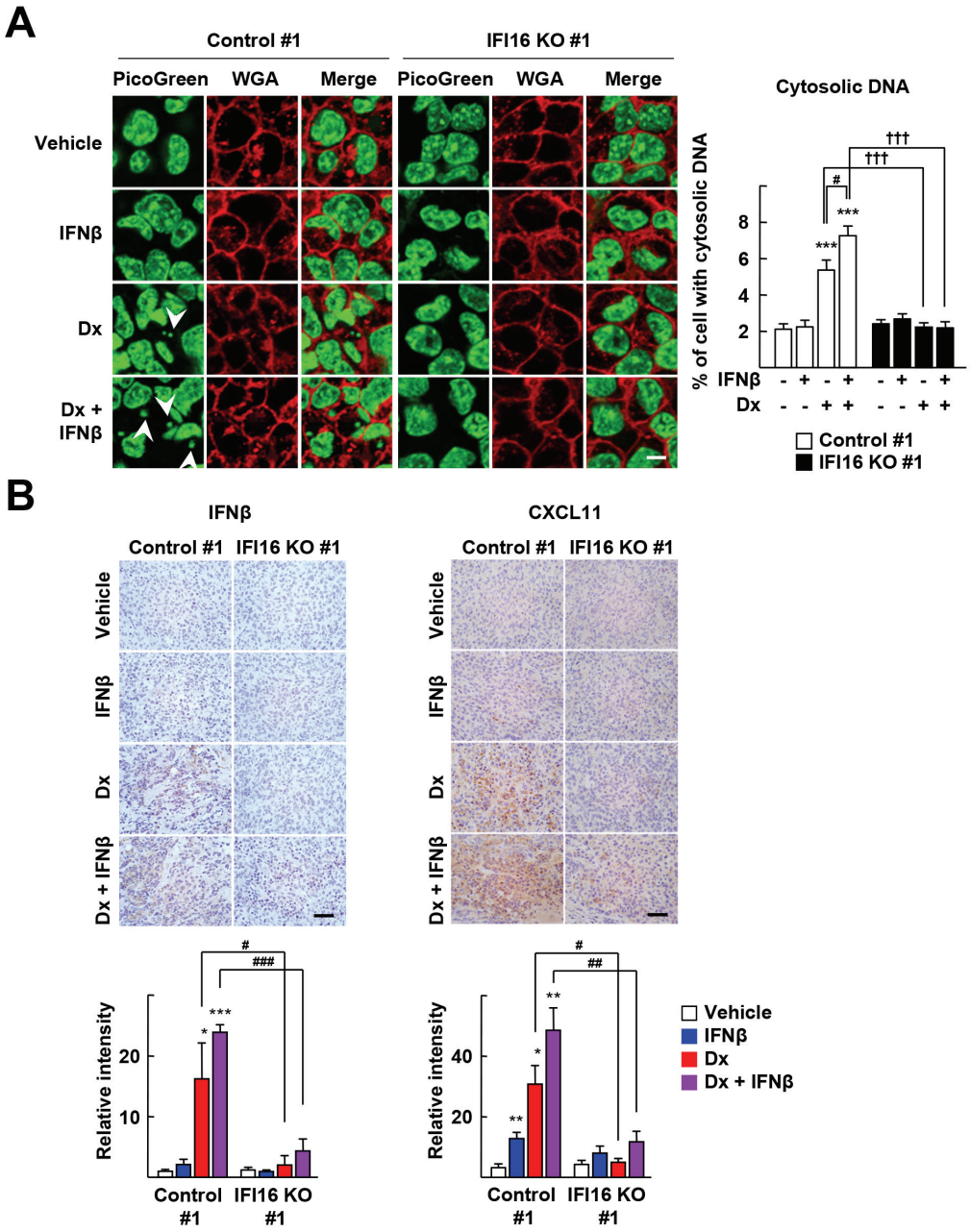
A
Control #1
IFI16 KO #1
PicoGreen
WGA
Merge
Vehicle
IFNβ
Dx
Dx + IFNβ
Cytosolic DNA
% of cell with cytosolic DNA
IFNβ
Dx
Control #1
IFI16 KO #1
B
IFNβ
CXCL11
Relative intensity
Control #1
IFI16 KO #1
Vehicle
IFNβ
Dx
Dx + IFNβ

Figure 36. Lack of IFI16 decreases the cytosolic DNA-induced STING signaling *in vivo*

(A) Tumor sections were stained with dsDNA-specific dye PicoGreen (green) and wheat germ agglutinin (WGA) (red) (left). Cytosolic intensity was quantified from three tumor samples from each group and five random field per sample using ImageJ software (right). $^{***}P < 0.001$ *vs* vehicle; $^{\#}P < 0.05$ *vs* Dx only; $^{\dagger\dagger\dagger}P < 0.001$ *vs* control cells. The arrows indicate cytosolic DNA.

(B) Immunohistochemistry staining of IFNβ and CXCL11 in tumor sections. Staining intensity was quantified in three tumor samples from each group and five random field per sample by densitometric analysis using ImageJ software (right). $^{*}P < 0.05$, $^{**}P < 0.01$ and $^{***}P < 0.001$ *vs* vehicle of each cell, $^{\#}P < 0.05$, $^{\#\#}P < 0.01$, and $^{\#\#\#}P < 0.001$ *vs* control cells.

2.8. High IFI16 expression is associated with better clinical outcomes in breast cancer patients

To evaluate the clinical significance of these experimental observations, I analyzed publicly available datasets, which included the gene expression profiles and clinical outcome information such as pCR and overall survival (OS). In four independent datasets, GSE22093, GSE34138, GSE16716, and GSE20271, the group of patients with high IFI16 expression showed higher pCR rate than those with low IFI16 expression (Iwamoto et al., 2011; de Ronde et al., 2013; MAQC Consortium, 2010; Tabchy et al., 2010) (Table 6). In agreement, the IFI16 expression levels were significantly higher in the achieved pCR group than in the nonachieved pCR group in these datasets (Figure 37A). To investigate the association of IFI16 expression with clinical outcome, survival analyses were performed using the Kaplan–Meier method with the log-rank test in three independent datasets, GSE1456, METABRIC, and GSE37751 (Pawitan et al., 2005; Pereira et al., 2016; Terunuma et al., 2014). In breast cancer patients who received chemotherapy, the OS was significantly improved in high IFI16 expression group compared with those in low IFI16 expression group (Figure 37B). These findings suggest that breast cancer patients with high intratumoral IFI16 expression are more sensitive to chemotherapy.

Finally, I analyzed the association of IFI16 with DDR and cytosolic DNA

signaling pathway in breast cancer patients. IFI16 was co-localized with 53BP1, a marker of DSBs, in TNBC specimens (Figure 38A). In addition, the level of cytosolic DNA was significantly higher in TNBC specimens compared with other types of breast cancer specimens, suggesting a probable role of IFI16 in cytosolic DNA-STING signaling pathway (Figure 38B).

Table 6. Increased therapeutic response in breast cancer patients with high IFI16 expression[a]

Data set	IFI16 expression[b]	Non-pCR	pCR	p-value	Odd ratio of pCR[c] (95% CI)
GSE22093	low	44 (91.7%)	4 (8.3%)	<0.0001	10.56 (3.288~33.9158)
	high	25 (51.0%)	24 (49.0%)		
GSE34138	low	68 (77.3%)	20 (22.7%)	0.0063	2.5333 (1.32~4.862)
	high	51 (57.3%)	38 (42.7%)		
GSE16716	low	118 (84.9%)	21 (15.1%)	0.0513	1.891 (1.0359~3.452)
	high	104 (74.8%)	35 (25.2%)		
GSE20271	low	81 (91.0%)	8 (9.0%)	0.055	2.5669 (1.0523~6.2615)
	high	71 (79.8%)	18 (20.2%)		

[a] The GSE22093, GSE34138, GSE16716 and GSE20271 datasets that have therapeutic response information were obtained from NCBI GEO site (Iwamoto et al., 2011; de Ronde et al., 2013; MAQC Consortium, 2010; Tabchy et al., 2010).

[b] Patients were categorized into a low (below median) IFI16 expression group and a high (above median) IFI16 expression group. The expression levels of IFI16 in individual patient in each IFI16 low and high group and their median values were shown in Figure 37A.

[c] The Fisher's exact probability test was performed for determination of significance by a web-based program (http://vassarstats.net/). CI, confidence interval.

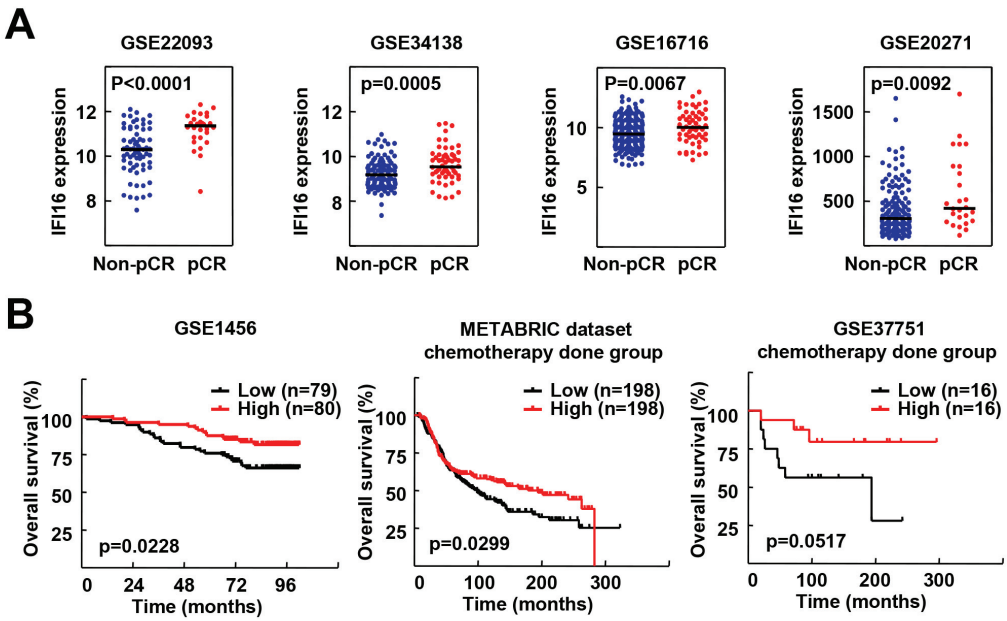

Figure 37. High IFI16 expression is correlated with an improved clinical outcome in breast cancer patients received chemotherapy

(A) Expression level of IFI16 was higher in pCR group of breast cancer. The GSE22093, GSE34138, GSE16716, and GSE20271 datasets were obtained from NCBI GEO site (Iwamoto et al., 2011; de Ronde et al., 2013; MAQC Consortium, 2010; Tabchy et al., 2010). Scattered dot plots show IFI16 expression level in Non-pCR group and in pCR group. Bars indicate the median IFI16 expression level in each group. Statistical significance was analyzed by Mann-Whitney *U* test.

(B) The GSE1456 and GSE37751 datasets were obtained from NCBI GEO site. The METABRIC dataset was obtained from a cBioPortal website. Patients were categorized into a low (below median) IFI16 expression group and a high (above median) IFI16 expression group. OS rate (%) was plotted for each group. To analyze statistical differences, Log-rank (Mantel-Cox) tests were performed.

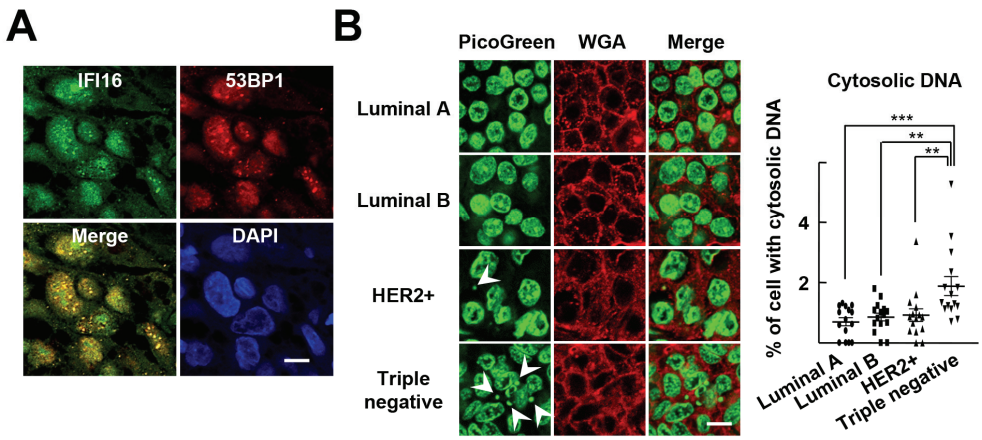

Figure 38. Clinical significance of IFI16 in TNBC

(A) Co-localization of IFI16 and 53BP1 in TNBC. TNBC tissue sections were subjected to immunostaining using antibodies against IFI16 (green) and 53BP1 (red). Nuclei were stained with DAPI (blue).

(B) Breast cancer specimens were stained with dsDNA-specific dye PicoGreen (green) and wheat germ agglutinin (WGA) (red) (left). Cytosolic intensity was quantified from 15 samples from each group using ImageJ software (right). $^{**}P < 0.01$ and $^{***}P < 0.001$ *vs* TNBC specimens. The arrows indicate cytosolic DNA.

V. DISCUSSION

1. NR1D1 as a crucial regulator for DNA damage response

In the first part of the study, I demonstrated that NR1D1 inhibits the recruitment of DDR complex to damaged DNA sites, which results in the impairment of proper DNA repair. Interestingly, NR1D1 was physically associated with PARP1 and PARylated form of NR1D1 was recruited to damaged DNA sites. Consistently, NR1D1 increased the sensitivity of breast cancer cells to chemotherapeutic agents *in vitro* and *in vivo* (Figure 39; Ka et al., 2017). Recently, it has been shown clearly that chromatin remodeling and histone-specific modifications directly control DNA damage sensing, signaling, and repair, which may provide an insight into the molecular mechanisms that allow NR1D1 to affect DNA repair (Price et al., 2013). Thus, a plausible mechanism for NR1D1 could involve its recruitment by PARP1 to hinder the recruitment of DDR factors to DNA damage sites by recruiting chromatin modifiers such as NcoR1 and HDAC3, which facilitate DNA winding by histone modifications. In addition, PARylation of NR1D1 could delay PARP1-mediated PARylation as well as the recruitment of other DDR factors such as γH2AX to damaged DNA sites.

Intriguingly, however, PARP inhibitors have been examined as sensitizing agents to chemotherapy and radiotherapy (Tangutoori et al., 2015).

Several PARP inhibitors including Olaparib, Veliparib and Talazoparib are in phase 2 and 3 clinical trials as monotherapy or combination therapies (Nur et al., 2018). Nevertheless, only about 40% of BRCA-deficient breast and ovarian cancers respond to PARP inhibitors, suggesting that PARP1 may function beyond a simple direction of DNA repair (Tutt et al., 2010, Audeh et al., 2010). The temporal- and spatial evaluation of posttranscriptional modifications of DDR components including NR1D1 could help to precise understanding of the regulation of DDR, which could provide better strategies for breast cancer treatment.

This study has identified NR1D1 as a negative regulator of DNA repair, which increases sensitivity to chemotherapeutic agents. However, it is widely recognized that defects in DNA repair system lead to genomic instability, which is one of the most prevalent characteristics of cancer (Venkatesan et al., 2015). Thus, although NR1D1 could provide therapeutic opportunities, it may cause genomic instability and ultimately drive mammary tumorigenesis. Indeed, NR1D1 gene is encoded within the ERBB2 amplicon and the expression level of this receptor is correlated with a poor prognosis (Chin et al., 2006, Davis et al., 2007). Further, NR1D1 enhances the survival of breast cancer cells, suggesting a potential role for NR1D1 in breast cancer development (Kourtidis et al., 2010). A better understanding of the NR1D1-induced cellular response to DNA damage

and repair at different steps of mammary tumorigenesis may provide benefits for developing strategies for prognosis and treatment of the disease.

2. Potential therapeutic use of NR1D1 ligands as adjuvant therapy

Although chemotherapy has contributed to the reduction of mortality of patients with cancer, it lowers quality of life due to severe side effects. Therefore, novel therapeutic options are required to reduce the dosages in chemotherapy to avoid unwanted toxicity. In this aspect, the DNA damage repair machinery may provide a target to establish the therapeutic options. Inhibitors of DNA repair components such as ATM, ATR, DNA-PK, Chk1, and Chk2 have been developed as chemosensitizers in clinical trials (Furgason and Bahassi, 2013). Here, I report that NR1D1 expression was negatively correlated with the DNA repair efficiency in breast cancer cell lines and that the NR1D1 agonist, GSK4112, sensitized breast cancer cells to doxorubicin (Fig. 7 and 18). Recently, several NR1D1 agonists that have sufficient plasma exposure and oral bioavailability have been developed and characterized *in vivo* (Table 1). These compounds could be used as potential chemosensitizers which could enhance the outcomes of adjuvant chemotherapy.

Interestingly, several other nuclear receptors have been reported to regulate the DNA damage repair machinery. NR4A is recruited to ionizing radiation- or ultraviolet-induced DNA damage sites and it promotes DNA repair (Malewicz et al., 2011, Jagirdar et al., 2013). Thyroid hormone receptor β

induces cellular senescence and DNA damage in mouse embryonic fibroblasts and hepatocytes (Zambrano et al., 2014). Testicular nuclear receptor 4 regulates ATM expression and functions as a tumor suppressor in prostate cancer (Lin et al., 2014). In addition, Izhar *et al.* (Izhar et al., 2015) reported that nine nuclear receptors, including ESRRA and RARB, were localized to the sites of DNA damage after laser microirradiation. These observations together with this study suggest that nuclear receptor ligands could provide better therapies when combined with current chemotherapeutic agents. Further investigations of the relationships between the expression levels of these receptors and the clinical outcomes of chemotherapy in breast cancer patients may expand the spectrum of therapeutic options.

3. Potential benefits of chronotherapy based on the oscillation of NR1D1 expression

NR1D1 is a well-known component of the circadian clock, which regulates the expression of circadian clock genes such as BMAL1 and CLOCK (Everett and Lazar, 2014). An increasing volume of evidences indicates that the efficiency of DNA repair oscillates with the circadian rhythm and the circadian clock system is closely linked to the sensitivity of chemotherapy (Sancar et al., 2015). For example, crucial DDR proteins such as xeroderma pigmentosum group A, N-methylpurine DNA glycosylase, and O^6-alkylguanine-DNA alkyltransferase (AGT) exhibited circadian oscillation in their expression and modulates the cellular sensitivity to genotoxic stress (Marchenay et al., 2001, Kim et al., 2009; Gaddameedhi et al., 2011). Recently, several attempts are being made to develop chronochemotherapy, a circadian-based anticancer approach that employs the optimal circadian time to achieve the best therapeutic index (Innominato et al., 2014). The application of chronotherapy to pathological diseases such as bronchial asthma, cardiovascular diseases and hypertension is well established and lead to successful outcome (Dallmann et al., 2014). However, the chronotherapeutic approach of cancer treatment is highly complicated and several attempts are being made to develop chronochemotherapy regimens (Innominato et al., 2014; Sancar et al., 2015). Recently, it has been reported that the

nucleotide excision repair rate exhibits circadian oscillation, and therefore administration of cisplatin at optical repair phase would improve the therapeutic index (Kang et al., 2009). According to a meta-analysis, chronotherapy with oxaliplatin, 5-fluorouracil, and leucovorin improved overall survival in men with metastatic colorectal cancer compared with conventional chemotherapy (Giacchetti et al., 2012). The finding that the efficacy of DSB repair was modulated by NR1D1 in breast cancer cells strongly supports the potential benefits of chronotherapy based on the oscillation of NR1D1 expression.

4. NR1D1 as a predictive biomarker for breast cancer chemotherapy

Many efforts have been made recently to search for useful markers to determine the outcome of chemotherapy. In the present study, I found that breast cancer patients with high NR1D1 expression levels had better clinical outcomes after chemotherapy in clinics (Table 5 and Figure 20). This observation may indicate that NR1D1 increases sensitivity of breast cancer cells to DNA damage-inducing chemotherpy, which result in successful achievement of pCR in patients. Because the achievement of pCR with primary chemotherapy is crucial for the successful treatment of patients with breast cancer, a careful attention should be made to determine best therapeutic options. We suggest NR1D1 as a novel predictive biomarker for breast cancer that allows for a more personalized treatment approach. Interestingly, most of cell lines we employed contain mutation of p53 and/or allelic loss of BRCA1, suggesting that loss of DNA repair capacity may facilitate the NR1D1-induced DNA repair impairment (Elstrodt et al., 2006, Hollestelle et al., 2010). Interestingly, when analyzed public patient datasets, NR1D1 expression is higher in luminal B and HER2-positive subtypes compared with luminal A and TNBC molecular subtypes (Figure 6). Therefore, luminal B and HER2-positive breast cancer could be a primary target for testing our hypothetical use of NR1D1 as a predictive biomarker for breast cancer

chemotherapy to facilitate a more personalized treatment approach in the future. Further detailed analyses of the NR1D1 gene expression level and alterations in genes involved with the DDR response may improve the prediction of outcomes with DNA damage-inducing chemotherapy.

5. Novel function of IFI16 - Sensor of endogenous damaged DNA

In the second part of the study, I demonstrated that IFI16 bound to doxorubicin-induced histone evicted dsDNA, leading to the inhibition of DNA repair. Subsequently, IFI16 moved into the cytoplasm along with dsDNA, activated STING signaling and induced type I IFN production. In turn, type I IFNs increased the expression of IFI16, thus forming an amplification loop to potentiate type I IFN signaling (Figure 40). This study identified for the first time that IFI16 senses endogenous dsDNA in the nucleus in response to DNA damage. It has been reported that IFI16 assembles into distinct oligomeric clusters and binds to dsDNA in a length-dependent manner: minimal length of 60 base pairs of exposed dsDNA are required for initiate assembly, and ~150 base pairs of dsDNA comprise an optimal binding cluster. Furthermore, IFI16 was shown to interacted di-nucleosomes when the spacer was longer than 70 base pairs (Stratmann et al., 2015). Thus it is recognized that chromatinization acts as crucial feature that distinguish between self and non-self DNA. However, upon DSBs, histones are evicted from the damaged DNA by chromatin remodeling enzymes (Price and D'Andrea, 2013), where IFI16 recognizes and binds rapidly as shown in this study (Figure 27). As 146 base pairs of DNA is wrapped by histone octamer, and linker dsDNA between two

nucleosomes is about 20 to 30 base pairs, histone eviction from chromatin would make enough space for IFI16 to form optimal cluster. The finding that IF16 recognizes endogenous self DNA in the nucleus is notable, in that IFI16 would act as an acute genomic stress sensor against physiological and pathological stress to modulate cell survival. Further studies on the role of IFI16 in endogenous DNA sensing in the context of chromatin challenge, such as transcription and DNA replication, would expand the understanding of the physiological role of IFI16 (Groth et al., 2007; Das and Tyler, 2013).

6. IFI16 as a key regulator in DNA damage-induced amplification of type I IFN signaling

The immune system recognizes and kills tumor cells in a process of tumor immunosurveillance, and type 1 IFN is critical for eliciting effective antitumor immunity by linking between innate and adaptive immunity (Dunn et al., 2006). In tumor microenvironment, cancer cell-derived nucleic acids are detected as danger-associated molecular patterns by pattern recognition receptors, including STING and Toll-like receptors, which then induce the production of type I IFNs (Bose, 2017; Zitvogel et al., 2015). Binding of type I IFNs to surface receptor leads to activation of Janus kinase (JAK)-signal transducer and activator of transcription (STAT) pathway, resulting in the transcriptional regulation of hudndreds of IFN-stimulated genes, which are responsible for the antitumor actions (Ivashkiv and Donlin, 2014; Parker et al., 2016). Type I IFN signaling is also shown to mediates the therapeutic effects of a wide range of conventional chemotherapies and radiotherapy by inducing the immunogenic cell death (Zitvogel et al., 2015; Galluzzi et al., 2017). Therefore, activation and amplification of type I IFN signaling are crucial to potentiate the efficacy of anticancer therapy.

Importantly, emerging evidences have suggested that innate immune pathway is closely associated with DDR pathway. Several DDR proteins are

reported to play active roles in innate immune signaling. For instance, Ku70, DNA-dependent protein kinase, Mre11, and Rad50 also serve asd cytosolic sensors for dsDNA (Chatzinikolaou et al., 2014). The other way, cGAS, a cytosolic dsDNA sensor, are recently known to play a role in DNA repair process in the nucleus (Liu et al., 2018). This study demonstrated that, as well as its role in inhibition of DNA repair in nucleus, IFI16 translocated from nucleus to cytoplasm along with DNA damage-induced dsDNA fragment (Figure 30). As previous reports that IFI16 cooperates with cGAS to activate STING signaling in macorphages and keratinocytes, IFI16, in the cytoplasm, also may contribute to activate STING signaling in breast cancer cells (Jønsson et al., 2017; Almine et al., 2017). Therefore, it is noted that sensing of IFI16 with damaged DNA initially elicits the impairment of DNA repair, and subsequently bring dsDNA into cytoplasm where it activates STING signaling. Dual mode of IFI16 action both in nucleus and cytoplasm may further promote STING activation and type I IFN signaling in response to cytotoxic agent-induced DNA damage. Indeed, breast cancer patients with high IFI16 expression levels had better clinical outcomes after chemotherapy in clinics (Figure 37). Therefore, I suggest that IFI16 is a critical factor interconnecting DDR and type I IFN signaling, thus potentiating the efficacy of anticancer therapy.

7. Potential therapeutic use of type I IFNs in treating TNBC

Although breast cancer was initially considered as a non-immunogenic tumor, TNBC is increasingly recognized as an immunogenic tumor, where the presence of tumor-infiltrating lymphocytes is correlated with favorable survival outcomes and therapeutic response (García-Teijido et al., 2016). Therefore, emerging efforts have focused on generating and amplifying T-cell responses, which is critical in converting cold breast cancer to hot (Tolba and Omar, 2018). In an effort, a PD-L1 blocking antibody, atezolizumab (TECENTRIQ®), was recently approved by the Food and Drug Administration (FDA) for patients with unresectable locally advanced or metastatic TNBC expressing PD-L1 (Cortés et al., 2019). It is the first approved immunotherapy regimen for breast cancer, expanding treatment options for breast cancer.

The type I IFNs has implicated as a key class of cytokines that triggers tumor immune infiltration and activation (Zitvogel et al., 2015). Indeed, type I IFNs, i.e., IFN-α2a (Roferon-A), IFN-α2b (Intron-A), IFN-β1a (Avonex, Rebif), and IFN-β1b (Betaferon, Betaseron) were approved for the treatment of various immunogenic cancer and virus-related cancer, such as melanoma, AIDS-related Kaposi sarcoma, and chronic hepatitis B and C (Booy et al., 2015). In breast cancer, several clinical studies have been carried out to evaluate the efficacy of

type I IFNs as a monotherapy or combination therapy, however, results were variable and somewhat disappointing (Parker et al., 2016). It suggests that type I IFNs may exert the antitumor effects in a subset of tumors, emphasizing the importance of identifying reliable biomarkers that predict response to therapy. In the present study, we identified a novel mechanism of action of type I IFNs, the inhibitory effect on DNA repair, which require IFI16 (Figure 23 and 24). Therefore, this study suggests that IFI16 would be a critical determinant of the response to type I IFNs and provides a potential therapeutic use of type I IFNs in TNBC.

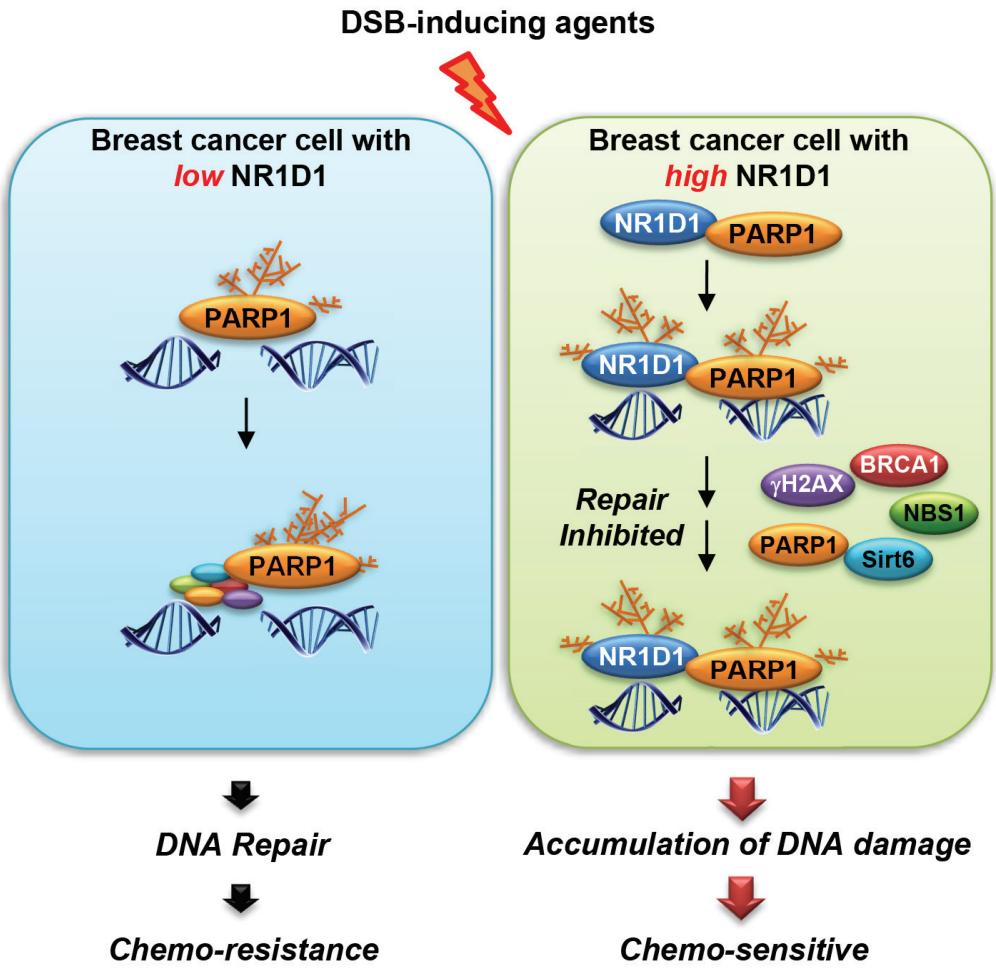

Figure 39. NR1D1 is a potent determinant of chemosensitivity in breast cancer

NR1D1 inhibits recruitment of the DDR complex to damaged DNA sites, thereby impairing proper DNA repair. Consequently, NR1D1 increases the sensitivity of breast cancer cells to chemotherapeutic agents.

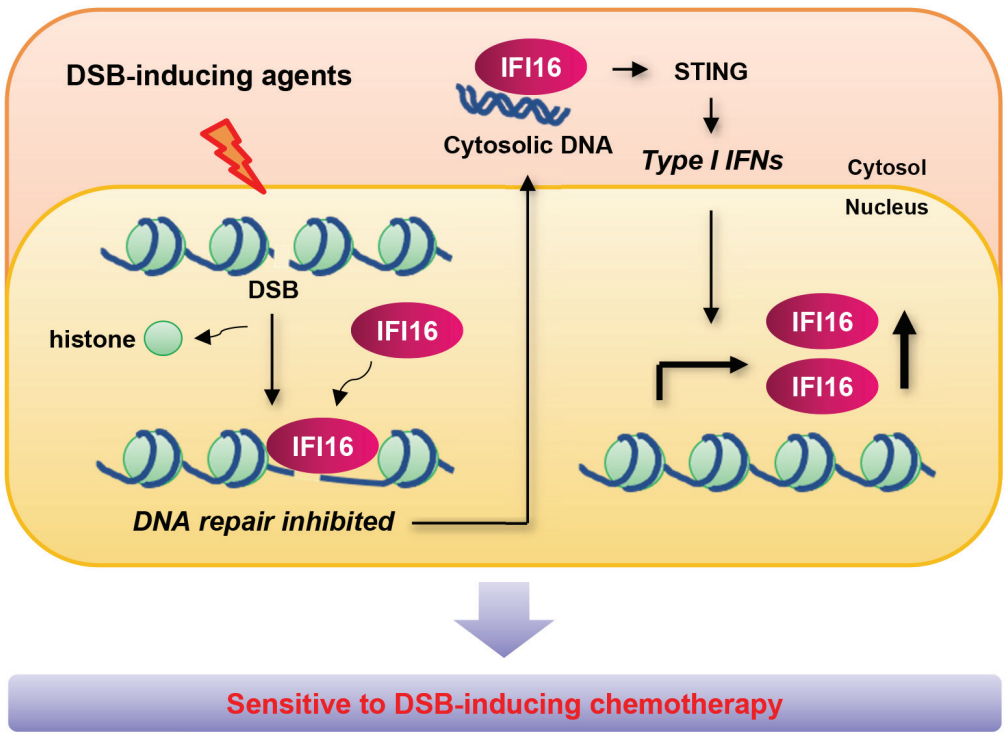

Figure 40. IFI16-mediated inhibition of DNA repair amplifies type I IFN signaling in TNBC

IFI16 binds doxorubicin-induced histone evicted dsDNA leading to inhibition of DNA repair, which amplifies type I IFN signaling in TNBC.

REFERENCES

Aglipay JA, Lee SW, Okada S, Fujiuchi N, Ohtsuka T, Kwak JC, et al. A member of the Pyrin family, IFI16, is a novel BRCA1-associated protein involved in the p53-mediated apoptosis pathway. Oncogene 22, 8931-8 (2003).

Albrecht M, Choubey D, Lengauer T. The HIN domain of IFI-200 proteins consists of two OB folds. Biochem Biophys Res Commun. 327, 679-87 (2005).

Alimirah F, Chen J, Xin H, Choubey D. Androgen receptor auto-regulates its expression by a negative feedback loop through upregulation of IFI16 protein. FEBS Lett. 580, 1659-64 (2006).

Almine JF, O'Hare CA, Dunphy G, Haga IR, Naik RJ, Atrih A, et al. IFI16 and cGAS cooperate in the activation of STING during DNA sensing in human keratinocytes. Nat Commun. 8, 14392 (2017).

Antoch MP, Kondratov RV, Takahashi JS. Circadian clock genes as modulators of sensitivity to genotoxic stress. Cell Cycle. 4, 901-7 (2005).

Audeh MW, Carmichael J, Penson RT, Friedlander M, Powell B, Bell-McGuinn KM, et al. Oral poly(ADP-ribose) polymerase inhibitor olaparib in patients with BRCA1 or BRCA2 mutations and recurrent ovarian cancer: a proof-of-concept trial. Lancet 376, 245-51 (2010).

Bhattacharya S, Srinivasan K, Abdisalaam S, Su F, Raj P, Dozmorov I, et al. RAD51 interconnects between DNA replication, DNA repair and immunity. Nucleic Acids Res. 45, 4590-4605 (2017).

Booy S, Hofland L, van Eijck C. Potentials of interferon therapy in the treatment of pancreatic cancer. J Interferon Cytokine Res. 35, 327-39 (2015).

Bose D. cGAS/STING Pathway in Cancer: Jekyll and Hyde Story of Cancer Immune Response. Int J Mol Sci. 18. pii: E2456 (2017).

Bouwman P, Jonkers J. The effects of deregulated DNA damage signalling on cancer chemotherapy response and resistance. Nat Rev Cancer 12, 587-98

(2012).

Caldecott KW. Single-strand break repair and genetic disease. Nat Rev Genet. 9, 619-31 (2008).

Cancer Genome Atlas Network. Comprehensive molecular portraits of human breast tumours. Nature 490, 61-70 (2012).

Chatzinikolaou G, Karakasilioti I, Garinis GA. DNA damage and innate immunity: links and trade-offs. Trends Immunol. 35, 429-35 (2014).

Chen Y, Kamili A, Hardy JR, Groblewski GE, Khanna KK, Byrne JA. Tumor protein D52 represents a negative regulator of ATM protein levels. Cell Cycle. 12, 3083-97 (2013).

Chin K, DeVries S, Fridlyand J, Spellman PT, Roydasgupta R, Kuo WL, et al. Genomic and transcriptional aberrations linked to breast cancer pathophysiologies. Cancer Cell 10, 529-41 (2006).

Choubey D, Deka R, Ho SM. Interferon-inducible IFI16 protein in human cancers and autoimmune diseases. Front Biosci. 13, 598-608 (2008).

Ciriello G, Gatza ML, Beck AH, Wilkerson MD, Rhie SK, Pastore A, et al. Comprehensive Molecular Portraits of Invasive Lobular Breast Cancer. Cell 163, 506-19 (2015).

Cridland JA, Curley EZ, Wykes MN, Schroder K, Sweet MJ, Roberts TL, et al. The mammalian PYHIN gene family: phylogeny, evolution and expression. BMC Evol Biol. 12, 140 (2012).

Cortés J, André F, Gonçalves A, Kümmel S, Martín M, Schmid P, et al. IMpassion132 Phase III trial: atezolizumab and chemotherapy in early relapsing metastatic triple-negative breast cancer. Future Oncol. (2019).

Cridland JA, Curley EZ, Wykes MN, Schroder K, Sweet MJ, Roberts TL, et al. The mammalian PYHIN gene family: phylogeny, evolution and expression. BMC Evol Biol. 12, 140 (2012).

Crumbley C, Burris TP. Direct regulation of CLOCK expression by REV-ERB. PLoS One. 6, e17290 (2011).

Crumbley C, Wang Y, Kojetin DJ, Burris TP. Characterization of the core

mammalian clock component, NPAS2, as a REV-ERBalpha/RORalpha target gene. J Biol Chem. 285, 35386-92 (2010).

Curigliano G, Burstein HJ, Winer EP, Gnant M, Dubsky P, Loibl S, et al. De-escalating and escalating treatments for early-stage breast cancer: the St. Gallen International Expert Consensus Conference on the Primary Therapy of Early Breast Cancer 2017. Ann Oncol. 28, 1700-1712 (2017).

Dallmann R, Brown SA, Gachon F. Chronopharmacology: new insights and therapeutic implications. Annu Rev Pharmacol Toxicol. 54, 339-61 (2014).

Das C, Tyler JK. Histone exchange and histone modifications during transcription and aging. Biochim Biophys Acta. 1819, 332-342 (2013).

Dasari S, Tchounwou PB. Cisplatin in cancer therapy: molecular mechanisms of action. Eur J Pharmacol. 740, 364-78 (2014).

Davis LM, Harris C, Tang L, Doherty P, Hraber P, Sakai Y, et al. Amplification patterns of three genomic regions predict distant recurrence in breast carcinoma. J Mol Diagn 9, 327-36 (2007).

De Andrea M, Gioia D, Mondini M, Azzimonti B, Renò F, Pecorari G, et al. Effects of IFI16 overexpression on the growth and doxorubicin sensitivity of head and neck squamous cell carcinoma-derived cell lines. Head Neck. 29, 835-44 (2007).

de Ronde JJ, Lips EH, Mulder L, Vincent AD, Wesseling J, Nieuwland M, et al. SERPINA6, BEX1, AGTR1, SfLC26A3, and LAPTM4B are markers of resistance to neoadjuvant chemotherapy in HER2-negative breast cancer. Breast Cancer Res Treat 137, 213-23 (2013).

Duan X, Ponomareva L, Veeranki S, Panchanathan R, Dickerson E, Choubey D. Differential roles for the interferon-inducible IFI16 and AIM2 innate immune sensors for cytosolic DNA in cellular senescence of human fibroblasts. Mol Cancer Res. 9, 589-602 (2011).

Dunn GP, Koebel CM, Schreiber RD. Interferons, immunity and cancer immunoediting. Nat Rev Immunol. 6, 836-48 (2006).

Dunphy G, Flannery SM, Almine JF, Connolly DJ, Paulus C, Jønsson KL,

Jakobsen MR, Nevels MM, Bowie AG, Unterholzner L. Non-canonical Activation of the DNA Sensing Adaptor STING by ATM and IFI16 Mediates NF-κB Signaling after Nuclear DNA Damage. Mol Cell. 71, 745-760.e5 (2018).

Edwards SL, Brough R, Lord CJ, Natrajan R, Vatcheva R, Levine DA, et al. Resistance to therapy caused by intragenic deletion in BRCA2. Nature. 451, 1111-5 (2008).

Elstrodt F, Hollestelle A, Nagel JH, Gorin M, Wasielewski M, van den Ouweland A, et al. BRCA1 mutation analysis of 41 human breast cancer cell lines reveals three new deleterious mutants. Cancer Res. 66, 41-5 (2006).

Everett LJ, Lazar MA. Nuclear receptor Rev-erbα: up, down, and all around. Trends Endocrinol Metab. 25, 586-92 (2014).

Fu L, Kettner NM. The circadian clock in cancer development and therapy. Prog Mol Biol Transl Sci. 119, 221-82 (2013).

Fu L, Pelicano H, Liu J, Huang P, Lee C. The circadian gene Period2 plays an important role in tumor suppression and DNA damage response in vivo. Cell. 111, 41-50 (2002).

Fujiuchi N, Aglipay JA, Ohtsuka T, Maehara N, Sahin F, Su GH, et al. Requirement of IFI16 for the maximal activation of p53 induced by ionizing radiation. J Biol Chem. 279, 20339-44 (2004).

Furgason JM, Bahassi el M. Targeting DNA repair mechanisms in cancer. Pharmacol Ther. 137, 298-308 (2013).

Gaddameedhi S, Selby CP, Kaufmann WK, Smart RC, Sancar A. Control of skin cancer by the circadian rhythm. Proc Natl Acad Sci U S A. 108, 18790-5 (2011).

Galluzzi L, Buqué A, Kepp O, Zitvogel L, Kroemer G. Immunogenic cell death in cancer and infectious disease. Nat Rev Immunol. 17, 97-111 (2017).

García-Teijido P, Cabal ML, Fernández IP, Pérez YF. Tumor-Infiltrating Lymphocytes in Triple Negative Breast Cancer: The Future of Immune Targeting. Clin Med Insights Oncol. 10, 31-9 (2016).

Gariglio M, Azzimonti B, Pagano M, Palestro G, De Andrea M, Valente G, et al. Immunohistochemical expression analysis of the human interferon-inducible gene IFI16, a member of the HIN200 family, not restricted to hematopoietic cells. J Interferon Cytokine Res. 22, 815-21 (2002).

Giacchetti S, Dugué PA, Innominato PF, Bjarnason GA, Focan C, Garufi C, et al. Sex moderates circadian chemotherapy effects on survival of patients with metastatic colorectal cancer: a meta-analysis. Ann Oncol. 23, 3110-16 (2012).

Goldstein M, Kastan MB. The DNA damage response: implications for tumor responses to radiation and chemotherapy. Annu Rev Med. 66, 129-43 (2015).

Gong F, Chiu LY, Cox B, Aymard F, Clouaire T, Leung JW, et al. Screen identifies bromodomain protein ZMYND8 in chromatin recognition of transcription-associated DNA damage that promotes homologous recombination. Genes Dev. 29, 197-211 (2015).

Gorbacheva VY, Kondratov RV, Zhang R, Cherukuri S, Gudkov AV, Takahashi JS, et al. Circadian sensitivity to the chemotherapeutic agent cyclophosphamide depends on the functional status of the CLOCK/BMAL1 transactivation complex. Proc Natl Acad Sci U S A. 102, 3407-12 (2005).

Grant D, Yin L, Collins JL, Parks DJ, Orband-Miller LA, Wisely GB, et al. GSK4112, a small molecule chemical probe for the cell biology of the nuclear heme receptor Rev-erbα. ACS Chem Biol. 5. 925-32 (2010).

Groth A, Rocha W, Verreault A, Almouzni G. Chromatin challenges during DNA replication and repair. Cell. 128, 721-33 (2007).

Gugliesi F, Mondini M, Ravera R, Robotti A, de Andrea M, Gribaudo G, et al. Up-regulation of the interferon-inducible IFI16 gene by oxidative stress triggers p53 transcriptional activity in endothelial cells. J Leukoc Biol. 77. 820-9 (2005).

Han YH, Kim HJ, Kim EJ, Kim KS, Hong S, Park HG, et al. RORα decreases oxidative stress through the induction of SOD2 and GPx1 expression and thereby protects against nonalcoholic steatohepatitis in mice. Antioxid Redox

Signal. 21, 2083-94 (2014).

Harbeck N, Gnant M. Breast cancer. Lancet. 389, 1134-1150 (2017).

Härtlova A, Erttmann SF, Raffi FA, Schmalz AM, Resch U, Anugula S, et al. DNA damage primes the type I interferon system via the cytosolic DNA sensor STING to promote anti-microbial innate immunity. Immunity. 42, 332-343 (2015).

Hernandez-Aya LF, Gonzalez-Angulo AM. Adjuvant systemic therapies in breast cancer. Surg Clin North Am. 93, 473-91 (2013).

Hollestelle A, Nagel JH, Smid M, Lam S, Elstrodt F, Wasielewski M, et al. Distinct gene mutation profiles among luminal-type and basal-type breast cancer cell lines. Breast Cancer Res Treat. 121, 53-64 (2010).

Hühn D, Bolck HA, Sartori AA. Targeting DNA double-strand break signalling and repair: recent advances in cancer therapy. Swiss Med Wkly. 143, w13837 (2013).

Innominato PF, Roche VP, Palesh OG, Ulusakarya A, Spiegel D, Lévi FA. The circadian timing system in clinical oncology. Ann Med. 46, 191-207 (2014).

Ivashkiv LB, Donlin LT. Regulation of type I interferon responses. Nat Rev Immunol. 14, 36-49 (2014).

Iwamoto T, Bianchini G, Booser D, Qi Y, Coutant C, Shiang CY, et al. Gene pathways associated with prognosis and chemotherapy sensitivity in molecular subtypes of breast cancer. J Natl Cancer Inst. 103, 264-72 (2011).

Izhar L, Adamson B, Ciccia A, Lewis J, Pontano-Vaites L, Leng Y, et al. A Systematic Analysis of Factors Localized to Damaged Chromatin Reveals PARP-Dependent Recruitment of Transcription Factors. Cell Rep. 11, 1486-1500 (2015).

Jagirdar K, Yin K, Harrison M, Lim W, Muscat GE, Sturm RA, et al. The NR4A2 nuclear receptor is recruited to novel nuclear foci in response to UV irradiation and participates in nucleotide excision repair. PLoS One. 8, e78075 (2013).

Jakobsen MR, Paludan SR. IFI16: At the interphase between innate DNA

sensing and genome regulation. Cytokine Growth Factor Rev. 25. 649-55 (2014).

Jian J, Wei W, Yin G, Hettinghouse A, Liu C, Shi Y. RNA-Seq analysis of interferon inducible p204-mediated network in anti-tumor immunity. Sci Rep. 8, 6495 (2018).

Jønsson KL, Laustsen A, Krapp C, Skipper KA, Thavachelvam K, Hotter D, et al. IFI16 is required for DNA sensing in human macrophages by promoting production and function of cGAMP. Nat Commun. 8, 14391 (2017).

Ka NL, Na TY, Na H, Lee MH, Park HS, Hwang S, et al. NR1D1 Recruitment to Sites of DNA Damage Inhibits Repair and Is Associated with Chemosensitivity of Breast Cancer. Cancer Res. 77, 2453-2463 (2017).

Kang HJ, Lee MH, Kang HL, Kim SH, Ahn JR, Na H, et al. Differential regulation of estrogen receptor alpha expression in breast cancer cells by metastasis-associated protein 1. Cancer Res. 74, 1484-94 (2014).

Kang TH, Leem SH. Modulation of ATR-mediated DNA damage checkpoint response by cryptochrome 1. Nucleic Acids Res. 42, 4427-34 (2014).

Kang TH, Reardon JT, Kemp M, Sancar A. Circadian oscillation of nucleotide excision repair in mammalian brain. Proc Natl Acad Sci U S A. 106, 2864-7 (2009).

Kerur N, Veettil MV, Sharma-Walia N, Bottero V, Sadagopan S, Otageri P, et al. IFI16 acts as a nuclear pathogen sensor to induce the inflammasome in response to Kaposi Sarcoma-associated herpesvirus infection. Cell Host Microbe. 9, 363-75 (2011).

Kim J, Matsunaga N, Koyanagi S, Ohdo S. Clock gene mutation modulates the cellular sensitivity to genotoxic stress through altering the expression of N-methylpurine DNA glycosylase gene. Biochem Pharmacol. 78, 1075-82 (2009).

Kizek R, Adam V, Hrabeta J, Eckschlager T, Smutny S, Burda JV, et al. Anthracyclines and ellipticines as DNA-damaging anticancer drugs: recent advances. Pharmacol Ther. 133, 26-39 (2012).

Kourtidis A, Jain R, Carkner RD, Eifert C, Brosnan MJ, Conklin DS. An RNA interference screen identifies metabolic regulators NR1D1 and PBP as novel survival factors for breast cancer cells with the ERBB2 signature. Cancer Res. 70, 1783-92 (2010).

Kojetin DJ, Burris TP. REV-ERB and ROR nuclear receptors as drug targets. Nat Rev Drug Discov. 13, 197-216 (2014).

Kumar N, Solt LA, Wang Y, Rogers PM, Bhattacharyya G, Kamenecka TM, et al. Regulation of adipogenesis by natural and synthetic REV-ERB ligands. Endocrinology. 151, 3015-25 (2010).

La Belle A, Khatib J, Schiemann WP, Vinayak S. Role of Platinum in Early-Stage Triple-Negative Breast Cancer. Curr Treat Options Oncol. 18, 68 (2017).

Lans H, Marteijn JA, Vermeulen W. ATP-dependent chromatin remodeling in the DNA-damage response. Epigenetics Chromatin. 5. 4 (2012).

Li T, Diner BA, Chen J, Cristea IM. Acetylation modulates cellular distribution and DNA sensing ability of interferon-inducible protein IFI16. Proc Natl Acad Sci U S A. 109, 10558-63 (2012).

Li W, Katoh H, Wang L, Yu X, Du Z, Yan X, et al. FOXP3 regulates sensitivity of cancer cells to irradiation by transcriptional repression of BRCA1. Cancer Res. 73, 2170-80 (2013).

Liedtke C, Kolberg HC. Systemic Therapy of Advanced/Metastatic Breast Cancer - Current Evidence and Future Concepts. Breast Care (Basel). 11, 275-281 (2016).

Lin W, Zhao Z, Ni Z, Zhao Y, Du W, Chen S. IFI16 restoration in hepatocellular carcinoma induces tumour inhibition via activation of p53 signals and inflammasome. Cell Prolif. 50 (2017).

Liu C, Srihari S, Cao KA, Chenevix-Trench G, Simpson PT, Ragan MA, et al. A fine-scale dissection of the DNA double-strand break repair machinery and its implications for breast cancer therapy. Nucleic Acids Res. 42, 6106-27 (2014).

Liu H, Zhang H, Wu X, Ma D, Wu J, Wang L, et al. Nuclear cGAS suppresses DNA repair and promotes tumorigenesis. Nature. 563, 131-136 (2018).

Lopez-Contreras AJ and Fernandez-Capetillo O. Signalling DNA Damage, Protein Phosphorylation in Human Health, Cai Huang, IntechOpen. (2012).

Lord CJ, Ashworth A. The DNA damage response and cancer therapy. Nature. 481, 287-94 (2012).

Luo J, Solimini NL, Elledge SJ. Principles of cancer therapy: oncogene and non-oncogene addiction. Cell. 136, 823-37 (2009).

Malewicz M, Kadkhodaei B, Kee N, Volakakis N, Hellman U, Viktorsson K, et al. Essential role for DNA-PK-mediated phosphorylation of NR4A nuclear orphan receptors in DNA double-strand break repair. Genes Dev. 25, 2031-40 (2011).

Manzella N, Bracci M, Strafella E, Staffolani S, Ciarapica V, Copertaro A, et al. Circadian Modulation of 8-Oxoguanine DNA Damage Repair. Sci Rep. 5, 13752 (2015).

Mao Z, Hine C, Tian X, Van Meter M, Au M, Vaidya A, et al. SIRT6 promotes DNA repair under stress by activating PARP1. Science 332, 1443-46 (2011).

MAQC Consortium. The MicroArray Quality Control (MAQC)-II study of common practices for the development and validation of microarray-based predictive models. Nat Biotechnol. 28, 827-38 (2010).

Marchenay C, Cellarier E, Lévi F, Rolhion C, Kwiatkowski F, Claustrat B, et al. Circadian variation in O6-alkylguanine-DNA alkyltransferase activity in circulating blood mononuclear cells of healthy human subjects. Int J Cancer. 91, 60-6 (2001).

Min S, Jo S, Lee HS, Chae S, Lee JS, Ji JH, et al. ATM-dependent chromatin remodeler Rsf-1 facilitates DNA damage checkpoints and homologous recombination repair. Cell Cycle 13, 666-77 (2014).

Morrone SR, Wang T, Constantoulakis LM, Hooy RM, Delannoy MJ, Sohn J. Cooperative assembly of IFI16 filaments on dsDNA provides insights into host defense strategy. Proc Natl Acad Sci U S A. 111, E62-71 (2014).

Muscat GE, Eriksson NA, Byth K, Loi S, Graham D, Jindal S, et al. Research resource: nuclear receptors as transcriptome: discriminant and prognostic value in breast cancer. Mol Endocrinol. 27, 350-65 (2013).

Nur Husna SM, Tan HT, Mohamud R, Dyhl-Polk A, Wong KK. Inhibitors targeting CDK4/6, PARP and PI3K in breast cancer: a review. Ther Adv Med Oncol. 10, 1758835918808509 (2018).

Norquist B, Wurz KA, Pennil CC, Garcia R, Gross J, Sakai W, et al. Secondary somatic mutations restoring BRCA1/2 predict chemotherapy resistance in hereditary ovarian carcinomas. J Clin Oncol. 29, 3008-15 (2011).

Oliver TG, Mercer KL, Sayles LC, Burke JR, Mendus D, Lovejoy KS, et al. Chronic cisplatin treatment promotes enhanced damage repair and tumor progression in a mouse model of lung cancer. Genes Dev. 24, 837-52 (2010).

O'Connor MJ. Targeting the DNA Damage Response in Cancer. Mol Cell. 60, 547-60 (2015).

Parker BS, Rautela J, Hertzog PJ. Antitumour actions of interferons: implications for cancer therapy. Nat Rev Cancer. 16, 131-44 (2016).

Pawitan Y, Bjöhle J, Amler L, Borg AL, Egyhazi S, Hall P, et al. Gene expression profiling spares early breast cancer patients from adjuvant therapy: derived and validated in two population-based cohorts. Breast Cancer Res. 7, R953-64 (2005).

Pereira B, Chin SF, Rueda OM, Vollan HK, Provenzano E, Bardwell HA, et al. The somatic mutation profiles of 2,433 breast cancers refines their genomic and transcriptomic landscapes. Nat Commun. 7, 11479 (2016).

Preitner N, Damiola F, Lopez-Molina L, Zakany J, Duboule D, Albrecht U, et al. The orphan nuclear receptor REV-ERBalpha controls circadian transcription within the positive limb of the mammalian circadian oscillator. Cell. 110, 251-60 (2002).

Price BD, D'Andrea AD. Chromatin remodeling at DNA double-strand breaks. Cell. 152, 1344-54 (2013).

Raghuram S, Stayrook KR, Huang P, Rogers PM, Nosie AK, McClure DB, et al.

Identification of heme as the ligand for the orphan nuclear receptors REV-ERBalpha and REV-ERBbeta. Nat Struct Mol Biol. 14, 1207-13 (2007).

Reis-Filho JS, Pusztai L. Gene expression profiling in breast cancer: classification, prognostication, and prediction. Lancet. 378, 1812-23 (2011).

Sakai W, Swisher EM, Karlan BY, Agarwal MK, Higgins J, Friedman C, et al. Secondary mutations as a mechanism of cisplatin resistance in BRCA2-mutated cancers. Nature. 451, 1116-20 (2008).

Sancar A, Lindsey-Boltz LA, Gaddameedhi S, Selby CP, Ye R, Chiou YY, et al. Circadian clock, cancer, and chemotherapy. Biochemistry 54, 110-23 (2015).

Sancar A, Lindsey-Boltz LA, Kang TH, Reardon JT, Lee JH, Ozturk N. Circadian clock control of the cellular response to DNA damage. FEBS Lett. 584, 2618-25 (2010).

Schärer OD. DNA interstrand crosslinks: natural and drug-induced DNA adducts that induce unique cellular responses. Chembiochem. 6, 27-32 (2005).

Sen T, Rodriguez BL, Chen L, Corte CMD, Morikawa N, Fujimoto J, et al. Targeting DNA Damage Response Promotes Antitumor Immunity through STING-Mediated T-cell Activation in Small Cell Lung Cancer. Cancer Discov. 9. 646-661 (2019).

Senkus E, Kyriakides S, Ohno S, Penault-Llorca F, Poortmans P, Rutgers E, et al. Primary breast cancer: ESMO Clinical Practice Guidelines for diagnosis, treatment and follow-up. Ann Oncol. 26 Suppl 5:v8-30 (2015).

Shah R, Rosso K, Nathanson SD. Pathogenesis, prevention, diagnosis and treatment of breast cancer. World J Clin Oncol. 5, 283-98 (2014).

Shanbhag NM, Rafalska-Metcalf IU, Balane-Bolivar C, Janicki SM, Greenberg RA. ATM-dependent chromatin changes silence transcription in cis to DNA double-strand breaks. Cell 141, 970-81 (2010).

Sokolowska O, Nowis D. STING Signaling in Cancer Cells: Important or Not? Arch Immunol Ther Exp (Warsz). 66, 125-132 (2018).

Solt LA, Wang Y, Banerjee S, Hughes T, Kojetin DJ, Lundasen T, et al. Regulation of circadian behaviour and metabolism by synthetic REV-ERB

agonists. Nature. 485, 62-8 (2012).

Soo Lee N, Jin Chung H, Kim HJ, Yun Lee S, Ji JH, Seo Y et al. TRAIP/RNF206 is required for recruitment of RAP80 to sites of DNA damage. Nat Commun. 7, 10463 (2016).

Sousa FG, Matuo R, Soares DG, Escargueil AE, Henriques JA, Larsen AK, et al. PARPs and the DNA damage response. Carcinogenesis. 33, 1433-40 (2012).

Stehlik C. The PYRIN domain in signal transduction. Curr Protein Pept Sci. 8, 293-310 (2007).

Stratmann SA, Morrone SR, van Oijen AM, Sohn J. The innate immune sensor IFI16 recognizes foreign DNA in the nucleus by scanning along the duplex. Elife. 4:e11721 (2015).

Sulli G, Rommel A, Wang X, Kolar MJ, Puca F, Saghatelian A, et al. Pharmacological activation of REV-ERBs is lethal in cancer and oncogene-induced senescence. Nature. 553, 351-355 (2018).

Swisher EM, Sakai W, Karlan BY, Wurz K, Urban N, Taniguchi T. Secondary BRCA1 mutations in BRCA1-mutated ovarian carcinomas with platinum resistance. Cancer Res. 68, 2581-6 (2008).

Tabchy A, Valero V, Vidaurre T, Lluch A, Gomez H, Martin M, et al. Evaluation of a 30-gene paclitaxel, fluorouracil, doxorubicin, and cyclophosphamide chemotherapy response predictor in a multicenter randomized trial in breast cancer. Clin Cancer Res. 16, 5351-61 (2010).

Tangutoori S, Baldwin P, Sridhar S. PARP inhibitors: A new era of targeted therapy. Maturitas 81, 5-9 (2015).

Terunuma A, Putluri N, Mishra P, Mathé EA, Dorsey TH, Yi M, et al. MYC-driven accumulation of 2-hydroxyglutarate is associated with breast cancer prognosis. J Clin Invest. 124, 398-412 (2014).

Thuerigen O, Schneeweiss A, Toedt G, Warnat P, Hahn M, Kramer H, et al. Gene expression signature predicting pathologic complete response with gemcitabine, epirubicin, and docetaxel in primary breast cancer. J Clin Oncol. 24, 1839-45 (2006).

Tolba MF, Omar HA. Immunotherapy, an evolving approach for the management of triple negative breast cancer: Converting non-responders to responders. Crit Rev Oncol Hematol. 122, 202-207 (2018).

Torre LA, Islami F, Siegel RL, Ward EM, Jemal A. Global Cancer in Women: Burden and Trends. Cancer Epidemiol Biomarkers Prev. 26, 444-457 (2017).

Trump RP, Bresciani S, Cooper AW, Tellam JP, Wojno J, Blaikley J, et al. Optimized chemical probes for REV-ERBα. J Med Chem. 56, 4729-37 (2013).

Tutt A, Robson M, Garber JE, Domchek SM, Audeh MW, Weitzel JN, et al. Oral poly(ADP-ribose) polymerase inhibitor olaparib in patients with BRCA1 or BRCA2 mutations and advanced breast cancer: a proof-of-concept trial. Lancet 376, 235-44 (2010).

Ukai-Tadenuma M, Yamada RG, Xu H, Ripperger JA, Liu AC, Ueda HR. Delay in feedback repression by cryptochrome 1 is required for circadian clock function. Cell. 144, 268-81 (2011).

Unterholzner L, Keating SE, Baran M, Horan KA, Jensen SB, Sharma S, et al. IFI16 is an innate immune sensor for intracellular DNA. Nat Immunol. 11, 997-1004 (2010).

van de Vijver MJ, He YD, van't Veer LJ, Dai H, Hart AA, Voskuil DW, et al. A gene-expression signature as a predictor of survival in breast cancer. N Engl J Med. 347, 1999-2009 (2002).

Vanpouille-Box C, Alard A, Aryankalayil MJ, Sarfraz Y, Diamond JM, Schneider RJ, et al. DNA exonuclease Trex1 regulates radiotherapy-induced tumour immunogenicity. Nat Commun. 8, 15618 (2017).

Veeranki S, Choubey D. Interferon-inducible p200-family protein IFI16, an innate immune sensor for cytosolic and nuclear double-stranded DNA: regulation of subcellular localization. Mol Immunol. 49, 567-71 (2012).

Venkatesan S, Natarajan AT, Hande MP. Chromosomal instability--mechanisms and consequences. Mutat Res Genet Toxicol Environ Mutagen 793, 176-84 (2015).

Wahba HA, El-Hadaad HA. Current approaches in treatment of triple-negative

breast cancer. Cancer Biol Med. 12, 106-16 (2015).

Wang QE, Han C, Zhao R, Wani G, Zhu Q, Gong L, et al. p38 MAPK- and Akt-mediated p300 phosphorylation regulates its degradation to facilitate nucleotide excision repair. Nucleic Acids Res. 41, 1722-33 (2013).

Wang Y, Kojetin D, Burris TP. Anti-proliferative actions of a synthetic REV-ERBα/β agonist in breast cancer cells. Biochem Pharmacol. 96, 315-22 (2015).

Williams RS, Williams JS, Tainer JA. Mre11-Rad50-Nbs1 is a keystone complex connecting DNA repair machinery, double-strand break signaling, and the chromatin template. Biochem Cell Biol. 85, 509-20 (2007).

Xin H, Curry J, Johnstone RW, Nickoloff BJ, Choubey D. Role of IFI 16, a member of the interferon-inducible p200-protein family, in prostate epithelial cellular senescence. Oncogene. 22, 4831-40 (2003).

Xu Y, Price BD. Chromatin dynamics and the repair of DNA double strand breaks. Cell Cycle. 10, 261-7 (2011).

Yan J, Kim YS, Yang XP, Li LP, Liao G, Xia F, et al. The ubiquitin-interacting motif containing protein RAP80 interacts with BRCA1 and functions in DNA damage repair response. Cancer Res. 67, 6647-56 (2007).

Yeo MG, Yoo YG, Choi HS, Pak YK, Lee MO. Negative cross-talk between Nur77 and small heterodimer partner and its role in apoptotic cell death of hepatoma cells. Mol Endocrinol. 19, 950-63 (2005).

Yersal O, Barutca S. Biological subtypes of breast cancer: Prognostic and therapeutic implications. World J Clin Oncol. 5, 412-24 (2014).

Yin L, Wu N, Curtin JC, Qatanani M, Szwergold NR, Reid RA, et al. Rev-erbalpha, a heme sensor that coordinates metabolic and circadian pathways. Science. 318, 1786-9 (2007).

Yin L, Wu N, Lazar MA. Nuclear receptor Rev-erbalpha: a heme receptor that coordinates circadian rhythm and metabolism. Nucl Recept Signal. 8:e001 (2010).

Zambrano A, García-Carpizo V, Gallardo ME, Villamuera R, Gómez-Ferrería

MA, Pascual A, et al. The thyroid hormone receptor beta induces DNA damage and premature senescence. J Cell Biol. 204:129-46 (2014).

Zitvogel L, Galluzzi L, Kepp O, Smyth MJ, Kroemer G. Type I interferons in anticancer immunity. Nat Rev Immunol. 15, 405-14 (2015).

국 문 초 록

유방암은 세계 전체 여성암의 약 1/4을 차지하며 여성암 중 최대 발병률을 보인다. 항암화학요법제는 대부분의 유방암 환자에게 사용되고 있으나 항암제 저항성이 빈번하게 발생하며 이는 암 치료에 있어서 가장 큰 난관이 되고 있다. 따라서 항암제의 효과를 증가시키고 저항성을 최소화할 수 있는 새로운 치료 전략의 도입이 필수적이다. 많은 항암화학요법제는 암세포에 과도한 DNA 손상을 일으킴으로써 세포독성 효과를 나타낸다. 따라서 암세포의 DNA 손상 반응을 조절하는 것은 항암화학요법제의 감수성을 극대화하고 저항성을 최소화하는 항암 전략을 수립하는 데 중요한 요인이 된다.

본 연구의 첫 번째 단원에서는 생체시계 유전자 nuclear receptor subfamily 1, group D, member 1 (NR1D1; Rev-erbα)이 DNA 손상 복구를 조절함으로써 항암화학요법에 대한 유방암 세포의 감수성을 증가시킴을 밝혔다. NR1D1은 DNA 이중 가닥 손상 복구 방법인 비상동 말단 연결과 상동 재조합을 모두 억제했으며, 항암제 독소루비신에 의해 증가한 DNA 손상의 복구를 지연시켰다. 그 분자적 기전으로는 NR1D1이 DNA 손상 복구 인자인 poly(ADP-ribose) polymerase 1에 의해 PARylation 됨으로써 DNA 손상 부위로 이동하고, 이는 DNA 손상 반응 인자들인 SIRT6, pNBS1, BRCA1 등의 DNA 손상 부위로의 이동을 저해하는 것으로 나타났다. 그 결과 NR1D1이 유방암 세포의 독소루비신에 대한 감수성을 증가시킴을 *in vitro*와 *in vivo* 모델 모두에서 관찰하였다. 마지막으로 공공데이터베이스 분석을 통해 NR1D1의 발현이 높은 유방암 환자에게서 항암 화학요법에 대한 감수성이 높음을 확인하였다.

두 번째 단원에서는 삼중음성 유방암에서 interferon γ-inducible protein 16 (IFI16)이 DNA 손상 복구를 억제하고, 이를 통해 1형 인터페론 신호 전달을 증폭시

킴으로써 항암화학요법에 대한 암세포의 감수성을 증가시킴을 밝혔다. 삼중음성유방암 세포주에서 DNA 손상 유도 약물 및 1형 인터페론 처리에 의해 IFI16의 발현이 증가하였다. IFI16은 DNA 이중 가닥 손상 시 히스톤 축출에 의해 생기는 이중 가닥 DNA를 인지하여 결합하고 DNA 손상 반응을 저해함으로써 DNA 손상 복구를 억제하였다. 이어 IFI16은 이중 가닥 DNA와 함께 세포질로 이동하고 stimulator of IFN genes 활성화를 통해 1형 인터페론의 생성을 증가시킴으로써 세포 사멸을 촉진하였다. 실제로 마우스에 독소루비신과 1형 인터페론 공동 투여 시 암세포 사멸의 시너지 효과를 나타냈으나 IFI16 저발현 암세포에는 효과가 미미하였다. 또한 IFI16 발현이 높은 유방암 환자에게서 항암 화학요법에 대한 감수성이 높음을 공공 데이터베이스 분석을 통해 확인함으로써 IFI16 발현의 임상적 중요성을 검증하였다.

본 연구를 통해 NR1D1 및 IFI16이 암세포의 DNA 손상 복구 과정을 억제하는 분자적 메커니즘을 규명하였고, 유방암 환자의 항암화학요법제에 대한 감수성을 증가시킬 수 있는 새로운 치료 타겟이 될 수 있음을 제시하였다.

주요어 : DNA 손상 반응, NR1D1, IFI16, PARP1, 1형 인터페론, 항암화학요법제 감수성, 유방암

학번 : 2013-21566